POLITECNICO
MILANO 1863

SCUOLA DI INGEGNERIA INDUSTRIALE
E DELL'INFORMAZIONE

# Thermodynamic analysis and optimal working fluid selection of a reversible Heat Pump-Organic Rankine Cycle coupled to a renewable energy based thermo-chemical energy storage

Tesi di Laurea Magistrale in
Energy Engineering - Ingegneria Energetica

Author: **Simone Montozzi**

Student ID: 10690966
Advisor: Prof. Marco Astolfi
Co-advisors: Dario Alfani, Andrea Giostri
Academic Year: 2020-21

# Abstract

In the present thesis work the author analyzes an innovative thermochemical storage system based on a heat pump charge cycle and a organic Rankine discharge cycle. Using a low temperature heat source (which could be an industrial waste source or a renewable heat source) a working fluid is evaporated in a low pressure heat exchanger. The fluid, after being compressed, it is condensed in a high pressure exchanger and releases heat which feeds a thermochemical reactor, in which a reversible reaction takes place. When there is a need to produce electricity, the inverse exothermic reaction takes place, which releases useful heat to evaporate the working fluid It is then expanded in the turbine, producing power. Furthermore, by condensing, this fluid heats the water of a district heating system.

The author has developed in Matlab® a set of codes in order to analyze the thermodynamics of the two cycles and evaluate which are the best fluids in terms of round-trip-efficiency. The discharge cycle is calculated by imposing the equality of the areas of the exchangers, as the components are the same for the two cycles.

Both for the base case and by carrying out sensitivity analyses on various generations of district heating and low temperature heat source temperatures, the best fluid is Benzene, which guarantees a round-trip-efficiency higher than 100% when using a fifth generation district heating network and a 110°C heat source.

**Keywords:** thermochemical storage, heat pump, ORC, heat exchangers, round-trip-efficiency

# Sommario

Nel presente lavoro di tesi si analizza un innovativo sistema di accumulo termochimico basato su un ciclo di carica a pompa di calore e un ciclo Rankine a fluido organico di scarica. Utilizzando una fonte di calore a bassa temperatura (che potrebbe essere una fonte di scarto industriale oppure da rinnovabili) si fa evaporare un fluido di lavoro in uno scambiatore di bassa pressione. Il fluido, dopo essere stato compresso, viene fatto condensare in uno scambiatore di alta pressione e rilascia calore che alimenta un reattore termochimico, nel quale avviene una reazione reversibile. Quando c'è necessità di produrre energia elettrica, si fa avvenire la reazione inversa, esotermica, che rilascia del calore utile per far evaporare il fluido di lavoro, che viene espanso in turbina producendo potenza. Inoltre, condensando, tale fluido riscalda dell'acqua di un sistema di teleriscaldamento.

L'autore ha sviluppato in Matlab® un set di codici per analizzare la termodinamica dei due cicli e valutare quali siano i fluidi migliori in termini di round-trip-efficiency. Il ciclo di scarica è calcolato imponendo l'uguaglianza delle aree degli scambiatori, in quanto i componenti sono gli stessi per i due cicli.

Sia per il caso base, sia effettuando delle analisi di sensibilità su varie generazioni di teleriscaldamento e di temperature della fonte di calore a bassa temperatura, il fluido migliore risulta essere il Benzene, che garantisce una round-trip-efficiency superiore al 100% quando si utilizza una moderna rete di teleriscaldamento e una fonte di calore a 110°C.

**Parole chiave:** Accumulo termochimico, pompa di calore, ciclo Rankine organico, scambiatori di calore

# Extended abstract

## 1 - Introduction

The exploitation of renewable energy sources is growing a lot due to the cost reduction of green technologies and due to the aim to reduce $CO_2$ production and fossil fuels consumption. But renewables sources are characterized by problems such as the control of the power output and the predictability. These aspects can lead to a lack of power produced when the request is high, and, on the contrary, there could be an excess of power injected in the grid when it is not needed. So, in order to deal with these problems, it is necessary to rely on energy storage systems, which can interact with the grid, absorbing or supplying electric energy when needed.

There are different types of energy storage, based on the different operating principle: the storage could be mechanical, electrochemical, chemical or thermal. The thermal energy storage is the most promising and still under-exploited in the world. In particular, it can be sensible heat storage (SHS), latent heat storage (LHS) or thermochemical heat storage (TCS).

The system studied in this thesis is based on a thermochemical energy storage system, coupled to a charging cycle (heat pump) and a discharging cycle (organic Rankine cycle).

## 2 - Bibliography review

In literature are present lot of different storage system prototypes and studies. The operating principles can be very different from each other. The author studied the technical aspects of the systems most similar to the one analyzed in this thesis.

In particular, the fluids used, the type (and temperature) of the low temperature heat source, the efficiencies assumed for the turbomachines and the round-trip-efficiency values obtained are are the main parameters of interest.

## 3 - Model description

Here is presented the functioning of the analyzed system. The charging and discharging cycles are depicted.

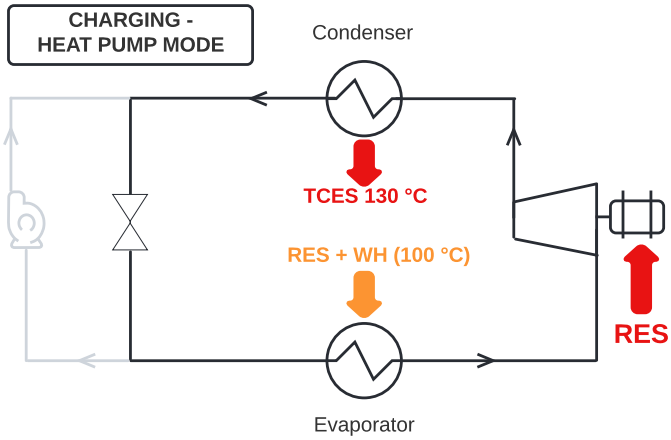


Figure 1: Plant configuration, Heat Pump mode

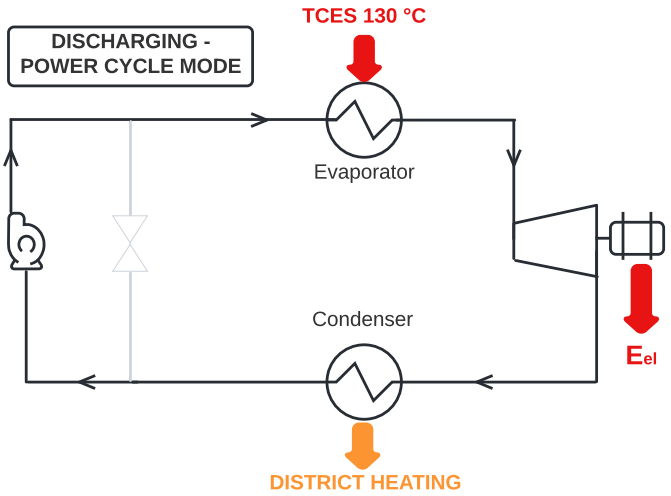


Figure 2: Plant configuration, Power Cycle mode

The low temperature heat source introduces energy into the cycle, causing evaporation of the working fluid. Then, the fluid is compressed and finally condensed. the working fluid. The condensation heat released is used into the chemical reactor to make the endothermic

reaction take place. When it is necessary to carry out the inverse reaction, the products of the reaction carried out previously, are made to react, releasing heat. This heat is introduced into the discharge cycle (Power Cycle), and serves to evaporate the working fluid. The fluid is then expanded in a turbine, generating electricity, and then condensed.

When the low temperature heat source is available throughout the winter, this is called thermal integration. If there is thermal integration, the heat source, in addition to evaporating the working fluid in the charging cycle, is used to contribute to the heating of the district heating water.

The thermodynamic cycles are depicted in Ts diagram:

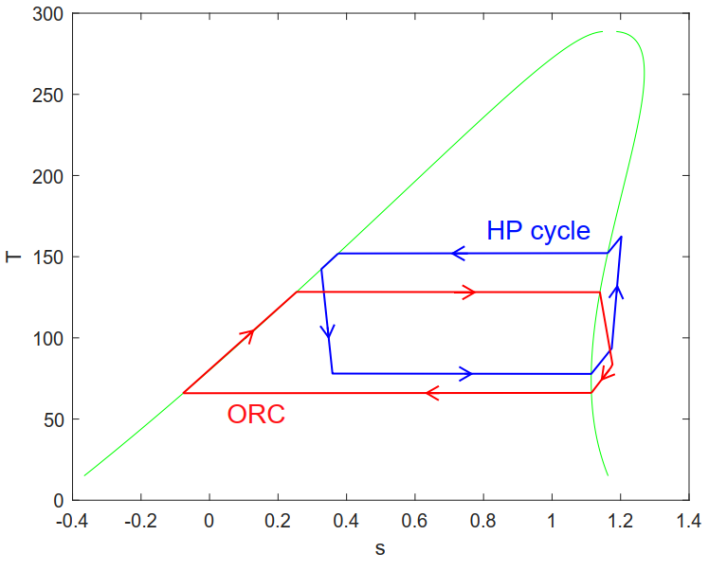


Figure 3: T-s diagram of the two cycles

After describing some basic model assumptions, such as the efficiency of the thermochemical energy storage (equal to 1), the isentropic efficiencies of the turbomachines used, the initial heat transfer coefficients for each heat exchangers, the pressure losses inside them and the temperature of the district heating system, the model is described.

The author created a set of Matlab codes in order to compute, as final result, the round-trip-efficiencies of the various fluids selected. The conceptual scheme is represented in the following figure:

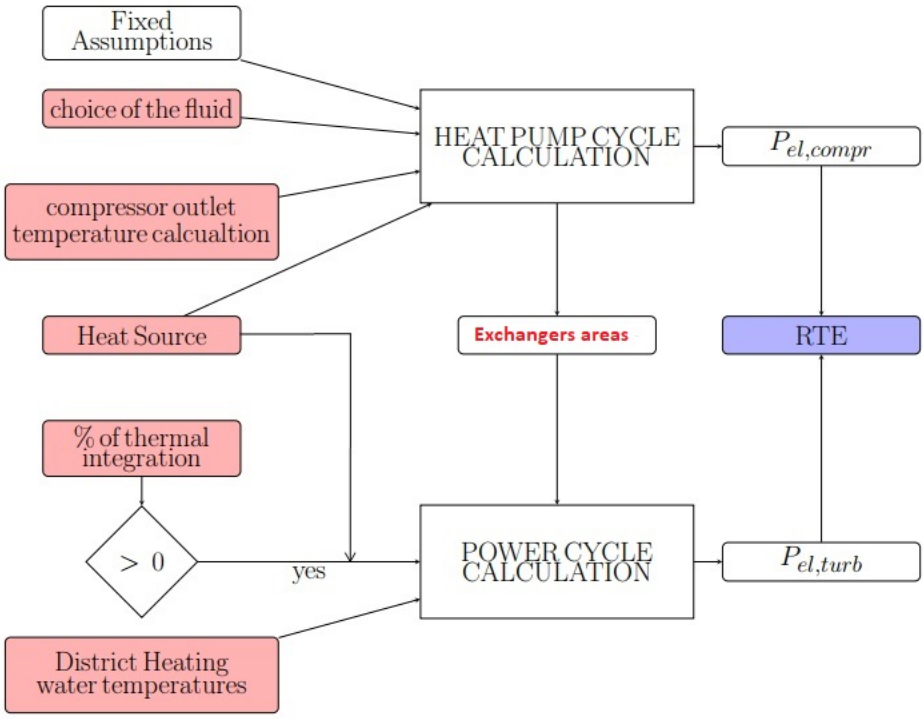


Figure 4: General conceptual scheme

Running the code for each fluid, and for each generation of district heating system, a classification of the best fluids is obtained.

The performance of the cycle is analyzed as the inlet and outlet temperatures of the compressor in the charging cycle vary. Therefore, the code calculated the minimum and maximum inlet and outlet temperatures at which compression can take place for each fluid. The code include a function that aims to avoid the unfavorable situations in which he compression end inside the saturation bell and in which he compression end outside the saturation bell but passing through it.

Furthermore, another function checks the temperature at the compressor outlet: if this temperature is lower than an imposed value (based on a pitch point with respect to the heat pump condensation temperature ), it is imposed to be equal to this minimum. Knowing the outlet temperature, the inlet one is calculated. If the outlet temperature is higher than the imposed value, that value represent the minimum outlet temperature.

After calculating the minimum inlet and outlet temperatures of the compression, the code calculates the maximum temperatures at which the compression can take place.

At this point, knowing the entire operating range of the compressor (in terms of temper-

atures), the reference parameters and performance can be calculated.

In particular, the areas of the exchangers are calculated using the classic heat exchange formula $Q = UA\Delta T_{ML}$, in which, for each section of each heat exchanger, the overall heat transfer coefficient U is calculated through an initially assumed set of $h_i$ and $h_e$. The values of these areas will then be used to calculate the discharge cycle, (which is then calculated in off design). This is because the exchangers, in this system, are the same both in the charge cycle and in the discharge cycle.

To increase the degree of precision of the results obtained, the values of $h_i$ and $h_e$ are calculated for each heat exchangers sections, through the appropriate heat exchange correlations for Shell&Tube heat exchangers.

## 4 - Results and fluids classification

After the definition of a reference case, the results are investigated. First of all, the trend of the RTE with the compressor outlet temperature is discussed. It is monotonously increasing for all fluids. This means that it is convenient, in terms of efficiency, to set the maximum compressor outlet temperature. The best fluids are Benzene, DMC and R1233ZD, as it can be seen in the following figure.

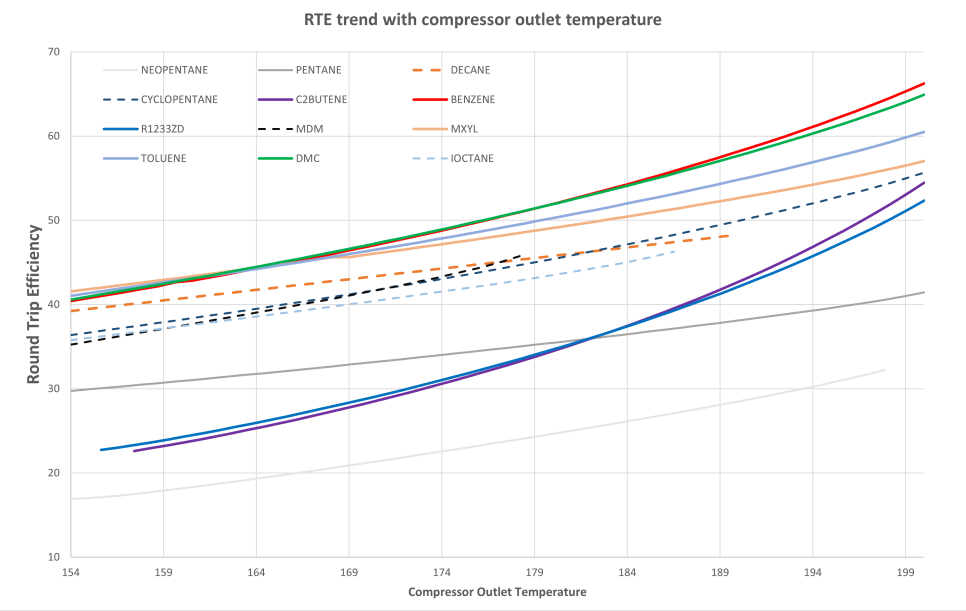


Figure 5: RTE trend as the compressor outlet temperature increases, for the reference case with no thermal integration

In order to have a more complete idea of the consequences of choosing a specific fluid, the

author has also chosen to investigate the behavior of the heat exchange areas. These are first analyzed individually: the area of the high pressure heat exchanger and that of the recuperator increases as the temperature increases, and the opposite happens for the low pressure heat exchanger.

The trends of the total area is depicted in the following figure:

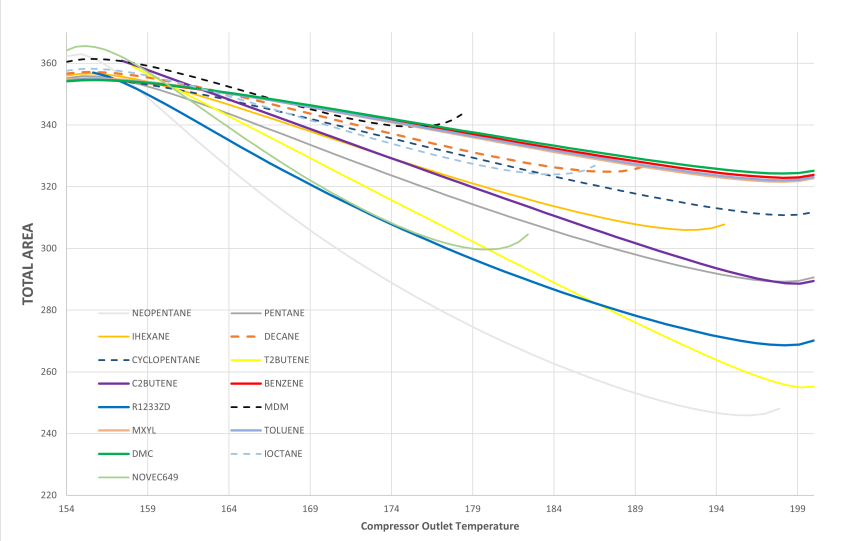


Figure 6: Total area trend with compressor outlet temperature

Finally, an analysis that simultaneously takes into account all these aspects is done. The parameter RTE/A is calculated (where A is the total area of the heat exchangers involved). Results are shown:

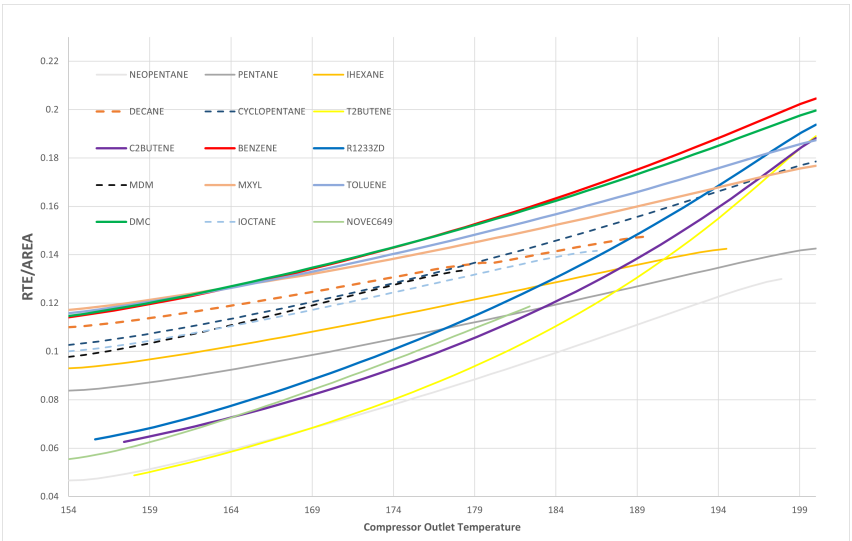


Figure 7: RTA/A trend with compressor outlet temperature

The best fluids remain the same: Benzene, R1233ZD and DMC. At this point, a sensitivity analysis is done: it is studied what happens when the temperatures of the district heating system and of the heat source that feeds the charging cycle change.

Adopting a more modern generation of district heating is beneficial for the whole system. Therefore, the lower is the supply and return temperatures, the higher will be the system RTE. The relative increase obtained by passing from the third generation to the most modern generation of district heating is shown graphically:

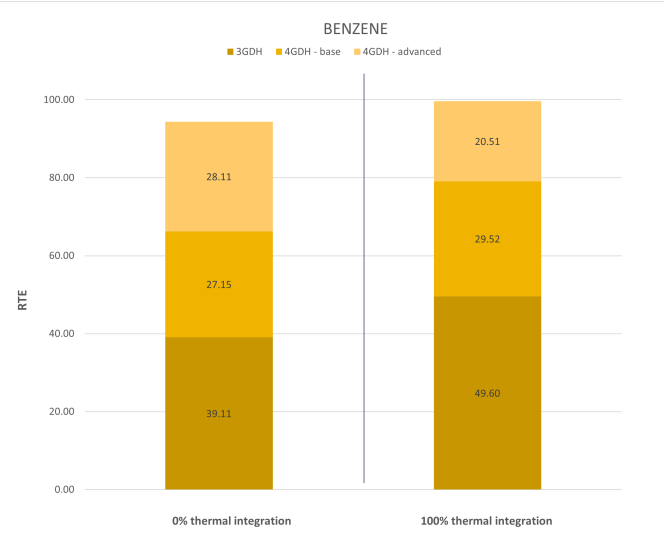


Figure 8: RTE relative increase in the three gen- erations

The use of benzene with a modern fourth generation system, in case of 100% thermal integration of the renewable/waste heat source, permit to reach the maximum RTE in those conditions (99.62).

Finally, the last result is that by varying the low temperature heat source (thus varying the water temperature), the RTE is not particularly affected. This is a positive factor, as it makes it clear that this system can be powered by different low temperature heat sources, while maintaining good performance.

## 5 - Conclusion

This thermochemical storage system produces excellent results when coupled with a modern district heating network. The most modern district heating networks (fourth generation) are being gradually installed all over the world, therefore the feasibility of these systems, with high performances, can be guaranteed in the years to come.

When this system is installed near an industrial plant, it can be thermally integrated throughout the year and the performance will be greater.

With regard to the best the working fluid, among the 34 fluids initially selected, Benzene is the one that guarantees the best performance in terms of RTE in any case. By changing the generation of district heating or the temperatures at which the heat source is available, it guarantees the best round-trip-efficiency, both in the case of thermal integration and in the stand-alone case. Benzene has an ODP equal to 0 and a GWP equal to 3.4, therefore it is an excellent fluid also from an environmental point of view.

# Contents

# 1 | Introduction

## 1.1. The need for energy storage

Recent projections made by the European Commission predict that the primary energy consumption will rise by 48% in 2040 [1]. On the other hand, the depletion of fossil resources (combined with their negative impact on the environment) has accelerated the shift toward sustainable energy sources. Therefore, renewable energy sources (RES) have been playing a dominant role in reforming the natural balance and providing the needs of the growing population demand.

However, intermittency and non-controllability are inherent characteristics of renewable energy-based electricity generation systems. So, due their stochastic nature, they are not programmable and they can't guarantee the stability of the power grid. The instant balance of temporal and spatial mismatch between generations and loads can be achieved introducing flexible elements in the power networks, where flexibility is defined as the capability to balance rapid changes in power generation.

A suitable energy storage system could provide an important (even crucial) approach to dealing with the intermittency of renewable sources and the unpredictability of their output as the surplus could be stored during the periods when intermittent generation exceeds the demand and then be used to cover periods when the load is greater than the generation. Energy storage systems (ESS) can be effective in improving the mismatch between energy generation and use in terms of time, temperature, power or site, leading to an increase of the overall efficiency and reliability.

An ESS includes a means by which electricity imported from a power grid is converted into a form that could be stored at off-peak demand, when energy cost is usually low or during surplus generation, and converted back to electricity at peak demand or when needed.

Another important aspect is that energy storage systems are urgently needed by the conventional electricity generating industry, because they have little or no storage facility.

The electricity transmission and distribution systems are operated for the simple one-way transportation from remote and large power plants to consumers. This means that electricity must always be used precisely when produces. However, the demand for electricity varies rapidly, daily and seasonally, and the maximum demand may only last for a few hours each year. This leads to inefficient, over-designed and expensive plants. ESS allows energy production to be de-coupled from its supply, self generated or purchased. This is particularly important to large utility generation systems, e.g. nuclear power plants, which must operate near full capacity for economic reasons. Therefore, energy storage systems can provide substantial benefits including load following, peaking power and standby reserve. Also by providing spinning reserve and a dispatched load, ESS can increase the net efficiency of thermal power sources while reducing harmful emissions [2].

Furthermore, ESS is regarded as an imperative technology for the distributed energy resource systems. They are installed at the distribution level, close to the place of utilisation, and generate power typically in the small range of a few kW to a few MW. A distributed system is regarded as a sustainable, efficient, reliable and environmentally friendly alternative to the conventional energy system. The energy system is undergoing the change to be a mixture of centralized and distributed sub-systems with higher and higher penetration of distributed energy resource systems.

However, drastic load fluctuations and voltage drops could occur, due to smaller capacity and higher possibility of line fault than the conventional power system. For this reason, EES are identified as a key solution to compensate the power flexibility and provide uninterruptible power supply in cases of instantaneous voltage drop for such a distributed energy network.

From a global pollution point of view, the IEA have concluded that an effective installed energy storage capacity will reduce global warming by 2°C, provided the installed capacity increases by 450 GW in 2050 as opposed to 140 GW in 2014 [3].

After briefly describing why there is a need to study and develop energy storage systems, the various ways to accumulate energy are presented.

## 1.2. Types of energy storage

In literature there are numerous descriptions of energy storage systems, with detailed classifications, features, advantages, environmental impacts, application and implementation possibilities [4] [5] [6]. The purpose of this section is to briefly describe the various types of energy storage that exist, focusing mainly on thermal energy storage.

Energy storage systems can be largely classified as mechanical, electrochemical, chemical and thermal storage systems.

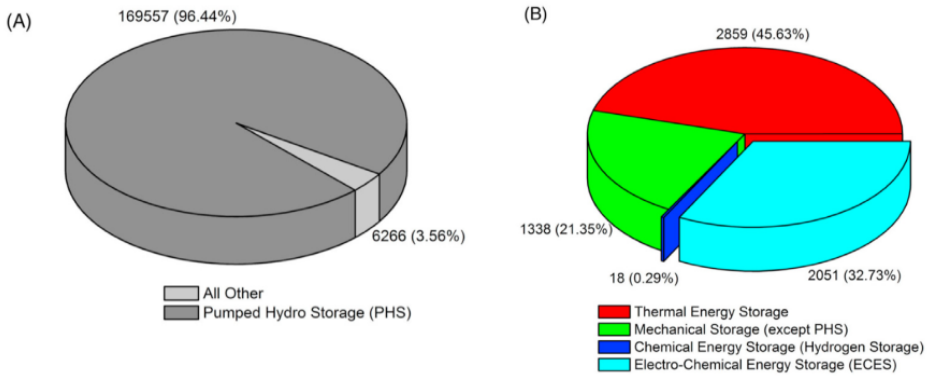


Figure 1.1: A) operational capacity for installed energy storage systems B) grid connected operational capacity for the other types of energy storage systems

The installed grid connected capacity for Energy Storage System was 140976 MW as of 2014. Nearly 99.3% of the capacity that was stored was in the form of pumped hydro storage [7]. The percentages of diffusion of the various storage systems are showed in 1.1.

### 1.2.1. Mechanical Energy Storage

Mechanical energy storage is based on the conversion of energy into both mechanical and electrical energy. During off-peak, when demand is low, the electrical energy is converted to mechanical energy, exploiting the principle of potential, kinetic or pressurized gas. Contrariwise, when demand is high, the energy is concerted to electrical energy [7]. A good feature of these types of energy storage systems is that the stored energy can be readily transformed to electrical or mechanical energy.

The common types of mechanical energy storage systems are pumped hydro energy storage, flywheel energy storage (FES), compressed energy storage (CAES) and gravity energy storage systems (GES).

## Pumped Hydro Energy Storage (PHES)

PHES is the most mature and widely used large scale energy storage technology. It uses gravity to store energy. During periods of low power demand, water is pumped from a lower reservoir to an upper reservoir. Then, when power demand is high, water flows from the upper reservoir to the lower reservoir, activating the turbines to generate electricity [8]. The volume and height of the water determines the amount of energy that can be stored. Currently, this system is a commercially available technology, and represent more than 99% installed energy storage capacity [9].

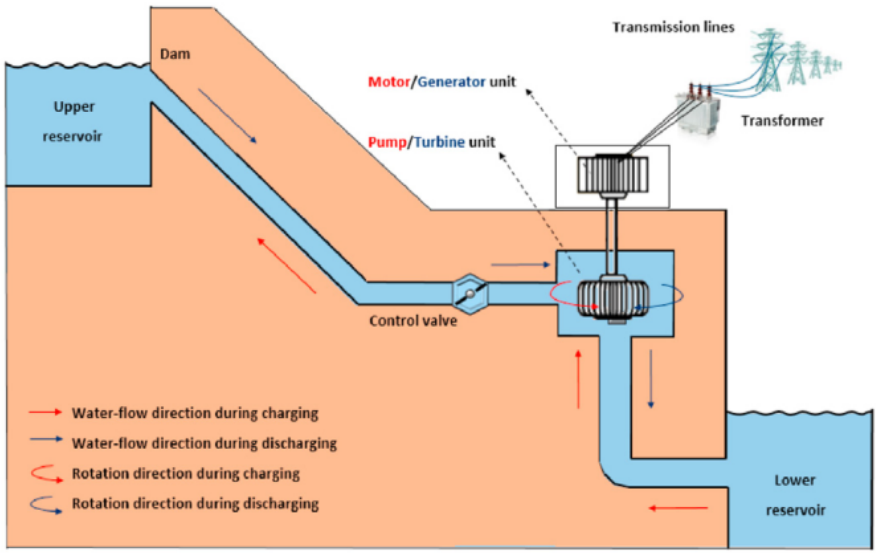


Figure 1.2: Pumped hydro storage system

Figure 1.2 shows the scheme of this storage system [7]. In general, the lifetime of PHES installations is around 30-50 years, with an acceptable round-trip efficiency of 65-85%. They are capable of providing reliable power within a short period of time (typically within one minute) [7]. Furthermore, flexible PHES generation will provide up and down control, which could stabilize the unstable power production coming from renewable energy sources. PHES act as fast response peaking plant to complement high inertia nuclear power and as an integrator for variable wind/solar power.

One limitation of PHES is that several natural geological features are needed, including adequate close land areas divided by adequate elevation. There must also be a massive supply of water.

## Flywheel energy storage systems (FESS)

This application is made up of a large cylinder fixed on a stator by magnetic glide bearings [10]. Figure 1.4 shows the schematic representation of a flywheel storage system. It take place in a vacuum, in order to reduce wind shear. Energy storage is done mechanically due to the kinetic energy of the rotor mass spinning at very high speeds. The energy stored in the flywheel can be reused by reducing the speed of the flywheel with a torque, while the kinetic energy is returned to the electrical motor, which acts as an electric generator. FESS is suitable for the storage of energy in electric locomotives to support movement via non-electrified sections of rail lines [11].

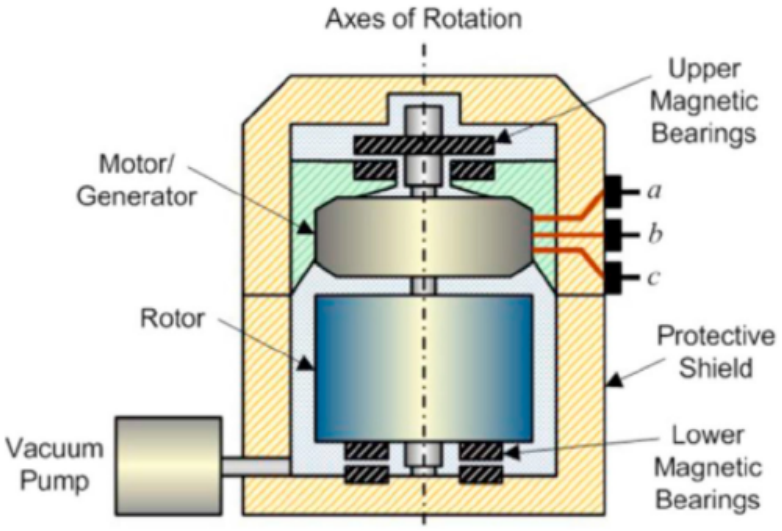


Figure 1.3: Main components of a flywheel storage system

Flywheels systems, in terms of cost of operation, are regarded ad perfect model of energy storage due to its low maintenance cost, long life cycle, high efficiency, free from depth of discharge effects, environmentally friendly, wide operating temperature range and ability to survive in harsh conditions. However, due to the high friction losses, flywheels are not good for long term energy storage.

## Gravity Energy Storage (GES)

Because of the geological limitations and water requirement encountered with PHES, there have been many adaptations to the pumped hydro concept. This technology uses a very large piston that is suspended in a deep water filled shaft with sliding seals which helps to prevent leakage around the piston. During the charging mode, the off peak electricity is used to drive the motor/generator which spins the pump to force water down the return pipe and into the shaft thus lifting the piston. In the discharging mode, the piston drops forcing water down the storage shaft up the return pipe and through the turbine which spins a motor/generator to produce electricity [12].

## Compressed Air Energy Storage (CAES)

In this application, air is compressed and stored in an underground cavern or an abandoned mine when excess energy is available. Upon energy demand, this pressurized air can be released to a turbine to generate electricity. Caverns can either be drilled in salt or rock formations, or existing cavities such as aquifer strata can be utilized. Such geological formations do not exist everywhere and large steel tanks that can maintain high pressures are sometimes installed under the ground at a higher system cost.

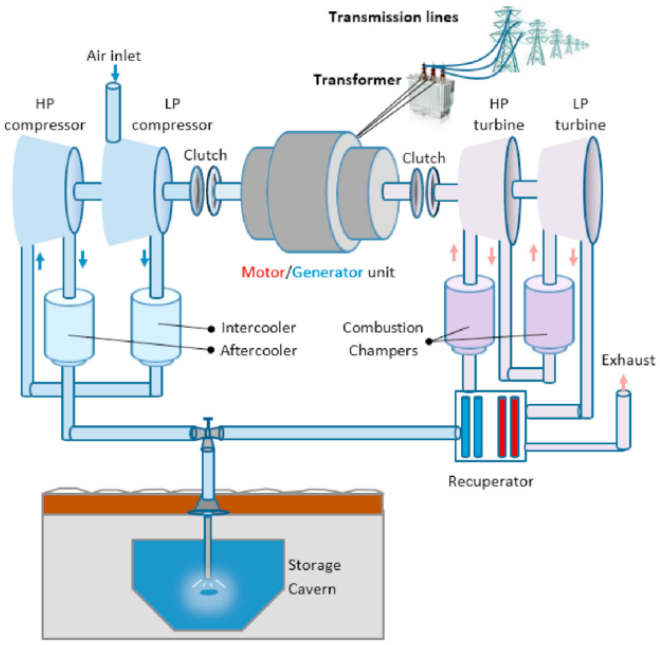


Figure 1.4: Schematic diagram for compressed air energy storage system

This application is dependent on the principles of how gas turbines functions and has a storage capacity of 50-300 MW [13]. The lifetime of CAES installations is approximately 40 years, with an energy efficiency of 71% [14]. Due to low self-discharge properties, they are being considered as long term scale storage installations.

To improve the efficiency of the system, heat generated from the compression stage of the cycle can be stored and utilised during the expansion process. This process results in the overall performance of the system improving by 10-15% [15]. The main challenge associated to compressed air energy storage has to do with the suitability of geological formations suitable for such projects

### 1.2.2. Electrochemical Energy Storage

Electrical energy can be stored electrochemically in batteries and capacitors.

Batteries are mature energy storage devices with high energy densities and high voltages. Among the various battery types, lithium batteries are playing an increasingly important role in electrical energy storage because of their high specific energy (energy per unit weight) and energy density (energy per unit volume) [12].

Capacitors can be classified as electrostatic capacitors, electrolytic capacitors, and electrochemical capacitors. Among these three types, electrochemical capacitors, also called supercapacitors or ultracapacitors (UCs), have the greatest capacitance per unit volume due to having a porous electrode structure. Several new electrode materials and electrolytes have been reviewed and suggested to improve the cost, energy density, power density, cycle life, and safety of batteries [16] [17].

### 1.2.3. Chemical Energy Storage

Chemical energy storage envelopes all technologies where the electrical energy is used to produce chemical compounds which can be stored and used when needed for energy generation. Most chemical compounds which are used as energy storage media has higher energy density than pumped hydro and compressed air and this makes them an ideal energy storage medium. They can be: hydrogen, methane, hydrocarbons, methanol, butanol and ethanol.

Hydrogen is produced through the electrolysis of water and all other compounds (i.e. methane, hydrocarbons and methanol) can be produced from hydrogen in the presence of a carbon source such as CO and CO2 using the Fischer-Tropsch synthesis.

Hydrogen is storable, transportable, highly versatile, efficient, and clean energy carrier. It also has a high energy density. Off-peak electricity is used to electrolyse water to produce hydrogen. The hydrogen can be stored either as compressed gas, liquefied gas, metal hydrides or carbon nanostructures. During the discharge phase, the stored hydrogen is either used in fuel cell or burnt directly to produce electricity.

Fuel cells are low power-density devices like batteries that convert chemical energy to electricity. They exhibit energy efficiencies of approximately 70–80%, while some power plants (e.g., combined cycle units) can achieve efficiencies as high as 60%. Fuel cells use oxygen and a fuel such as hydrogen. They can be combined with supercapacitors to improve their power densities.

One major drawback in using hydrogen for electricity storage is the substantial energy losses during a single cycle. For example, electrolysis currently have an efficiency of 60%, transport and compression for storage may lead to another 10% efficiency loss (although this can be lower) while reconversion to electricity has a efficiency of about 50% for fuel cell application (higher efficiency is anticipated for combustion based power generation if cogeneration of heat is integrated). Thus, the overall round trip efficiency may be in the neighbourhood of 30%. This is partially compensated by the high storage density.

### 1.2.4. Thermal energy storage

Thermal energy storage systems (TES) typically consist of a storage medium and equipment for heat injection and extraction to/from the medium. The storage medium can be a naturally occurring structure or region (e.g., ground) or it can be artificially made using a container that prevents heat loss or gain from the surroundings (water tanks).

TES systems can be effective in improving the mismatch between energy generation and use in terms of time, temperature, power or site, leading to an increase of the overall efficiency and reliability [18]. Coupling thermal energy storage to a power-to-heat technology (based on the conversion of electricity into heat) to provide flexibility to the power system is a promising option of the demand-side management. In particular, turning surplus of variable renewable electricity into heat to be stored as thermal energy offers a significant additional flexibility with a great potential in stabilizing the grid voltage [19]. During off-peak times, heating or cooling can be generated by thermal energy and then used during peak-hours flattening the customer's load profile.

Several studies examine the coupling of thermal storage with power-to-heat systems for several purposes. In general, small-scale power-to-heat and TES applications can be

applied in the residential and commercial sectors while large scale are mainly focus on industrial applications such as district heating grids [4].

The thermal energy storage installed capacity is nearly 3.3 GW, nearly 1.9% of total world energy storage noted for 2017 [20]. This value is expected to progressively rise in future years, and thermal storage technologies will play a key role in the energy storage sector.

TES systems have as their main purpose the prevention of loss of thermal energy by storing excess heat until it is consumed. Although there are many sources of heat from human activities that is wasted, it is not practical to implement TES system at every heat source. However, for large heat sources like solar thermal energy, geothermal energy, fossil-fuel power plants, nuclear power plant, industrial waste heat, there is scope to implement TES system in an economical way.

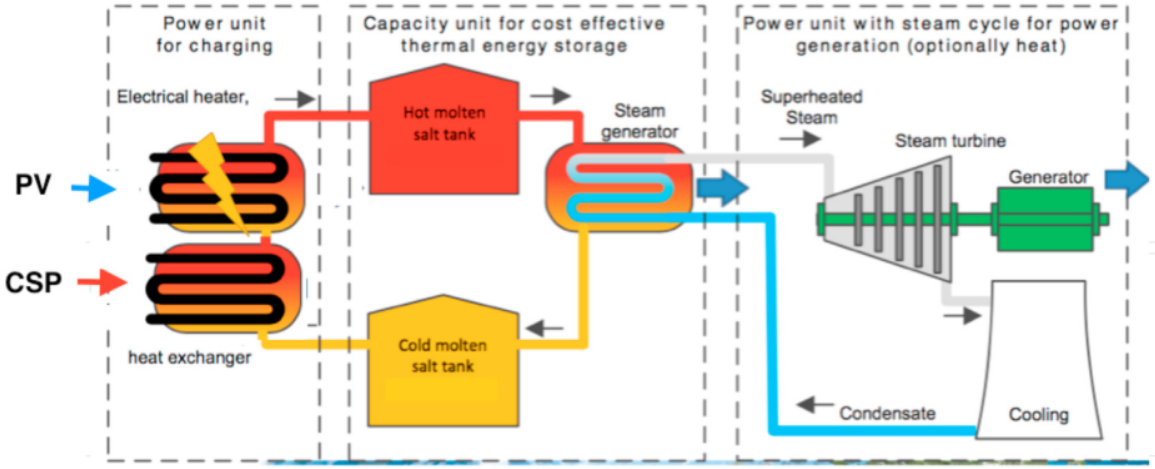


Figure 1.5: Schematic diagram of thermal energy storage system

Figure 1.6 contains a list of operational plants around the globe and the thermal energy storage systems in operation in those plants [21] [22] [23].

Large scale operational TES systems.

| Location | Energy source | | TES system | | | Remarks |
|---|---|---|---|---|---|---|
| | Primary | Secondary | Type | Storage medium | Annual capacity (MWh) | |
| Friedrichshafen, Germany | Solar | Natural gas | Underground, Seasonal | Water | 4106 | District heating network |
| Marstal, Denmark | Solar | Biomass | Underground, Seasonal | Water, Pit storage | 19,000 | District heating network |
| Kungalv, Sweden | Industry waste heat | Waste incineration | Underground, Seasonal | Water | 90,000 | District heating network |
| Chemnitz, Germany | Solar | Natural gas, fuel oil | Underground, Seasonal | Gravel/water | 573 | District heating network |
| Neckarsulm, Germany | Solar | | Underground, Seasonal | Borehole/duct | 3960 | District heating network |
| Rostock, Germany | Solar | | Underground, Seasonal | Aquifer | 497 | District heating network |
| Kutch, India | Solar | | Diurnal | Solar pond | 1357 | Industrial process heat supply |
| Solar two, Nevada, USA | Solar | | Diurnal two tank system | Solar salt | 105 | Electrical power generation. Hot tank (565 °C, 875 $m^3$) |
| THEMIS, Pyrenees, France | Solar | | Diurnal two tank system | Hitect salt | 40 | Electrical power generation. Hot tank (450 °C, 310 $m^3$) |
| Andasol Andalusia, Spain | Solar parabolic trough | | Diurnal, Two–tank, Indirect | Molten salt | 1010 | Electrical power generation Hot tank (384 °C) |
| Extresol Torre de Miguel Sesmero, Spain | Solar parabolic trough | | Diurnal, Two–tank, Indirect | Molten salt | 1010 | Electrical power generation Hot tank (384 °C) |
| Arcosol 50 San José del Valle, Spain | Solar parabolic trough | | Diurnal, Two–tank, Indirect | Molten salt | 1010 | Electrical power generation Hot tank (384 °C) |
| La Florida Badajoz, Spain | Solar parabolic trough | | Diurnal, Two–tank, Indirect | Molten salt | 1010 | Electrical power generation Hot tank (384 °C) |
| La Dehesa La Garrovilla, Spain | Solar parabolic trough | | Diurnal, Two–tank, Indirect | Molten salt | 1010 | Electrical power generation Hot tank (384 °C) |
| Gemasolar (Solar Tres) Fuentes de Andalucía, Spain | Solar power tower | | Diurnal, Two–tank, Direct | Molten salt | 600 | Electrical power generation Hot tank (565 °C) |

Figure 1.6: List of some TES systems in operation

Storage technologies can be classified with respect to the storage principle: sensible, latent and thermochemical [4].

Traditionally, heat storage has been in the form of sensible heat. Sensible heat storage (SHS) is based on storing thermal energy by cooling or heating of a liquid/solid storage medium. Sensible heat determines a temperature linear change (increase or decrease) in the thermal storage material, without changing its chemical composition or phase.

Sensible heat $Q_S$ depends on the temperature change and the specific heat capacity of the storage material. The amount of energy stored (J) is calculated ad follows:

$$Q_s = mc_p\Delta T \tag{1.1}$$

where: $m$ is the mass of the storage medium (kg), $c_p$ is the heat capacity of the storage medium (J/(kg K)) and $\Delta T$ is the temperature difference (°C).

It is important for sensible heat storage systems to use a heat storage material having high specific heat, good thermal conductivity, long-term stability under thermal cycling, compatibility with its containment, recyclability, a low $CO_2$ footprint and low cost [24].

Nowadays, sensible heat storage based on hot water is the State of the Art in district heating systems. SHS systems are successfully applied both in small-scale (residential application with the use of water tanks) and large-scale water volumes, for seasonal storage (aquifer, borehole, cavern, or pit thermal storage). Regarding the low-temperature thermal energy storage, water is the preferred fluid, since it has low cost, non-hazardous behaviour and it is easy to integrate with solar thermal heating.

The State of the Art of the seasonal storage is the underground thermal energy storage (UTES). The four different types of UTES which has been developed are briefly described. An important common disadvantage is that a suitable geological formation is required, in order to guarantee structure feasibility.

- Tank Thermal Energy Storage (TTES): this system is based on reinforced tanks filled with cold-hot water thermocline, connected with charging and discharging loops. TTES can be designed for ground-level or underground (up to 15 meter deep). In order to limit heat losses, the outside of the tank must be insulated by a complex envelope which must guarantee protection from moisture penetration.
- Pit Thermal Energy Storage (PTES): it is made by an artificial pool, which is heat insulated and close by a lid. The storage is filled with water or with a mixture

of gravel saturated with water, and covered by a well-insulated roof. Common pit depths are between 5 to 15 meters.

- Borehole Thermal Energy Storage (BTES): it consists of an heat storage directly underground, without the use of water tanks. A huge heat exchanger with soil is created, by means of ducts inserted into vertical boreholes. BTES must be implemented in grounds with high thermal capacity and impermeability. The ground can be heated up. BTES shows lower storage capacities than other technologies.
- Aquifer Thermal Energy Storage (ATES): it takes advantage of the natural occurring selfcontained layers of ground water (aquifers). During the charging cycle, the water leaves the cold well, it is heated up and injected in the warm well. During the discharge cycle, the flow is inverted. The main drawback is the difficulty in finding suitable aquifers. In general, this solution presents low storage capacities.

Latent heat storage (LHS) is a developing technology that involves changing the phase of a storage material. Recently, this type of thermal energy storage has attracted considerable attention, due to the isothermal nature of the phase-change process, and its lower weight per unit of storage capacity and compactness. Its improved thermal properties compared to sensible heat storage materials, such as stable phase-change temperature and a high latent heat, are also factors that contribute to its emergence.

The amount of energy stored (J) is given by the following equation:

$$Q_l = m\Delta h \tag{1.2}$$

where $\Delta h$ is the melting or phase change enthalpy (J/kg).

Solid-liquid phase change is mainly used, but also solid-solid phase changes are used in some applications. Although for solid-solid phase change the specific latent heat is less, it has advantages like no leakage and no need for encapsulation. Liquid-gas phase change has the highest latent heat of phase change [25].

The materials used for LHS can be organic materials, paraffin, fatty acids, esters, alcohols, glycols, inorganic and salts. Unlike conventional (sensible) storage materials, PCM absorbs and release heat at a nearly constant temperature. Studies using various types of PCMs show that latent heat storage using PCMs can store 5–14 times more heat than sensible heat materials [26].

A large number of phase-change materials are known to melt with a heat of fusion in

any required range. However, for their employment as latent heat storage materials these materials must exhibit certain desirable thermodynamic, kinetic and chemical properties. Moreover, economic considerations and easy availability of these materials has to be kept in mind [27].

The desirable thermophysical, kinetics and chemical properties that a good PCM must have are: suitable phase-transition temperature, high latent heat of transition (especially on a volumetric basis, in order to minimize the physical size of the heat store) and good heat transfer.

In the following figure are reported some phase-chanege materials, classified according to their melting point.

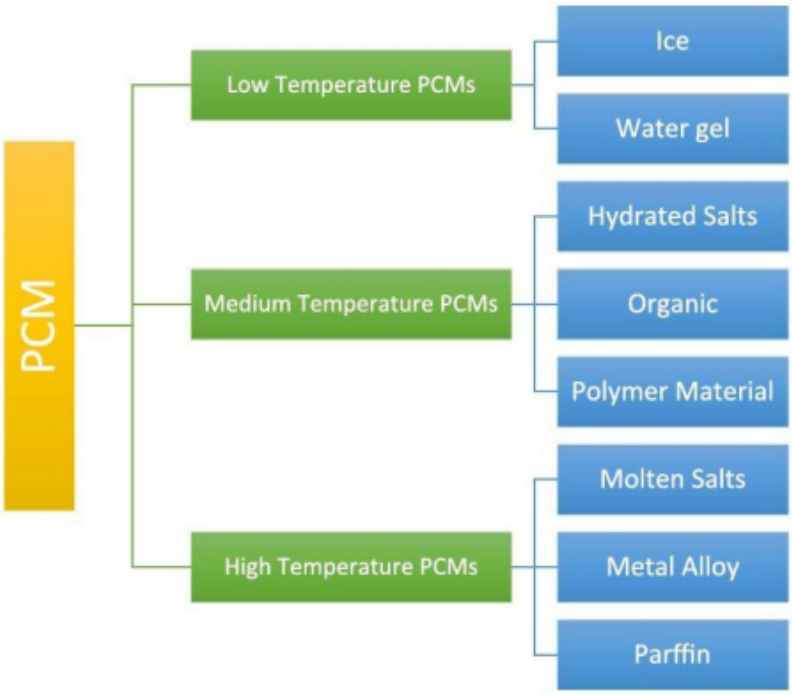


Figure 1.7: Phase-change materials

## 1.3. Thermochemical Heat Storage

This form of heat storage involves a reversible reaction in which heat is stored during the endothermic reaction step and released during the exothermic one. During the charging step, thermal energy is used to dissociate a chemical reactant into products, as shown by the reaction:

$$C + heat \Rrightarrow A + B \tag{1.3}$$

The products are stored separately and, when heat is required, they are mixed and the reverse reaction happens. The initial reactant is formed. The heat released during the reaction is utilised as an energy source.

$$A + B \Rrightarrow C + heat \tag{1.4}$$

This concept is shown graphically in Figure 1.8

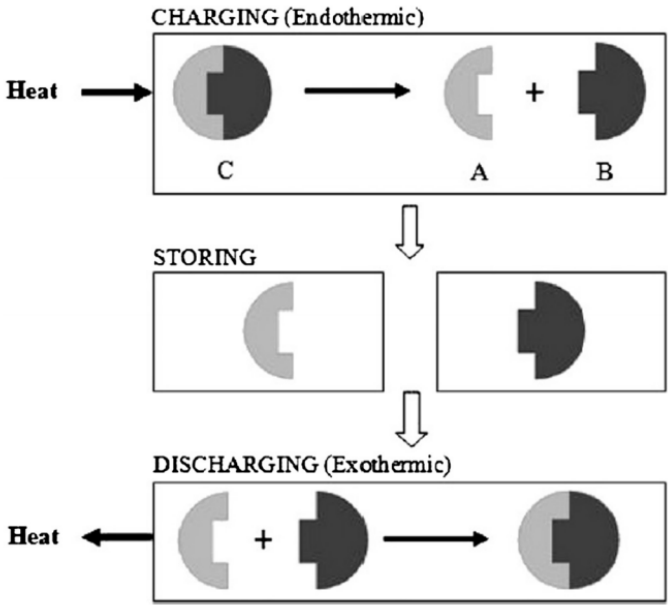


Figure 1.8: Process of thermochemical heat storage

In order to make the endothermic reaction happen, any system can be used as heat source: solar energy [28] or micro combined heat and power (CHP) [29] are the most common examples of heat source. The system analyzed in this thesis is based on a generic heat

source at fixed temperatures.

The energy density of these systems is about 5–10 times higher than latent and sensible heat storage systems respectively. Their storage period and transport are theoretically unlimited because there is no thermal loss during storage as products can be stored at ambient temperature. Indeed, it is demonstrated that the physical thermal storage systems (sensible heat or phase change) progressively lose thermal energy, so they are not suitable for long-term storage.

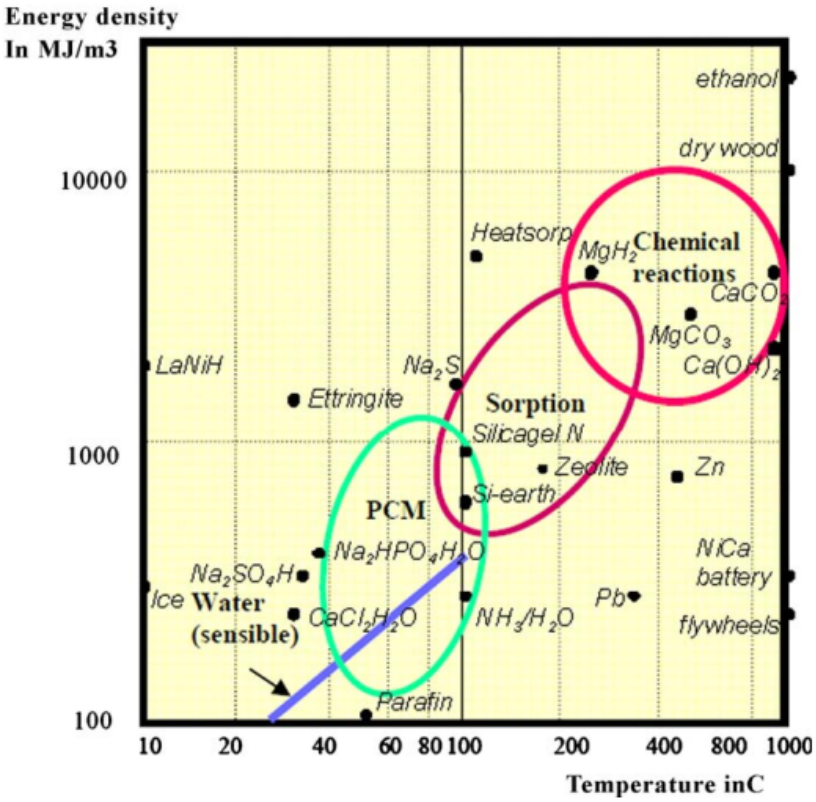


Figure 1.9: Energy density of high energy storage methods

Figure 1.9 [30] shows the energy density of the thermochemical storage materials (indicated in the 'sorption' and 'chemical reactions' circles compared to those of PCM and water (sensible heat storage).

Although these energy densities are much higher than other types of thermal storage, the development status of this technology is still in the early stages. The possibility of achieving more compact systems, little energy losses during the storing operation and higher energy densities compared to other types of thermal energy storage are the most prominent advantages of thermochemical energy storage systems.

As regards the thermal storage of energy, the next chapter deals with the bibliographic review of some of the systems studied or installed in the past years.

In the following pages a comparison between the three types of thermal storage is shown. Figure 1.10 summarizes the technical aspects, while in Figure 1.11 the operating temperatures are listed and the pros and cons of this technology are summarized.

| | SHS System | LHS System | TCES System |
|---|---|---|---|
| Fundamental principle | • Energy stored by raising temperature<br>• Depends on rise in ΔT | • Energy stored during phase change of material at constant temperature<br>• Depends on latent heat of material | • Energy stored during reversible reactions (endothermic and exothermic)<br>• Depends on reaction enthalpy |
| Amount of heat stored | $Q = m \cdot C_p \cdot \Delta T$ | $Q = m \cdot L$ | $Q = n_A \cdot \Delta H_r$ |
| Volumetric energy density | Small (< 50 kWh/m$^3$) | Medium (100 kWh/ m$^3$) | High (> 500 kWh/m$^3$) |
| Gravimetric energy density | Small (0.02–0.03 kWh/kg) | Medium (0.05–0.1 kWh/kg) | High (0.5–1 kWh/kg) |
| Storage temperature | Charging step temperature | Charging step temperature | Ambient temperature |
| Storage period | Limited due to thermal losses to surroundings | Limited due to thermal losses to surroundings | Theoretically unlimited |
| Energy transport | Shorter distance | Shorter distance | Theoretically long distance |
| Maturity | Industrial scale | Pilot-scale | Laboratory and pilot-scale |
| Technology | Simple | Simple | Complex |
| Pros/cons | Pros:<br>• Low-cost materials<br>• Reliable<br>• Simple system<br>Cons:<br>• Low-energy storage density<br>• Higher thermal insulation requirement<br>• Shorter storage duration | Pros:<br>• Higher storage density compared to SHS<br>• Compact system<br>Cons:<br>• Poor thermal conductivity<br>• Higher thermal insulation requirement<br>• Some materials highly corrosive | Pros:<br>• Highest storage density<br>• Long-term storage<br>• Minor heat losses<br>• Heat storage at ambient condition<br>Cons:<br>• Expensive<br>• Complex system |

Figure 1.10: Comparison of various TES technologies

| Technologies | Temperature Range | Advantages | Drawbacks | Storage Period | Storage Density | Life Span |
|---|---|---|---|---|---|---|
| Sensible heat storage (SHS) | ■ up to 50 °C (ground storage and acquifer)<br>■ up to 110 °C (water tank)<br>■ up to 400 °C (concrete) | ■ thermally stable at high temperatures<br>■ low cost materials (excepting liquid metals and thermal oils)<br>■ easy availability<br>■ mature technology at industrial scale | ■ high freezing point (about 100 °C) leading to considerable heat losses<br>■ temperature stability during the discharge process<br>■ thermal energy storage density less than LHS density<br>■ specific heat of materials is less than specific heat of LHS<br>■ large volume required | limited (heat losses) | reduced | long |
| Latent heat storage (LHS) | ■ 20 ÷ 40 °C (paraffins)<br>■ 30 ÷ 80 °C (salt hydrates) | ■ non-toxicity of the PCMs<br>■ compact TES systems due to the use of PCM<br>■ specific heat of LHS is 50–100 times higher than SHS<br>■ energy storage density close to phase change temperature is very high<br>■ no temperature rise occurs during the process leading to an accurate temperature control<br>■ reduced volumes | ■ low thermal conductivity<br>■ organic PCM are flammable<br>■ inorganic PCM are corrosive | Limited (heat losses) | medium | limited |
| Thermochemical heat storage (THS) | ■ 20 ÷ 200 °C | ■ the thermal energy storage density is the highest<br>■ there is no thermal loss during storage considering that products are stored at the environment temperature<br>■ highly compact energy storage<br>■ the reactants are stored for a long time without provoking any degradation of the stored heat | ■ rate of dehydration reaction is slow<br>■ high cost<br>■ low reliability<br>■ potential toxicity<br>■ low system lifetime<br>■ issues about recyclability | long | high | limited |

Figure 1.11: Comparison of various TES technologies, part 2

# 2 | Bibliography review

Starting from the last decade, for the reasons mentioned in Chapter 1, including the deregulation of the electricity market, the growth of renewable energies and the need for network flexibility in terms of load leveling [2], electric energy storage began to gain interest. In this chapter a bibliographic review is made. Various storage systems are compared, underlining the common points with the system studied in this thesis and summarizing the different results.

The first to be studied were systems that consist of a high pressure (HP) tank and a low pressure (LP) tank, four turbomachines (one compressor/turbine pair used during the loading period, and another one during the delivery period), and two heat exchangers, as represented in Figure 2.1 (only one of the two pairs of turbomachines is shown).

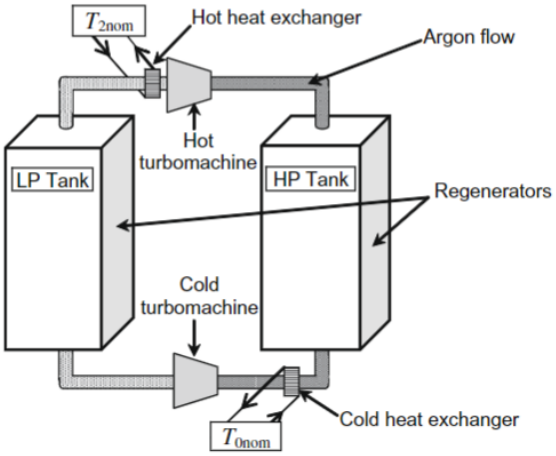


Figure 2.1: Schematic representation of the storage principle

Desrues et al. [31] presented this new type of thermal energy storage process for large scale electric applications. The working fluid used is Argon (gas) and the thermodynamic cycle is a closed Bryton. The gas flows clock-wise during the loading period and counter clock-wise during the delivery period. The initial temperature of the HP tank is assumed to be

equal to the outside temperature ($T_{0,nom} = 25^oC$), while the initial temperature od the LP tank is $T_{2,nom} = 500^oC$. They developed a numerical model that shows the feasibility of the process. Moreover, they stated that the development of reciprocating compressors and turbines with higher polytropic efficiencies could lead to lower temperature and smaller scale applications still showing decent efficiencies. The results, in terms of performances, allow to compare this large scale process with the two mature other ones (Pumped Hydro Energy Storage and Compressed Air Energy Storage). A big pro is that the process suffers for practically no geographical or geological constraints and no safety or environmental issues, and seems to be able to reach similar efficiency, capacity and power performances.

White et al. expanded the study of this system, with particular focus on how various sources of loss affect the round-trip efficiency [32].

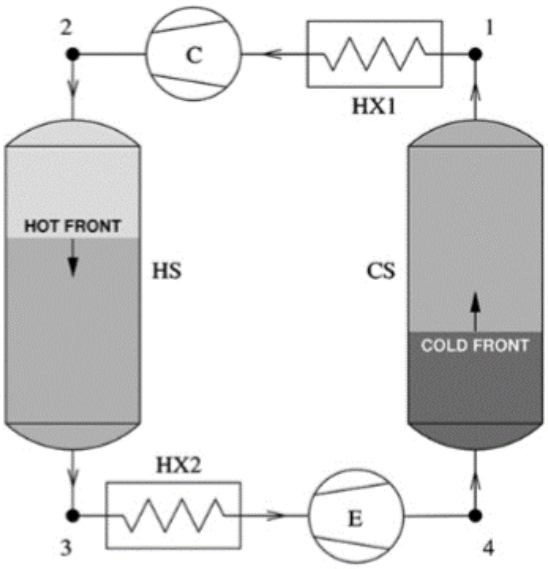


Figure 2.2: Layout of PTES system [32]

The main components are a compressor (C), an expander (E) and two thermal stores: one hot (HS) and one cold (CS) (Figure 2.2). The energy is stored as sensible heat. The compressor and the expander may be either turbomachinery-based or reciprocating devices. They are mechanically coupled and linked to a motor-generator. As in the previous case, the working fluid is Argon which flows in the direction indicated by the arrows during charge, but is reversed for discharge. During charge, the system operates as a high temperature ratio heat pump, using electrical energy to extract heat from the cold front and deliver heat to the hot front. During discharge, the processes are reversed so that the device operates as a heat engine: heat is returned from the hot to the cold store

and electrical energy is retrieved. The heat engine and heat pump operate on the Joule-Brayton and reverse Joule-Brayton cycles respectively. Although this type of storage, was in 2013 (year of publication of this study) in the early stages of development, it is based on well-established technologies and it is therefore possible to estimate its likely performance (round-trip efficiency, storage density and capital cost) with a reasonable level of confidence.

The results shows that the round-trip efficiency and storage density both increase with the compressor temperature ratio. High temperature ratios, however, imply high pressure ratios which in turn imply high cost for the hot reservoir. This is mitigated by the use of a monatomic gas such as Argon for the working fluid. Obtaining a satisfactory RTE clearly requires highly efficient compression and expansion processes: this may be achieved by the use of reciprocating devices. For a turbomachinery-based system, the effects of compression and expansion irreversibility can be mitigated by reducing the ratio between hot and cold store discharged temperatures, which also has the advantage of increasing the energy and power densities. In general, the authors confirmed that this kind of storage system may well be able to compete with CAES and PHES, but without the associated geographic limitations.

Wang et al. [33] have proposed an innovative thermal storage system, similar to the previous ones (based on Joule-Bryton cycle) but with more tanks, which can be connected in series or in parallel. The best solution is represented by the solution with series-connected reservoirs. It shows a round-trip efficiency of 64.9%.

Other studies based on the Joule-Bryton thermodynamic cycle have been carried out in the past years. Given that the proposed storage system is based on a thermal energy storage coupled with a reversible heat pump/organic Rankine cycle, such type of systems are now analyzed.

Eppinger et al. [34] identify the optimal fluids for a heat storage configuration based on a heat pump that receives energy from a low temperature source, coupled to a organic Rankine cycle. Both latent and sensible storage systems are considered for different fluids and are examined for their suitability for different operating conditions with a focus on the behaviour of Cyclopentane, R1233zd(E), Novec649 and R365mfc. The complete list of the analyzed fluid in reported below.

| Name | Abbreviations |
|---|---|
| Butane | BUTANE |
| Methylcyclohexane | C1CC6 |
| *cis*-Butene | C2BUTENE |
| Propylcyclohexane | C3CC6 |
| Cyclohexane | CYCLOHEX |
| Cyclopentane | CYCLOPEN |
| D4 | D4 |
| Dimethyl carbonate | DMC |
| Ethylbenze | EBENZENE |
| Heptane | HEPTANE |
| Hexane | HEXANE |
| Isopentane (2-methylpentane) | IPENTANE |
| MD2M (Decamethyltetrasiloxane) | MD2M |
| MD3M (Dodecamethylpentasiloxane) | MD3M |
| MDM (Octamethyltrisiloxane) | MDM |
| MM (Hexamethyldisiloxane) | MM |
| m-Xylene | MXYLENE |
| Neopentane (2,2-dimethylpropane) | NEOPENTN |
| Novec 649 ® (Dodecafluoro-2-methylpentan-3-one) | NOVEC649 |
| o-Xylene | OXYLENE |
| Pentane | PENTANE |
| p-Xylene | PXYLENE |
| R113 (1,1,2-Trichloro-1,2,2-trifluoroethane) | R113 |
| R114 (1,2-Dichloro-1,1,2,2-tetrafluoroethane) | R114 |
| R123 (2,2-Dichloro-1,1,1-trifluoroethane) | R123 |
| R1233zd(E) (*trans*-1-Chloro-3,3,3-trifluoro-1-propene) | R1233ZD |
| R141b (1,1-Dichloro-1-fluoroethane) | R141B |
| R245ca (1,1,2,2,3-Pentafluoropropane) | R245CA |
| R245fa (1,1,1,3,3-Pentafluoropropane) | R245FA |
| R365mfc (1,1,1,3,3-Pentafluorobutane) | R365MFC |
| R347mcc (1,1,1,2,2,3,3-Heptafluoro-3-methoxypropane) | RE347MCC |
| Trans-Butene | T2BUTENE |
| Toluene | TOLUENE |

Figure 2.3: Overview of fluid names and abbreviations

Most of the fluids analyzed are common to those selected by the author of this thesis. The system analyzed by Eppinger et al. is the same as the one presented in this work, with the only difference in the storage section. But since the thermochemical storage system itself will not be analyzed (only the temperatures at which the reaction takes place and at which the reactor releases the heat to the discharge cycle will be chosen), thermodynamics can be considered similar and the authors' analyzes and conclusions can be compared.

They conclude that with current technologies and a heat source above 80°C, it is possible to achieve a round-trip-efficiency above 60%, even on a small scale. R1233zd(E) appears to be the best choice with a small trade-off between lesser efficiency against environmental

sustainability and safety. For latent storages, cyclopentane achieves the highest efficiency with a downside regarding safety.

Jockenhofer et al. [35] developed a thermal energy storage based on a subcritical Rankine cycle. The system is named ORC-CHEST (Organic Rankine Cycle based Compressed Heat Energy Storage).

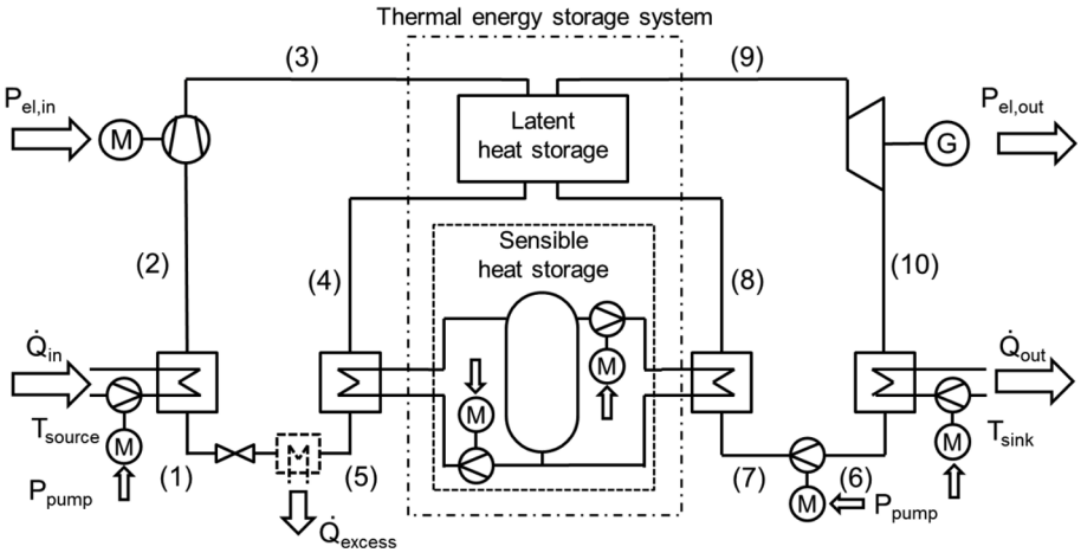


Figure 2.4: Process diagram of the subcritical PTES with low temeprature heat integration

The system is shown in Figure 2.4. It is very similar to the one analyzed in the present thesis, which will be described in detail in the next chapter. The working fluid is evaporated by adding low temperature thermal energy in a heat exchanger (from 1 to 2). Excess electrical energy is used to compress the fluid (from 2 to 3). Afterward there is the thermal energy storage system: firstly, the working fluid is condensated (latent heat storage, from 3 to 4) and then the saturated liquid is aftercooled, whereby the sensible heat is transferred to a pressurized water thermocline storage (from 4 to 5). Before entering the evaporator, the fluid in laminated till the evaporation pressure.

Regarding the discharge cycle, after compression to evaporation pressure (from 6 to 7), the working fluid is preheated to saturation state using the thermal energy from the sensible heat storage (from 7 to 8). The evaporation takes place in the latent heat storage (from 8 to 9) and the thermal energy is converted back to electrical energy by an expander, driving a generator (from 9 to 10). The working fluid is liquefied in a condenser (from 10

to 6).

In this ORC-CHEST the working fluid is initially chosen according to its saturation bell.

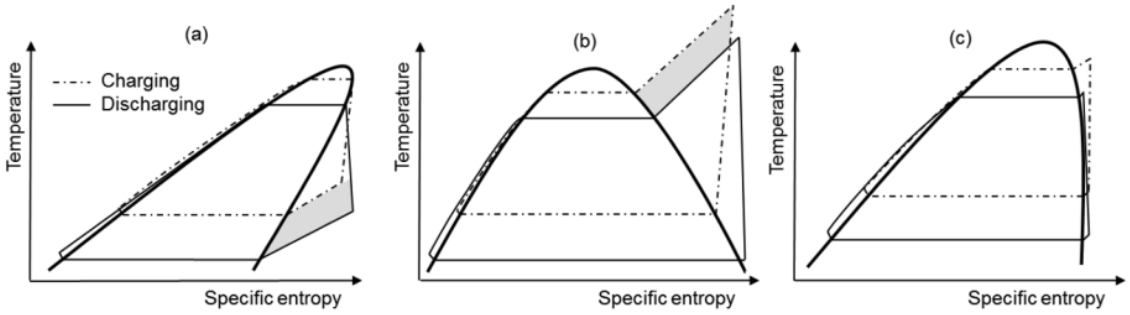


Figure 2.5: saturation bells for (a) retrograde (dry) fluid, (b) anterograde (wet) fluid, (c) isentropic fluid

In fact, looking at the saturation bells shown in Figure 2.5, it can be seen that a dry fluid (cycle a) requires additional thermal energy storage, represented by the shaded area, for vapor preheating before entering the compressor and cooling to the saturation temperature after the expander to avoid a mismatch between charging and discharging half cycles. A wet fluid would require an additional sensible heat storage to cool down the vapor at the compressor outlet as well as superheating the vapor before entering the expander. A fluid with an isentropic saturation line allows for minimizing the mismatch between the charging and discharging cycles.

These considerations on the working fluid are always necessary when the thermal storage is latent or sensible. The thermodynamic mismatch between the charging and discharging cycles is not a problem when the storage is thermochemical. In fact, as explained in the following chapters, in this thesis some working fluids have been selected regardless of the shape of their saturation bell.

The authors of [35] concluded that the ORC-CHEST system, with butene as working fluid, can provide an exergetic efficiency of 0.59 when a heat source temperature of 100°C is available. Most exergy losses occur in storage.

Staub et al. [36] proposed a storage system illustrated in Figure 2.6, powered by energy from a geothermal plant.

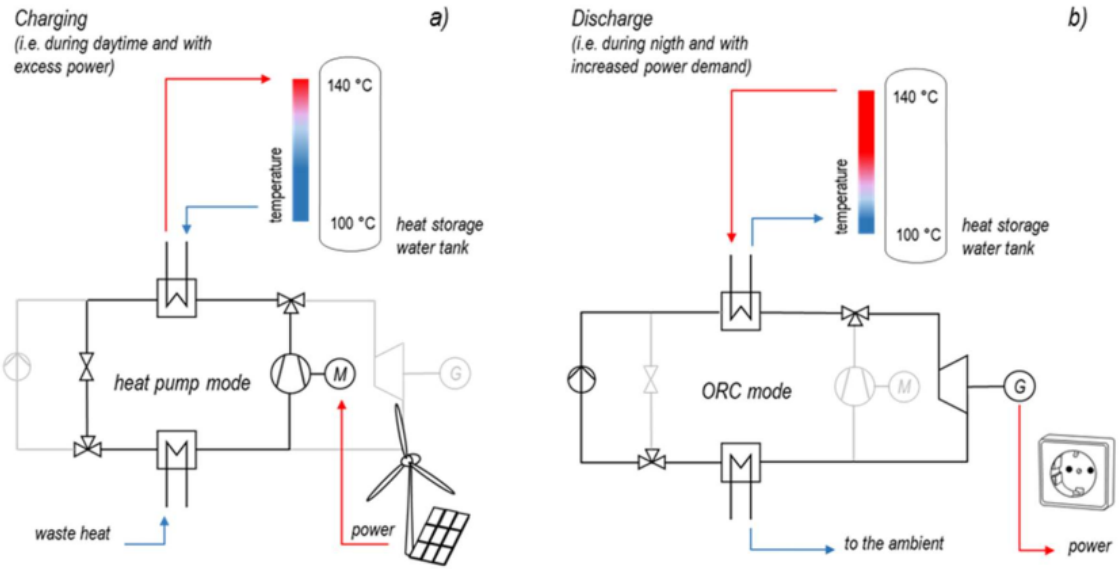


Figure 2.6: Reversible heat pump-organic Rankine cycle storage system during charging (a) and discharging (b)

The main advantage of this concept is that the process requires just one single apparatus. Most components of a heat pump can serve as components for an Organic Rankine Cycle. In particular the costly heat exchangers can comprise both, the condenser and the evaporator in the heat pump as well as in ORC mode. Even the compressor of the heat pump can be used as expander of the Rankine cycle. The components are commercially available or easily adoptable according to the proposed cycle, especially for small-scale systems in the range below 100 kW. Therefore, a strong point of this plant is the easy realization in technical-economic terms.

They consider a temperature of the waste heat source of 90°C, and the chosen working fluid was R365mfc, widely used for heat pump applications.

The negative point concerns the RTE results: it is lower than 50%, limited by the application of commercially available heat pump components in this power range.

For short-term storage, the system will compete with more efficient battery systems. They conclude that for a more promising prospect, larger applications (with turbines and centrifugal or axial compressors) would be better. With an isentropic efficiency of the turbomachinery above 80%, the RTE would be greater than 70%.

Steger et al. [37] studied a reversible heat pump-organic Rankine cycle system, depicted in the following figure.

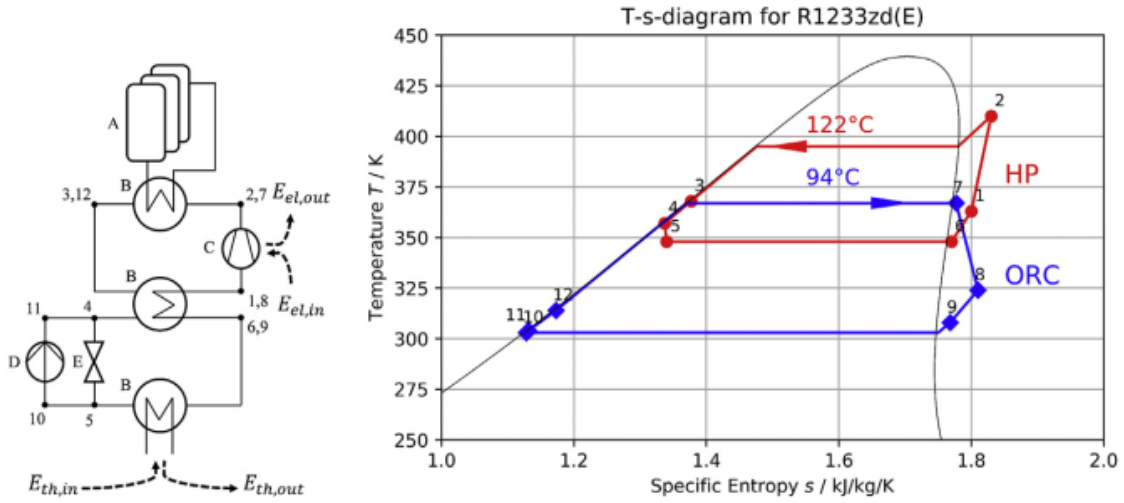


(a) Flow scheme of the reversible HP- (b) T-s-diagram of the heat pump (dots, red) and organic Rankine cycle (diamonds, ORC concept with A: storage, B: heat blue) for R1233zd(E)
exchanger, C: reversible machine, D:
ORC pump, E: HP expansion valve

Figure 2.7: Concept of reversible HP-ORC

In their system, in heat pump mode the condensation takes place at 125°C and the evaporation at 85°C. In ORC mode the condensation takes place at 30°C and the evaporation at 95°C. Since the system uses the same components (and therefore the same turbomachinery) the pressure ratio is a fundamental parameter. Therefore, among various fluids initially selected, they conclude that the R1233ZD(E) is a good solution for the pilot plant setup (also considering the low GWP and the other good fluid properties).

Frate et al. [38], after a bibliographic review of Pumped Thermal Energy Storage (PTES), proposed a thermal integrated system to achieve a round trip efficiency higher than 0.6, which was the value that they demonstrate to be the limit.

In the previously studied configurations, the heat pump takes the heat at the same temperature at which the heat exchanger gives it back. They proposed a system that takes advantage of a suitable heat source, in order to enable the heat pump to absorb the heat at temperatures higher than those at which it is discharged. They found that, by means of reducing the operational $\Delta T$ of the heat pump, it enhances the round-trip efficiency of the storage system.

They studied a number of heat source temperatures in the range from 80°C to 110°C and they simulated the performance of the system for several working fluids. R1233zd(E) was the most promising, since such fluid showed a maximum round-trip efficiency equal to 1.3

when the heat source temperature was 110 °C.

Abarr et al.[39] proposed a Pumped Thermal Energy Storage and Bottoming System (Bot-PTES). After having presented the new concept [40], described some of the design decisions, described the modeling approach and validated the key components of the model, analyzed the Bot-PTES system as an addiction to a natural gas peaker plant.

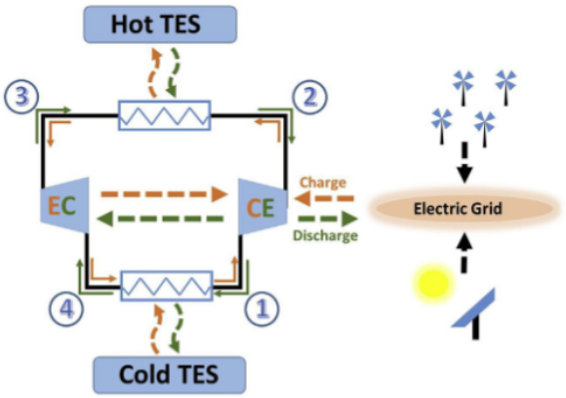


Figure 2.8: PTES system

Connecting the Bot-PTES system to a natural gas peaker plant allows the Bot-PTES system to harvest heat leaving the peaker plant that would otherwise be wasted. The Bot-PTES could then be used as a utility-scale energy storage system for the hours of the day when the peaker plant is not running, including times when excess power from solar or wind is available.

The working fluid used is ammonia. The obtained round-trip-efficiency in nominal conditions is 52.3%. The Bot-PTES system as a stand-alone energy storage system is less efficient when compared to other state-of-the-art technologies. The fundamental advantage of the Bot-PTES system is that it can operate more hours per day (high capacity factor) compared to other energy storage systems, which in turn leads to more revenue generation on the capital investment.

Manente et al. [41] proposed a system named 'integrated ORC-TSHT', composed by the combination of a heat-to-power conversion unit, namely a subcritical ORC, and a heat transformation unit, namely a two-salt solid–gas sorption heat transformer. The aim of the system is the power production and heat upgrade by the thermochemical heat transformer. The two sections interact by means of the cascaded utilization of the heat source and the transport of the upgraded heat from the TSHT to the ORC, as depicted in Figure 2.9.

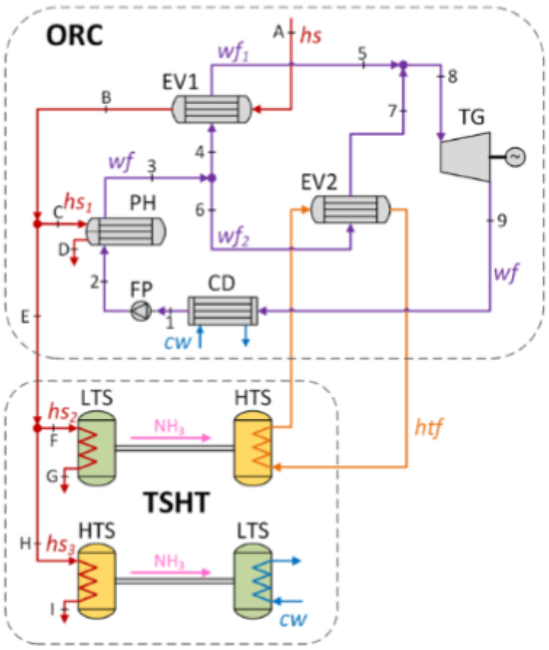


Figure 2.9: Layout of the novel integrated ORC-TSHT system for power production proposed by Manente et al. [41]

The results demonstrate that the proposed system achieves performances that surpass traditional waste heat-to-power solutions in terms of power output, exergetic efficiency and heat utilization. The heat source inlet temperatures is assumed to be 120°C. So, the combination of ORCs with a thermochemical reactor can offer performance and efficiencies exceeding those of conventional, stand-alone ORC systems. The involved fluids was R134a and R245fa.

The various thermal storage systems presented in recent years in the literature show good results, which can be improved in the future. The utilization of a thermochemical energy storage system coupled to an heat pump and an organic Rankine cycle has not yet been studied in detail.

The table on the following page collects some of the thermal storage systems analyzed in the literature. It should be noted that only systems based on an ORC power cycle are listed. Moreover, only the papers whose figure of merit is the round-trip-efficiency were selected. Some of the parameters listed, as the mid temperature heat source, the efficiencies of the machines and the investigated fluids, will be taken into consideration in the next chapter, in which the model used in this thesis and all the hypotheses made will be described.

| Reference | HP electrical input | Mid T heat source | Power | Storage type | Machines efficiencies | Investigated fluids | Figure of merit |
|---|---|---|---|---|---|---|---|
| Dumont, Lemort [42] | renewable generic | Waste Heat 30-100 °C | 4 kW | Latent | $\eta_{is,turb} = 0.75$ $\eta_{is,pump} = 0.50$ | R1233zd(e) R1234yf R245fa R11 | RTE |
| Hencoz, Buchter, et al. [43] | solar PV | - | 50 MW | Latent | $\eta_{is,compr} = 0.80$ $\eta_{is,turb} = 0.90$ $\eta_{is,pump} = 0.85$ | ammonia | RTE |
| Jockenhofer, Steinmann [35][44] | renewable generic | 100 °C | - | Latent and Sensible | $\eta_{is,compr} = 0.80$ $\eta_{is,turb} = 0.88$ $\eta_{is,pump} = 0.80$ | butene | RTE, entropy |
| Staub et al. [36] | geothermal | 90°C | small scale | Latent and Sensible | $\eta_{iscompr} = 0.70$ $\eta_{is,turb}0.70$ | R265mfc | RTE |
| Steger et al. [37] | renewable generic | 90°C | small scale | Sensible | - | Cyclopen R365mfc R1233ZD(E) R123 Novec649 | RTE |
| Frate et al. [38] | renewable generic | 80-110°C | - | Latent and Sensible | $\eta_{is,compr} = 0.80$ $\eta_{is,turb} = 0.80$ | R1233zd(E) R1234ze(Z) Ammonia | RTE |
| Eppinger et al. [34] | renewable generic | 110 °C | - | Latent/ Sensible | $\eta_{is,compr} = 0.07$ $\eta_{is,turb}0.70$ $\eta_{is,pump} = 0.80$ $\eta_{storage} = 1$ | Figure 2.1 | RTE |

Table 2.1: Characteristics of some plants analyzed in the bibliographic review

# 3 | Model description

This chapter explains in detail the system analyzed and the calculation method used. The assumptions adopted for the simulations and the main elements present in the structure of the codes are analyzed. The simulations are carried out in MATLAB, and all the properties of the fluids necessary for the simulations, are provided by REFPROP.

## 3.1. Plant Layout

To have an indication of the plant layout of the analyzed system, one can refer to Figure 3.1, in which the charging phase is shown.

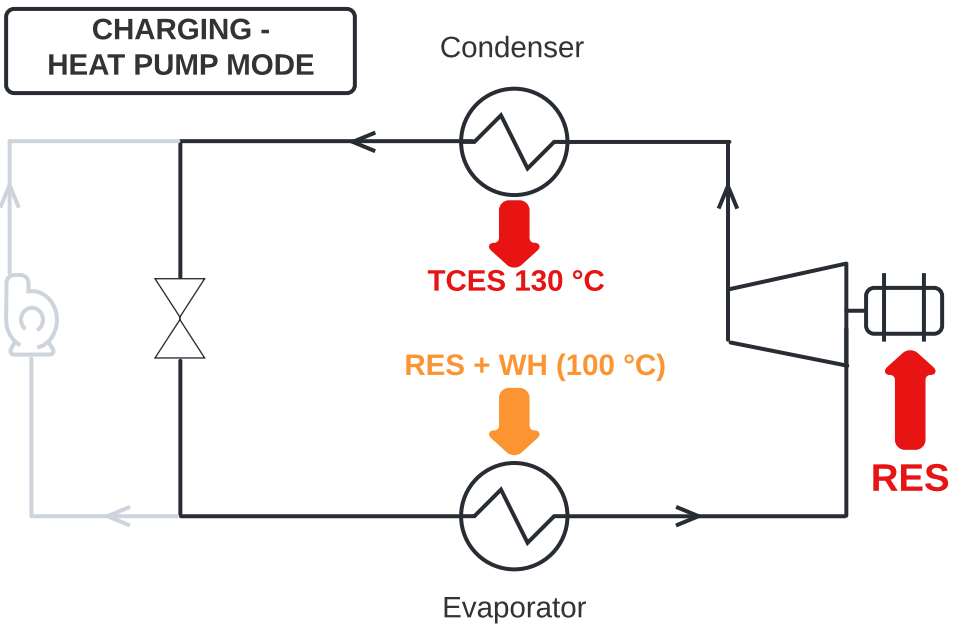


Figure 3.1: Plant configuration, Heat Pump mode

A low temperature heat source, that could be a renewable energy source (RES) or an industrial waste heat source (WH) introduces energy into the cycle, causing evaporation of the working fluid. Then, the fluid is compressed and finally condensed. The condensation heat released is used into the chemical reactor to make the endothermic reaction take place.

The benefit of a suitable heat pump coupled to a low temperature heat source is that it can upgrade that heat to a higher temperature. This is achieved by consumption of electricity.

When it is necessary to carry out the inverse reaction, the products of the reaction carried out previously, are made to react, releasing heat. This heat is introduced into the discharge cycle (Power Cycle), and serves to evaporate the working fluid. Figure 3.2 shows this cycle.

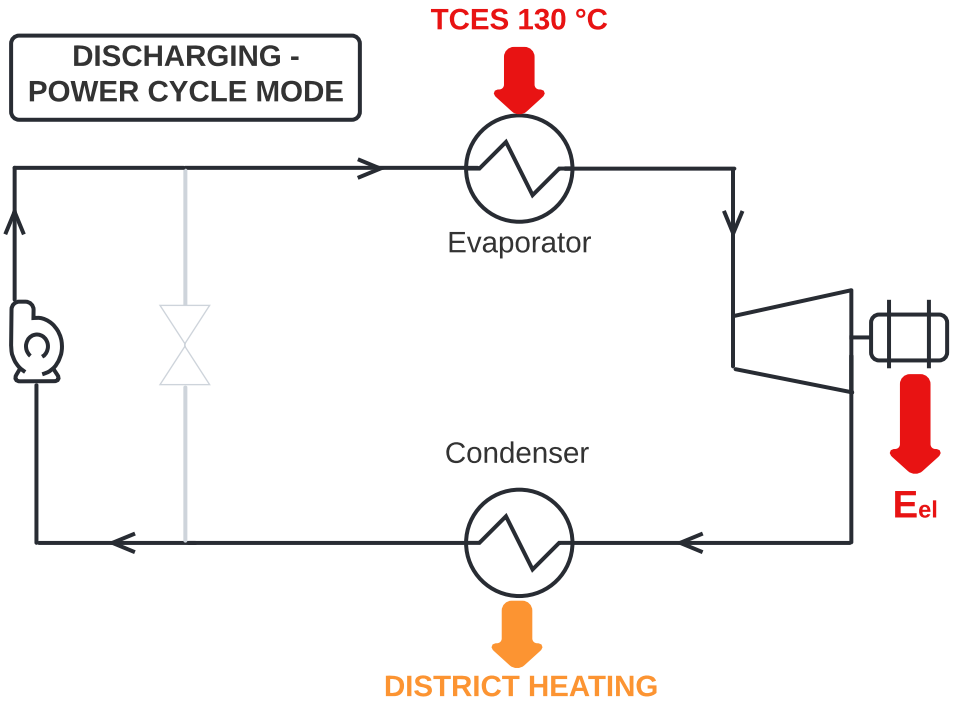


Figure 3.2: Plant configuration, Power Cycle mode

The fluid is then expanded in a turbine, generating electricity, and then condensed. Condensation heat is used to heat the fluid (water) of a district heating system.

This is the basic configuration examined in this thesis, where the district heating water

is heated exclusively by the heat released by the discharge cycle. A further configuration that will be analyzed in this thesis consist consists of thermal integration of the medium temperature heat source: there are cases where the source is available throughout the year, and therefore it is used not only to feed the charging cycle, but also to contribute to the heating of the district heating water.

In figure 3.6 the two thermodynamic are depicted.

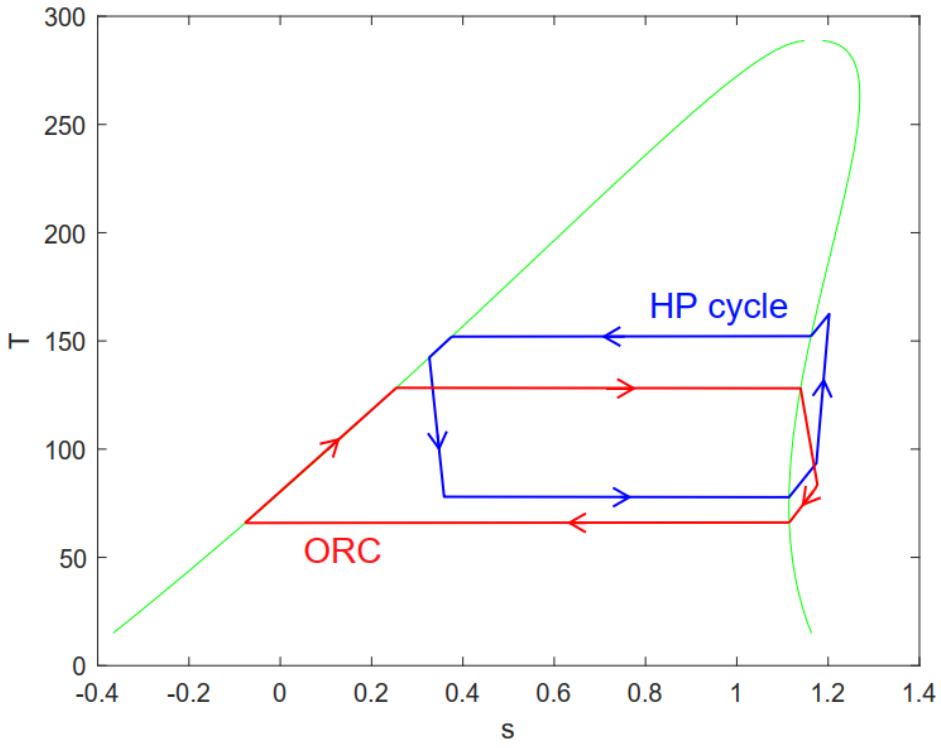


Figure 3.3: T-s diagram of the two cycles

## 3.2. Model assumptions

The purpose of this thesis is to identify the optimum working fluid in the various analyzed configurations. The parameter of merit that will be mainly considered is the round-trip-efficiency (RTE) of the system. Another important aspect for this system concerns the areas of the heat exchangers: in this thesis there is no economic analysis, but the area of the exchangers will be taken into account for the choice of the best working fluid.

The RTE is computed according to the following equation:

$$\eta_{roundtrip} = COP_{HP} * \eta_{TCS} * \eta_{PC} \tag{3.1}$$

### 3.2.1. Termochemical Energy Storage

According to Equation 3.1 The influence of the thermochemical energy storage on the performance of the system is related to its efficiency, defined ad the ratio between the thermal energy input and the thermal energy output during a complete charge and discharge cycle.

The thermochemical energy storage has also a strong influence on the performance of the heat pump and of the power cycle. Since the energy input is stored as chemical energy, it is possible to store the reactants at ambient temperature, therefore the system does not lose any energy from the charge to the discharge cycle.

Hence, thermochemical energy storage has an efficiency equal to one.

### 3.2.2. Turbomachinery

The RTE strongly depends on the performance of the adopted equipment.

The values used in all the simulations carried out in this thesis are adopted in many studies investigating storage systems similar to the one considered here.

A more detailed analysis should investigate deeper the fluid dynamic of the processes involved, in order to find more reliable values for the efficiencies of the components. However, the values adopted are not expected to differ significantly.

The values of the turbine and the compressor isentropic efficiency are supposed to be adequate only if the components work inside the superheated vapor region, where no liquid phase is present. Therefore, the cases involving a transformation inside the saturation dome will not be considered, because there would be a strong reduction of the efficiencies

and would require different turbomachinery blades, adept to resist to the liquid droplets and to remove them.

Hence, in all the investigated cases, the heat pump cycle and the power cycle are always programmed to have the expansion and the compression process outside the saturation bell, in the superheated vapor region.

In the following table the efficiency values used are listed.

| | Turbine | Compressor | Pumps |
|---|---|---|---|
| Isentropic efficiencies | 88 % | 80 % | 80 % |
| Mechanical efficiencies | 99 % | 99 % | 98 % |

Table 3.1: Turbine, compressor and pump efficiencies assumptions

### 3.2.3. Heat Exchangers

Also the heat exchangers have a strong influence on the roundtrip efficiency of the system. The parameters which can strongly affect the performance and the cost of the system are the pinch point temperature difference, the global heat transfer coefficient and the pressure losses occurring inside the component.

As regard the pinch point temperature differences, they are not superimposed. As regards the global heat transfer coefficients, they are calculated both in the charging cycle and in the discharging cycle. This parameter depends primarily on the internal and external heat transfer coefficients, on the internal and external fouling factor and on a geometrical term. This is shown in the following relation.

$$U = f(h_{int}, h_{ext}, C_{int}^{fouling}, C_{ext}^{fouling}, AreaRatio) \tag{3.2}$$

$$U = (\frac{1}{h_{int}\frac{A_{int,pt}}{A_{ext,pt}}} + \frac{1}{h_{ext}\frac{A_{ext,TOT}}{A_{ext,pt}}} + \frac{R_{f,int}}{\frac{A_{int,pt}}{A_{ext,pt}}} + \frac{R_{f,ext}}{\frac{A_{ext,TOT}}{A_{ext,pt}}})^{-1}[\frac{W}{m^2K}] \tag{3.3}$$

The terms $R_{f,ext}$ and $R_{f,ext}$ are the fouling resistance coefficients which model the deposit formation during operation and they are evaluated as the average between two cleaning cycles. They are assumed according to realistic values coming from the literature and are reported in 3.2. The same for the area ratios of the heat exchangers [45] [46].

| | |
|---|---|
| $\frac{A_{int,pt}}{A_{ext,pt}}$ | 0.87 |
| $\frac{A_{int,pt}}{A_{ext,pt}}$ | 1 |
| $\frac{A_{int,pt}}{A_{ext,pt}}rec$ | 14 |
| $\frac{A_{int,pt}}{A_{ext,pt}}rec$ | 0.87 |
| $R_{f,int,DSH}$ | 0.00018 |
| $R_{f,ext,DSH}$ | 0.0004 |
| $R_{f,int,COND}$ | 0.0002 |
| $R_{f,ext,COND}$ | 0.0004 |
| $R_{f,int,REC}$ | 0.00018 |
| $R_{f,ext,REC}$ | 0.00018 |

Table 3.2: Area ratios and fouling factor assumptions

Regarding the heat transfer coefficient, they are assumed depending on the heat exchanger section [47]. Indeed, the heat transfer depend on the state of the two fluids that are involved in the exchange. In the literature there are detailed studies on these coefficients for each section of each heat exchanger [48] [49].

The assumed values are reported in Table 3.3.

| | $W/(m^2K)$ |
|---|---|
| $h_{i,DSH}$ | 300 |
| $h_{e,DSH}$ | 1000 |
| $h_{i,COND}$ | 2000 |
| $h_{e,COND}$ | 1000 |
| $h_{i,EVA}$ | 2000 |
| $h_{e,EVA}$ | 5000 |
| $h_{i,REC}$ | 600 |
| $h_{e,REC}$ | 1900 |
| $h_{i,ECO}$ | 300 |
| $h_{e,ECO}$ | 1000 |

Table 3.3: Heat transfer coefficients for each heat exchangers sections

The other important parameter regarding heat exchangers are the pressure losses. They could have an appreciable influence on the roundtrip efficiency of the system. in order to get a good estimation of the pressure losses inside a heat exchanger, a computational fluid dynamic simulation would be required. This analysis is beyond the purpose of this project, since it would require the exact knowledge of the geometry of the component. Hence, the losses are assumed. They are summarized in the following equalities.

$$\Delta P_{liquid} = 0.5[bar] \tag{3.4}$$

$$\Delta P_{gas} = 0.02 * P_{inlet} \tag{3.5}$$

Even in a phase change transformation there is a pressure drop. For an ideal phase change process, the pressure and the temperature are constant. Actually, this is not verified because irreversibility and pressure losses are present.

Usually, the losses happening during a phase change process, are not expresses in *bar* or in the form of a percentage of the inlet pressure: they are expressed ad a temperature difference.

The values adopted in the simulations are the following.

$$\Delta T^{HP}_{sat,evaporation} = 0.2 \tag{3.6}$$

$$\Delta T^{HP}_{sat,condensation} = 0.5 \tag{3.7}$$

$$\Delta T^{PC}_{sat,evaporation} = 0.2 \tag{3.8}$$

$$\Delta T^{PC}_{sat,condensation} = 0.5 \tag{3.9}$$

### 3.2.4. Low Temperature Heat Source

The heat source is a low temperature heat source, that could be a waste heat or a low temperature energy source. In this project work, the thermal energy source adopted is supposed to be water (that could be heated up by a solar camp or by exhaust gasses coming from an industrial process) at 100°C. This water is then supposed to lower its temperature down to 80 °C, in order to make the working fluid of the heat pump cycle evaporate.

### 3.2.5. District Heating systems generations

District heating systems are a determining factor in increasing the use of renewable energy. Indeed, it is shown that through modern district heating networks the European energy system could achieve the same reductions in primary energy use and carbon dioxide emissions that would be obtained with the six strategies proposed in the European Commission's report, *EnergyRoadmap*2050 [50].

At present, five generations of district heating networks can be distinguished according to operating temperatures.

The first generation of district heating systems ($1GDH$) used steam as the heat carrier. These systems were first introduced in USA in the 1880s. Today, systems which use steam can be considered an outdated technology, since high steam temperatures generate strong heat losses.

The second generation of systems ($2GDH$)used pressurised hot water as the heat carrier, with supply temperatures mostly over $100^oC$. These systems emerged in the 1930s and dominated until the 1980s, when heat sources from solar, biomass or industrial waste began to be available and the thermal needs of buildings began to decrease.

This led to a third generation of district heating networks ($3GDH$), which also uses pressurized water as a working fluid, but at temperatures between $100^oC$ and $80^oC$. This generation is sometimes referred to as "Scandinavian district heating technology", since

many district heating component manufacturers are Scandinavian. All extensions and all new systems in China, Korea, Europe, USA and Canada use this $3GDH$.

The trend throughout these three generations has been towards lower distribution temperatures and material lean components. Following these identified directions, a fourth generation of district heating technology was developed. The recent fourth generation ($4GDH$) implies a further lowering of supply temperatures (in the range between $30^oC$ and $70^oC$), greater energy efficiency and integration of more renewable sources.

Although 2020-2050 was initially indicated in the literature as the $4GDH$ development period, the growing interest in low-temperature district heating and rapid technological advances in heat pumps have laid the foundation for a further decrease in water temperature in the network. distribution below $30^oC$.

Therefore we refer to a fifth generation o district heating and cooling systems ($5GDHC$). This new generation has conceptual characteristics different from those proposed in the definition of $4GDH$ found in the literature [50].

The strengths of a low supply temperature in the network show several advantages. Firstly, it permits recovering all possible kind of excess heat available in a complete Circular Economy strategy exploiting energy synergies among heat sources and sinks available at a district level [51]. Urban low-grade excess heat can be recovered directly in $5GDHC$ without the need of heat pumps, contrary to what occurs in traditional high-temperature DH systems. Moreover, the fact that the excess heat sources are close to the heat demand avoids the construction of transmission pipelines in outer-city areas. $5GDHC$ networks are bi-directional so that different substations can extract or supply heat simultaneously from the network, providing both heating and cooling services independently from the network temperature. This fact gives to the owner a freedom in operation of the substation equivalent to having an individual heating system.

A 2019 article summarizes 40 fifth generation district heating systems in operation in Europe. Six of these are located in Italy [52]. The average water supply and return temperatures are $20^oC$ and $10^oC$.

## District Heating water temperatures

After a brief description of the different district heating networks, it is explained which generations have been taken into account in this thesis.

A widely used approach to studying district heating systems in Germany, Austria and

Switzerland defines the following four study classes [53]:

- High temperatures district heating, represented by most of the systems currently in use, i.e. those of the third generation.
- Fourth generation district heating with supply temperatures of about $60/70^oC$, in which heat can be supplied directly to heat the rooms and sanitary water.
- Fourth generation district heating with supply temperatures of about $30^oC$, in which the heat cannot be directly supplied for space heating and domestic water: a heat pump is required. A cooling system is required, but the heat produced is transferred directly to the network and can be reused.
- Fifth generation district heating at temperature below $20^oC$ C. They use waste heat available at very low temperatures. This heat cannot be directly supplied for space heating and domestic water: a heat pump is required. The system temperatures are suitable for direct cooling of buildings by means of a heat exchanger.

Taking inspiration from the previous approach and considering that using a $5GDHC$ systems in this discussion would be thermodynamically disadvantageous given the temperatures involved in the system analyzed here, three case studies are distinguished:

1. $3GDHC$. Supply and return temperatures of 90 $^oC$ and 65 $^oC$.
2. $4GDHC - base$. Supply and return temperatures of 65 $^oC$ and 35 $^oC$.
3. $4GDHC - advanced$. Supply and return temperatures of 35 $^oC$ and 20 $^oC$.

### 3.2.6. Working Fluid

Regarding the working fluid, 34 fluids were initially selected from the $REFPROP$ database. $REFPROP$ is a computer program, distributed through the Standard Reference Data program of NIST, that provides thermophysical properties of pure fluids and mixtures over a wide range of fluid conditions including liquid, gas, and supercritical phases [54]. It has proven to be an extremely useful tool used by industry, government, and academia, and it is a primary method for the dissemination of work done by the Thermophysical Properties of Fluids Group.

The first selection of fluids was made on the basis of their thermodynamic characteristics. The ideal working fluid should have suitable critical parameters (temperature and pressure) for the application. The critical temperature should be high enough to permit the condensation in the heat pump cycle at a proper temperature. So, fluids whose critical

temperature is lower than the temperature at which the reaction takes place have been discarded. Furthermore, according to a study concerning the selection of optimal fluids for heat pumps, only those that have a critical pressure below 50 *bar* are considered [55].

In addition to the thermodynamic properties, an ideal fluid must satisfy other characteristics. A suitable fluid should have:

- high availability and affordable specific cost
- contained flammability value
- contained toxicity value
- compatibility with materials
- low pollution rates. Two values must be considered:
  - $ODP$ - Ozone Depletion Potential. It is defined as the ratio of global loss of ozone due to given substances over the global loss of ozone due to the release of the same mass of CFC-11 [56].
  - $GWP$ - Global Warming Potential. It was developed to allow comparisons of the global warming impacts of different gases. It is a measure of how much energy the emissions of 1 ton of a gas will absorb over a given period of time, relative to the emissions of 1 ton of carbon dioxide ($CO2$) [57].

For many years the refrigerating and air-conditioning industry adopted a category of fluids called CFC (chloro-fluoro-carbons), known as "freons". They were ideal for many aspects, like low flammability, low toxicity, low cost and they have also good thermodynamic characteristics, but they have the serious problem of a high ODP. For this reason they were progressively banned and they are not listed in the table.

Subsequently, a new family of refrigerants was developed: the Hydro Fluoro Carbons (HFCs). They have a low ODP value and they are nonflammable, recyclable and non-toxic. HFCs are used worldwide, but modern laws are asking for a GWD much lower than those exhibited by HFCs.

Taking into account environmental acceptability, the necessary high coefficient of performance (COP) and relative high critical point, the only characteristic that may be viewed as relatively unimportant is non-flammability.

Table 3.4 lists the fluids initially selected.

| | Critical temperature $[^oC]$ | Critical pressure $[bar]$ |
|---|---|---|
| BENZENE | 288.87 | 49.1 |
| RE347MCC | 164.55 | 24.8 |
| C1CC6 | 299.05 | 34.7 |
| C2BUTENE | 162.6 | 42.3 |
| C3CCC6 | 357.65 | 28.6 |
| C11 | 365.65 | 19.9 |
| CYCLOHEXANE | 280 | 40.8 |
| CYCLOPENTANE | 239 | 45.7 |
| D5 | 346 | 11.6 |
| DECANE | 344.55 | 21 |
| DMC | 283.85 | 49.1 |
| HEPTANE | 266.98 | 27.4 |
| HEXANE | 234.67 | 30.3 |
| IHEXANE | 224.55 | 30.4 |
| IOCTANE | 270.85 | 25.7 |
| IPENTANE | 187.20 | 33.8 |
| MD2M | 326.25 | 12.3 |
| MDM | 290.94 | 14.2 |
| MM | 245.6 | 19.4 |
| MXYLENE | 343.74 | 35.3 |
| NEO-PENTANE | 160.59 | 32 |
| NONANE | 321.40 | 22.8 |
| NOVEC649 | 168.66 | 18.7 |
| OCTANE | 296.17 | 25 |
| OXYLENE | 357.109 | 37.4 |
| PENTANE | 196.55 | 33.7 |
| PXYLENE | 343.018 | 35.3 |
| R123 | 183.681 | 36.6 |
| R245CA | 174.42 | 39.4 |
| RE245FA2 | 171.73 | 34.3 |
| R365MFC | 186.85 | 32.7 |
| R1233ZD | 165.6 | 36.2 |
| T2BUTENE | 155.46 | 40.3 |
| TOLUENE | 318.6 | 41.3 |

Table 3.4: List of fluids initially selected

## 3.3. Model Description

This section describes the MATLAB code created to simulate the various configurations analyzed in this thesis.

First of all, the functioning of the code is described in general, giving an overview of the inputs, the variables subject to sensitivity analysis and the outputs. Subsequently, the simulation of the charging cycle is explained: starting from the analysis of the compression of the fluid, all the other thermodynamic points are calculated. Eventually, the discharging cycle is analyzed.

### 3.3.1. General description of the code

First of all, the charging cycle (heat pump cycle) is simulated. The required parameters for the simulation are:

- fixed assumptions
- working fluid
- compressor inlet and outlet temperatures
- temperature of the heat source

The last three terms (represented inside red blocks in the diagram in Figure 3.4) are the variable parameters on which we act to calculate the optimal performances of the system.

Knowing these parameters, the charging cycle is calculated. The areas of the heat exchangers of the cycle are obtained. They represent an input for the power cycle, which is simulated in order to keep these values constant.

The discharge cycle (power cycle) calculation requires as inputs the district heating water temperatures and, in the percentage in which it is present, the temperature of the heat source.

Among the outputs obtained, the electrical power of the cycle is used to calculate the RTE of the system. The equation for the calculation of the RTE is the following:

$$RTE = \frac{P_{PC}}{P_{compr,HP}} \tag{3.10}$$

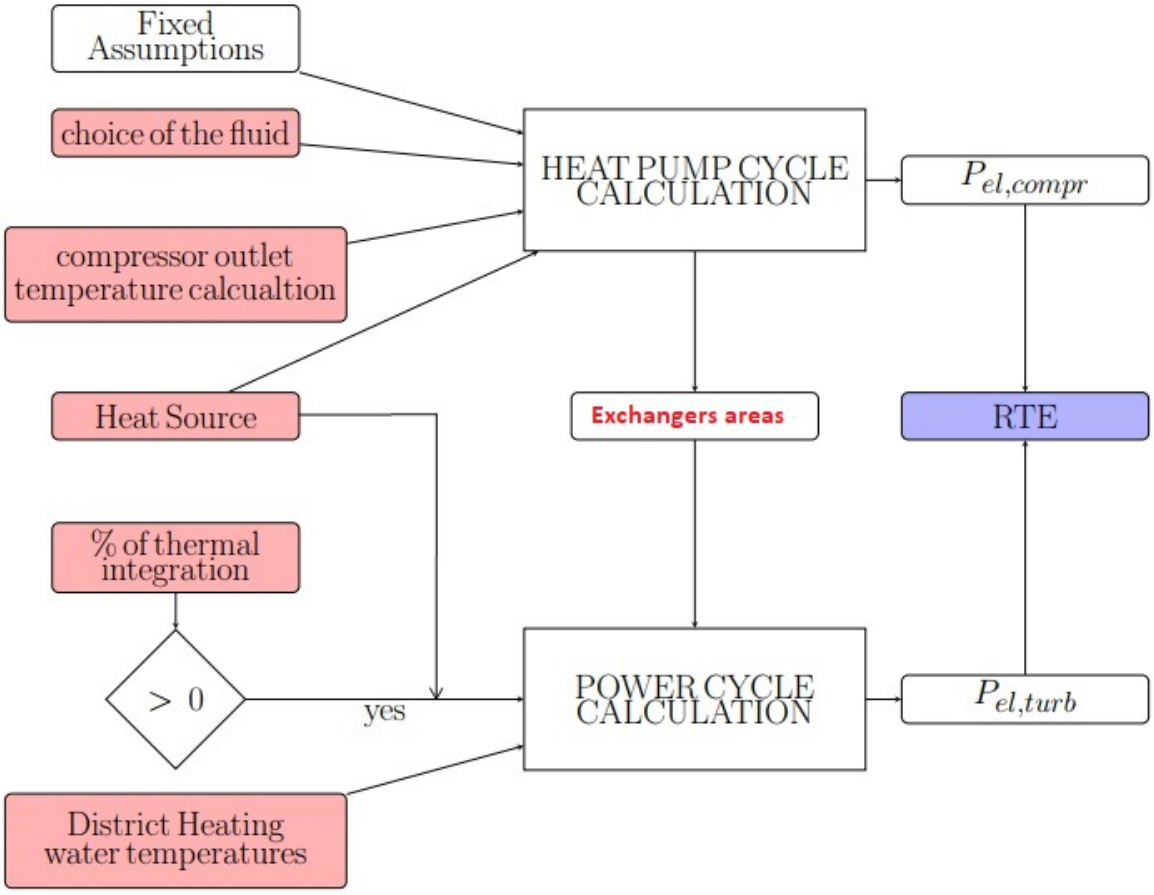


Figure 3.4: General conceptual scheme

Therefore, the final result is the RTE. Running the code for each fluid, and for each generation of district heating system, a classification of the best fluids is obtained.

### 3.3.2. Plant Configuration

Here the thermodynamic path of the working fluid in the two cycles is shown.

Figure 3.5 shows the thermodynamic points during the heat pump mode.

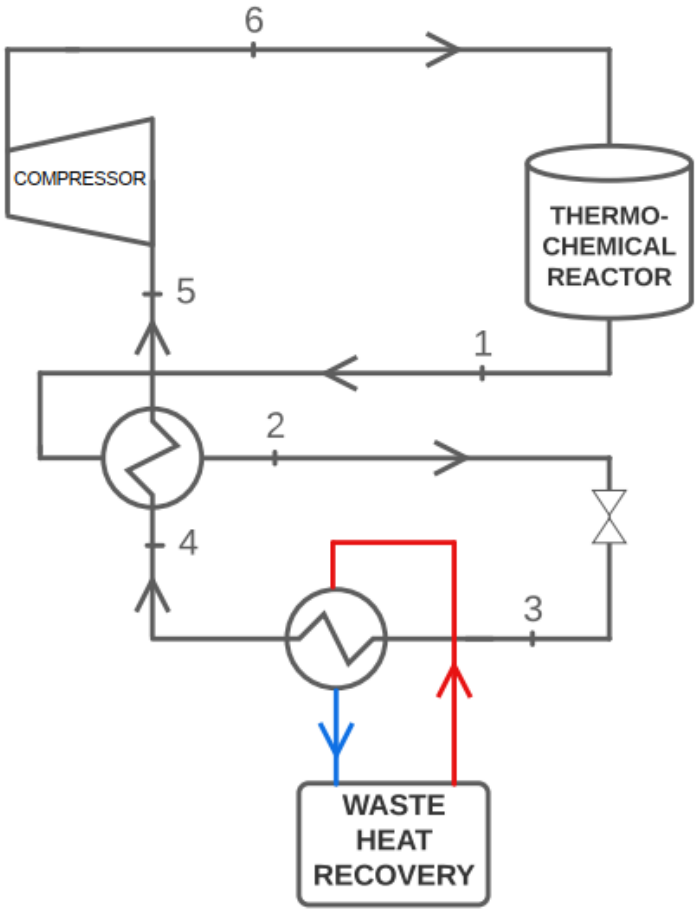


Figure 3.5: Charging Cycle scheme

The low temperature heat source (indicated as waste heat recovery in Figure 3.5) introduces energy into the cycle, evaporating the working fluid (from 3 to 4). The fluid is then preheated in the recuperator up to point 5 and enters the compressor. At the outlet of the turbomachine, point 6, the fluid at high temperature and pressure is condensed to release the heat necessary for the chemical reaction to take place. Finally, the condensed fluid (point 1) is cooled down to point 2 in the recuperator and finally laminated to close the cycle.

The two thermodynamic cycles are shown in Figure 3.6.

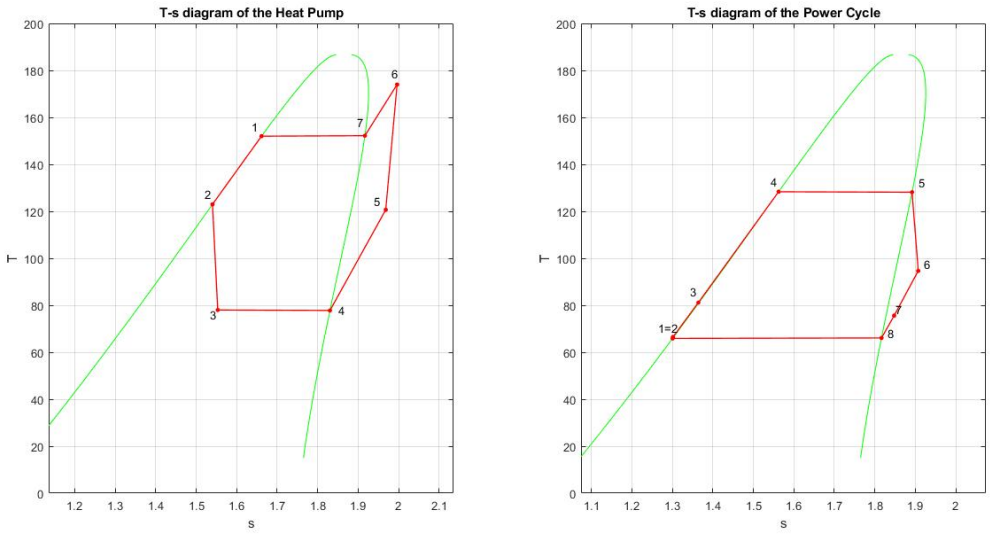


Figure 3.6: T-s diagram

When switching to power cycle operation, the reverse exothermic reaction occurs inside the reactor. Thanks to the energy released in the reactor, the preheated liquid fluid (point 3 in Figure 3.7) is evaporated up to point 5 (point 4 is the thermodynamic point at which the economization ends and the evaporation begin, as shown in Figure 3.6).

The working fluid is then expanded till point 6, producing electric power. Then, the recuperator cools the fluid up point 7. Afterwards, the fluid is firstly desuperheated and then condensed, releasing heat useful for heating the district heating water. The cycle closes with the compression of the liquid fluid (from 1 to 2) and its preheating.

Figure 3.7 shows the thermodynamic path of the working fluid during the power cycle operation of the system.

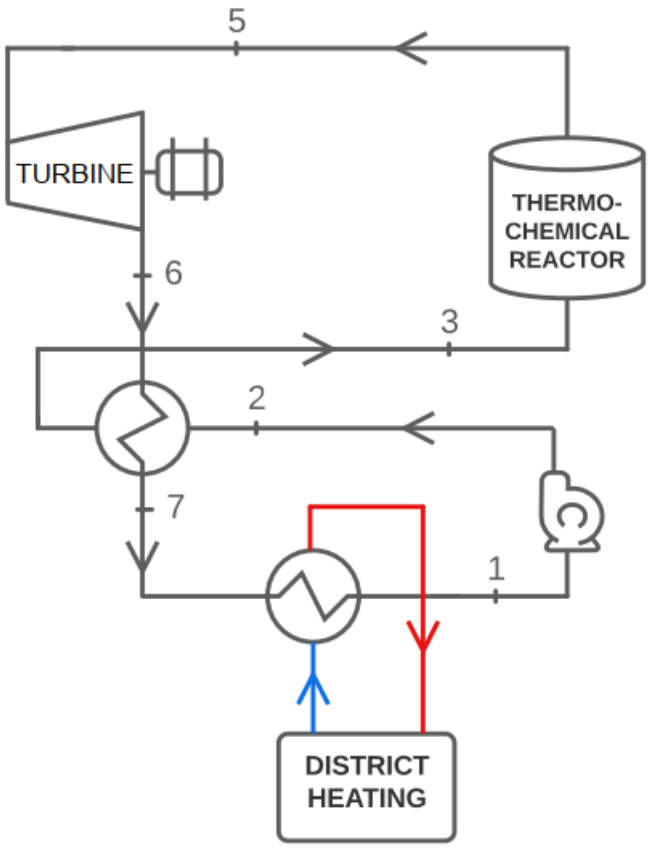


Figure 3.7: Power Cycle scheme

## 3.4. Heat Pump Cycle simulation

The performance of the cycle is analyzed as the inlet and outlet temperatures of the compressor in the charging cycle vary. Therefore, the first step is to calculate the minimum and maximum inlet and outlet temperatures at which compression can take place for each fluid analyzed.

Figure 3.8 illustrates the conceptual scheme used.

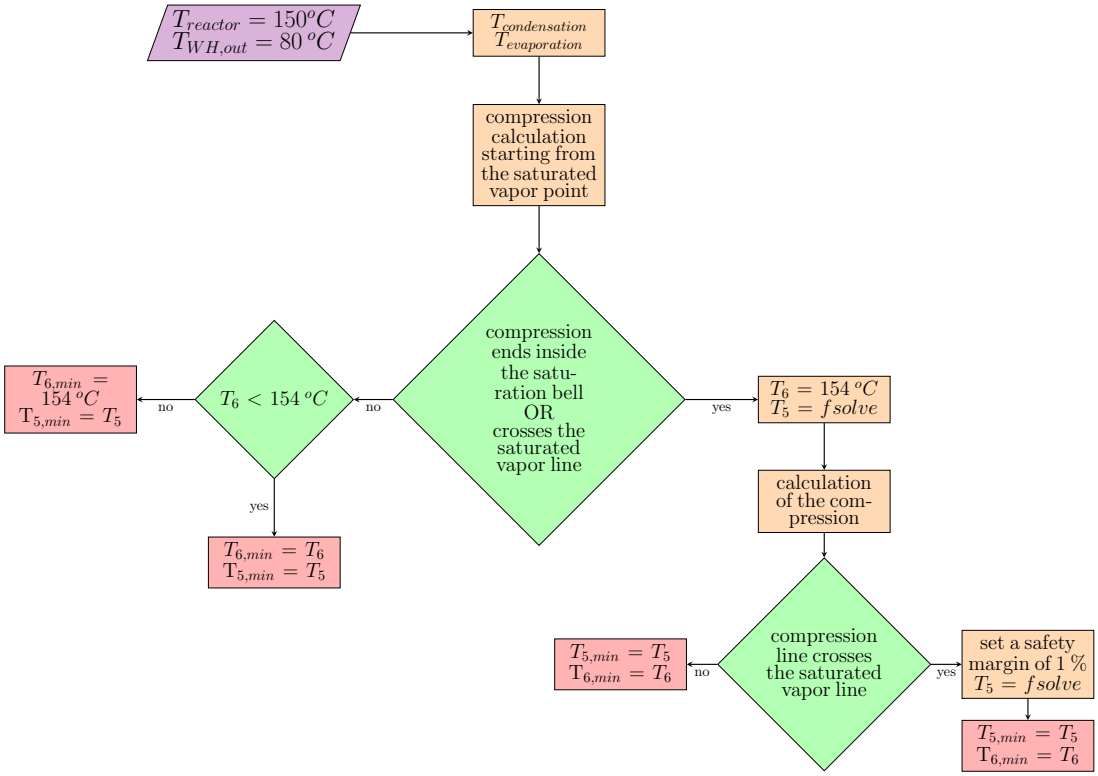


Figure 3.8: Calculation of $T_{5,min}$ and $T_{6,min}$

Starting from the knowledge of the temperature at which the reaction takes place ($T_{reactor} = 150^oC$) and the temperature up to which the energy source is cooled down ($T_{WH,out} = 80^oC$), the condensation end temperature and the evaporation start temperature are immediately calculated:

$$\begin{aligned} T_1 &= T_{reactor} + \Delta T_{PP,cond} \\ T_3 &= T_{WH,out} - \Delta T_{PP,liq-liq} \end{aligned} \tag{3.11}$$

where $\Delta T_{PP,cond}$ and $\Delta T_{PP,cond}$ are supposed to be equal to 2 °C.

From these temperatures, the condensation start temperature and the evaporation end temperature are calculated, taking into account the losses present during phase changes.

$$\begin{aligned} T_7 &= T_1 + \Delta T_{cond,HP} \\ T_4 &= T_3 - \Delta T_{eva,HP} \end{aligned} \tag{3.12}$$

Regarding the points that lie on the saturation bell, the relative thermodynamic properties are calculated taking advantage of the knowledge of the title. This is done by calling REFPROP:

$$\begin{aligned} [P_1, h_1, s_1, d_1] &= refprop(T_1, Q = 0) \\ [P_4, h_4, s_4, d_4] &= refprop(T_4, Q = 1) \\ [P_7, h_7, s_7, d_7] &= refprop(T_7, Q = 1) \end{aligned} \tag{3.13}$$

At this point, the code calculates the compression starting from the saturated vapor point (point 4). The steps are as follows:

$$\begin{cases} P_6 = P_7 \\ h_{6,is} = refprop(P_6, s_5) \\ h_6 = h_5 + \frac{(h_{6,is} - h_5)}{\eta_{is,compr}} \\ [P_6, s_6, d_6] = refprop(h_6, P_6) \end{cases} \tag{3.14}$$

It was used the definition of compressor isentropic efficiency:

$$\eta^{is}_{compressor} = \frac{h_{out} - h_{in}(T_{in}, s_{in})}{h^{is}_{out}(T_{in}, s_{in}) - h_{in}(T_{in}, s_{in})} \tag{3.15}$$

Based on the complexity of the analyzed fluid, two situations could occur:

- the compression end inside the saturation bell
- the compression end outside the saturation bell but passing through it

These two situations are not accepted, so it must be checked if they occur.

For this reason, a specific function was created. This function takes as input the inlet and outlet points of the compression and returns the minimum distance of the compression line from the saturation bell.

Furthermore, the function indicates if the compression ends inside the bell. Thermodynamically, this situation is described by the following relation:

$$h_6 < h_7 \tag{3.16}$$

As can be seen from the flow chart, if none of these situations occur, the previously obtained compression end point is analyzed.

In order to keep an adequate $\Delta T$ from the temperature at which the reaction occurs, it has been chosen to set the minimum compressor outlet temperature at $154^oC$.

At this point, another control is necessary: if $T_6$ is less than the previously mentioned minimum, $T_6$ is imposed to be equal to this minimum ($154^o$). Knowing the outlet temperature, the inlet one, $T_5$, is then calculated using a MATLAB solver ($fsolve$).

The procedure carried out by the solver is described in Figure 3.9. A first guess of the inlet temperature is assumed. Then, after calculating the inlet pressure, the inlet thermodynamic properties are calculated. Thanks to the definition of the isentropic efficiency of the compressor it is possible to obtain the outlet enthalpy, through which, using REFPROP, the outlet temperature is obtained. The 'fsolve' function repeats these operations until the output temperature calculated corresponds to the imposed temperature.

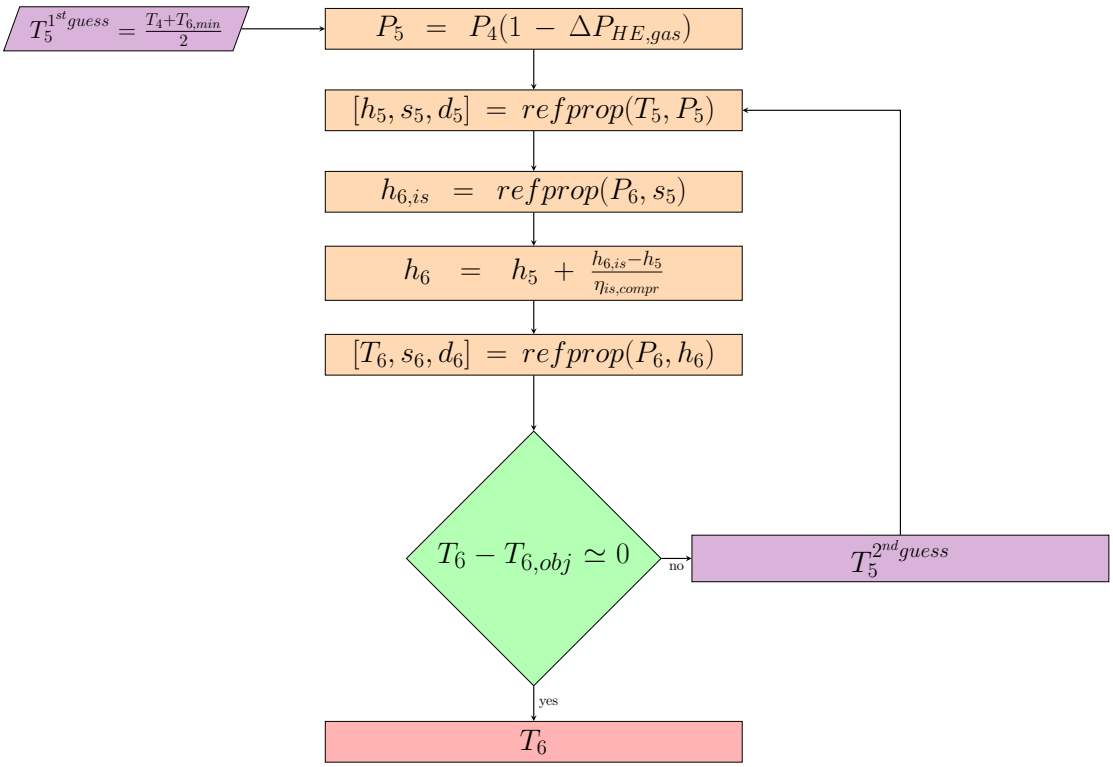


Figure 3.9: Calculation of $T_6$

Returning to the scheme of Figure 3.8, if $T_6$ is higher than the minimum compressor output value imposed, that value represent the minimum outlet temperature. The corresponding $T_5$ is the minimum compressor input value.

After calculating the minimum inlet and outlet temperatures of the compression, the code calculates the maximum temperatures at which the compression can take place.

The conceptual scheme is reported in Figure 3.10.

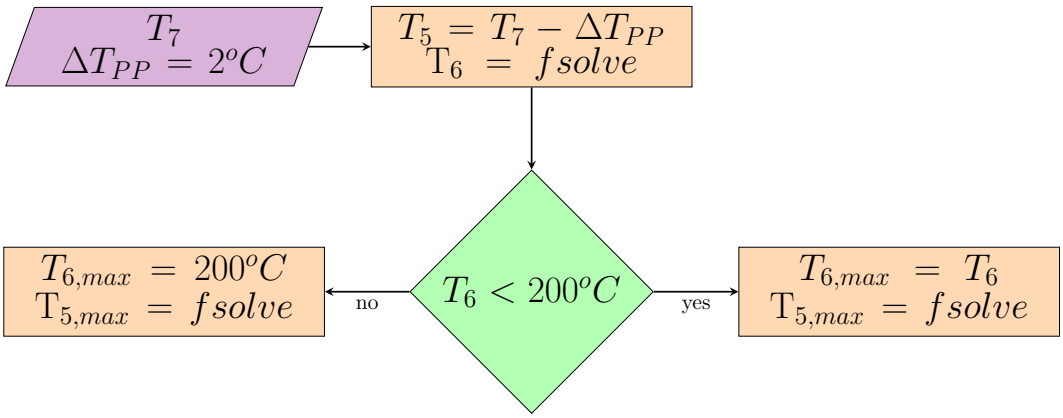


Figure 3.10: Calculation of $T_{5,max}$ and $T_{6,max}$

A maximum inlet temperature, $T_5$, is imposed using a $\Delta T_{PP} = 2^oC$. From this, using the MATLAB solver, the corresponding outlet temperature is calculated.

At this point it is checked whether the temperature value obtained at the outlet is greater or less than the set limit, imposed at $200^oC$. This value is due to the thermodynamic limits of the turbomachinery.

If $T_6$ is less than $200^oC$, the value is acceptable and correspond to the maximum outlet temperature. On the contrary, if $T_6$ exceeds the imposed limit, a $T_{6,max}$ of $200^oC$ is set and the corresponding $T_{5,max}$ is calculated using the solver.

At this point, for each pair of inlet and outlet temperatures, starting from the minimum one, all the other thermodynamic properties of the two points are calculated. This can be made knowing the inlet and outlet pressures, which can be calculated as follow:

$$\begin{cases} P_5 = P_4 * (1 - \Delta P_{HE,gas}) \\ P_6 = P_7 \end{cases} \tag{3.17}$$

Therefore, the thermodynamic properties are calculated as:

$$\begin{aligned}[h_5, s_5, d_5] &= refprop(T_5, P_5) \\ [h_6, s_6, d_6] &= refprop(T_6, P_6)\end{aligned} \tag{3.18}$$

Up to now, the minimum and maximum temperatures of the compressor inlet and outlet have been calculated. The two extremes thermodynamic cycles are represented in Figure 3.14. They refer to the fluid *mxylene*.

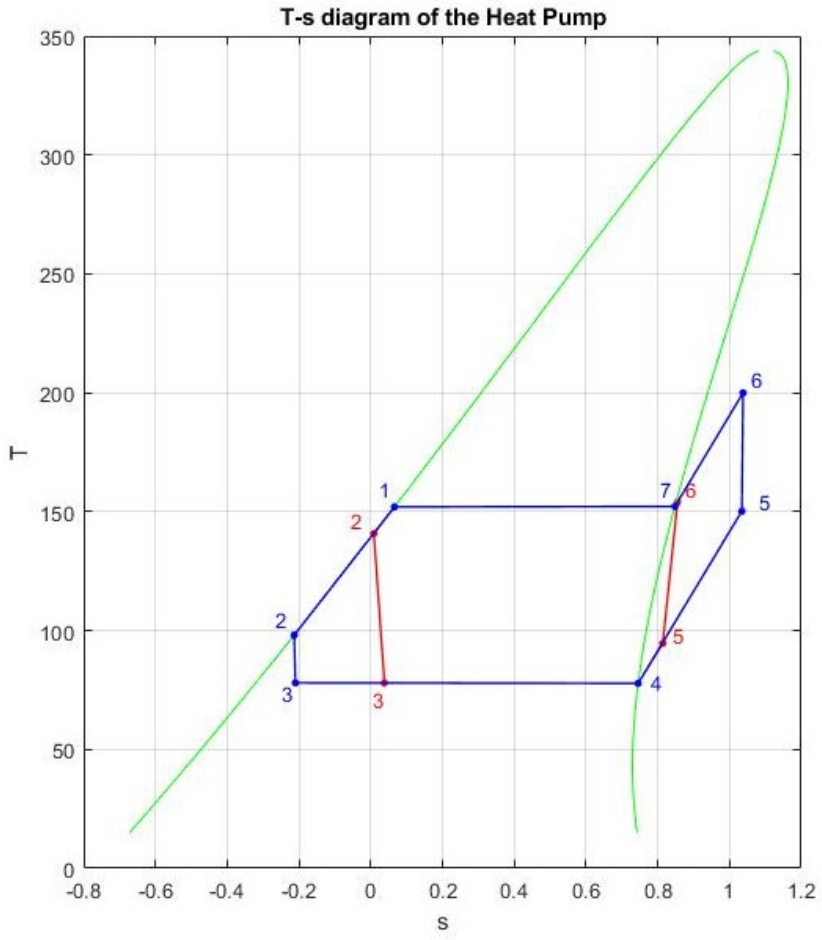


Figure 3.11: Heat Pump $T - s$ diagram

The cycle with the minimum temperatures is represented in red, while the one with the maximum temperatures, in blue.

Through an energy balance at the recuperator, it is now possible to calculate the enthalpy of *point*2, which corresponds to the enthalpy value in *point*3, due to isentalpic lamination:

$$\dot{m}_{HP}(h_1 - h_2) = \dot{m}_{HP}(h_5 - h_4) \tag{3.19}$$

$$h_3 = h_2 \tag{3.20}$$

Having information of all the thermodynamic points of the cycle, it is possible to calculate some parameters of interest. The heat released by the condensation of the charge cycle corresponds to the heat necessary to make the endothermic reaction take place in the reactor. So, through equations 3.21 and 3.22, the flow rate of fluid circulating in the charging cycle is calculated.

$$Q_{reaction} = \dot{m}_{HP} * (h_6 - h_1) \tag{3.21}$$

$$\dot{m}_{HP} = \frac{Q_{reaction}}{h_6 - h_1} \tag{3.22}$$

As for the heat entering the cycle, it is given by the low temperature source. This heat is used to evaporate the working fluid of the charging cycle. Analytically, this is expressed through the following two equations:

$$\dot{Q}_{eva}^{HP} = \dot{Q}_{in,WH} \tag{3.23}$$

$$\dot{m}_{HP} * (h_4 - h_3) = \dot{m}_{water,HP} * 4.2 * (T_{in,WH} - T_{out,WH}) \tag{3.24}$$

From this, one can obtain the requested water flow.

$$\dot{m}_{water,HP} = \frac{\dot{m}_{HP} * (h_4 - h_3)}{4.2 * (T_{in,WH} - T_{out,WH})} \tag{3.25}$$

Going on with the calculation of the parameters of interest, the electrical power absorbed by the compressor is obtained

$$P_{el,compr} = \dot{m}_{HP}(h_6 - h_5) \tag{3.26}$$

The most important parameter for a heat pump cycle is the COP, which can be calculated as follows.

$$COP = \frac{\dot{Q}_{reaction}}{P_{el,compr}} \tag{3.27}$$

### 3.4.1. Areas of the heat exchangers

The code continues with the calculation of the areas of the exchangers. This is done applying the basic overall heat transfer equation for the heat transfer in the heat exchanger:

$$Q = UA\Delta T_{ML} \tag{3.28}$$

where $\Delta T_{ML}$ is the logarithmic mean temperature difference, defined as:

$$\Delta T_{ML} = \frac{\Delta T_A - \Delta T_B}{\ln \frac{\Delta T_A}{\Delta T_B}} \tag{3.29}$$

#### High pressure heat exchanger

The heat exchange that takes place in the high pressure exchanger is shown in the figure below.

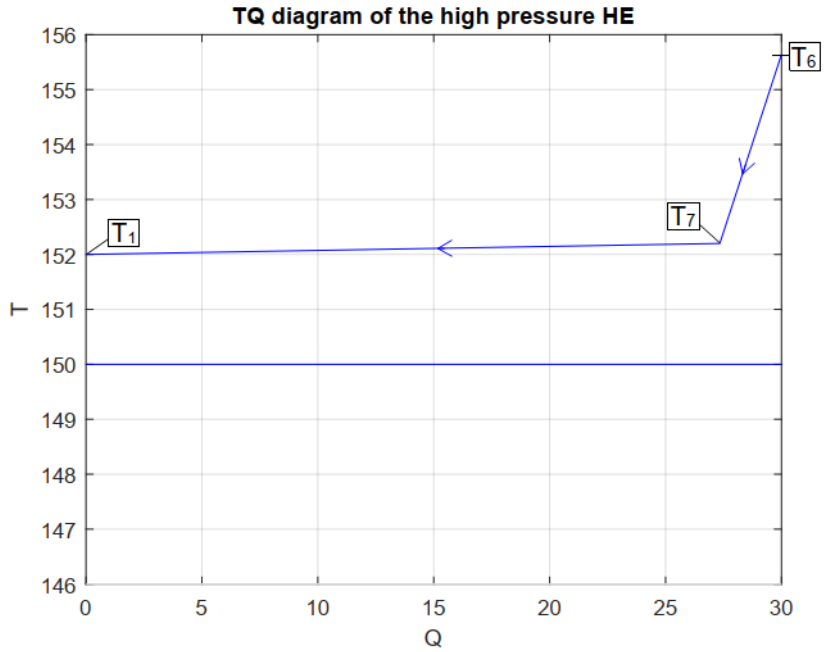


Figure 3.12: $TQ$ diagram of the high pressure heat exchanger

Firstly, the heat exchanged in the condenser and in the desuperheater is calculated.

$$\dot{Q}_{cond}^{HP} = \dot{m}_{HP}(h_7 - h_1) \tag{3.30}$$

$$\dot{Q}_{DSH} = \dot{m}_{HP}(h_6 - h_7) \tag{3.31}$$

Then, the $\Delta T_{ML,cond}$ of the two sections are calculated.

$$\Delta T_{ML,cond} = \frac{(T_7 - T_{reactor}) - (T_1 - T_{reactor})}{\ln \frac{(T_7 - T_{reactor})}{(T_1 - T_{reactor})}} \tag{3.32}$$

$$\Delta T_{ML,DSH} = \frac{(T_6 - T_{reactor}) - (T_7 - T_{reactor})}{\ln \frac{(T_6 - T_{reactor})}{(T_7 - T_{reactor})}} \tag{3.33}$$

Eventually, the $UA$ parameter of the high pressure heat exchanger is obtained:

$$UA_{cond} = \frac{\dot{Q}_{cond}}{\Delta T_{ML,cond}} + \frac{\dot{Q}_{DSH}}{\Delta T_{ML,DSH}} \tag{3.34}$$

At this point it is possible to calculate the overall heat transfer coefficient U, using the relation 3.3 with the assumptions of Table 3.2 and Table 3.3.

Finally, the area of the heat exchanger is calculated.

## Low pressure heat exchanger

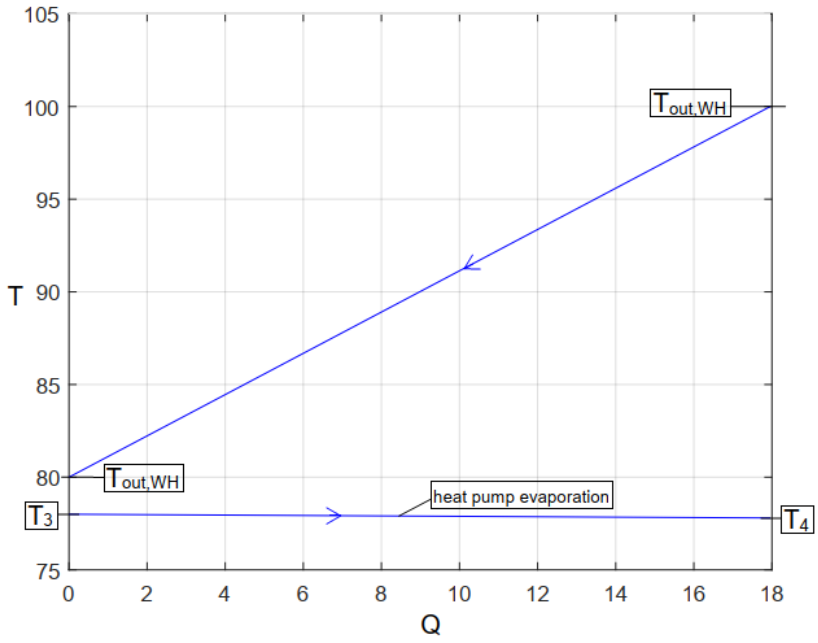


Figure 3.13: $TQ$ diagram of the low pressure heat exchanger

Figure 3.13 shows the $TQ$ diagram of the evaporation of the working fluid. The evaporation heat is calculated according to Equation 3.35.

$$Q_{eva}^{HP} = \dot{m}_{HP}(h_4 - h_3) \tag{3.35}$$

$$\Delta T_{ML,eva} = \frac{(T_{in,WH} - T_4) - (T_{out,WH} - T_3)}{\ln \frac{(T_6 - T_5)}{(T_2 - T_4)}} \tag{3.36}$$

$$UA_{eva}^{HP} = \frac{Q_{EVA}^{HP}}{\Delta T_{ML,eva}^{HP}} \tag{3.37}$$

As for the previous exchanger, at this point the value of U parameter is calculated through relation 3.3, and then the area of the low pressure heat exchanger is obtained.

## Recuperator

In this component, the working fluid at the evaporator outlet (at temperature $T_4$) is preheated up to temperature $T_5$ by cooling the hot fluid exiting the condensation from $T_1$

to $T_2$.

Therefore, the heat exchanged, $\Delta T_{ML,rec}$ and the $UA$ parameter are calculated as follows.

$$Q_{rec}^{HP} = \dot{m}_{HP}(h_1 - h_2) \tag{3.38}$$

$$\Delta T_{ML,rec} = \frac{(T_1 - T_5) - (T_2 - T_4)}{\ln \frac{(T_1 - T_5)}{(T_2 - T_4)}} \tag{3.39}$$

$$UA_{rec}^{HP} = \frac{Q_{rec}^{HP}}{\Delta T_{ML,rec}^{HP}} \tag{3.40}$$

Now it is possible to calculate the value of the global heat transfer coefficient and therefore the area of the recuperator.

## 3.5. Power Cycle Simulation

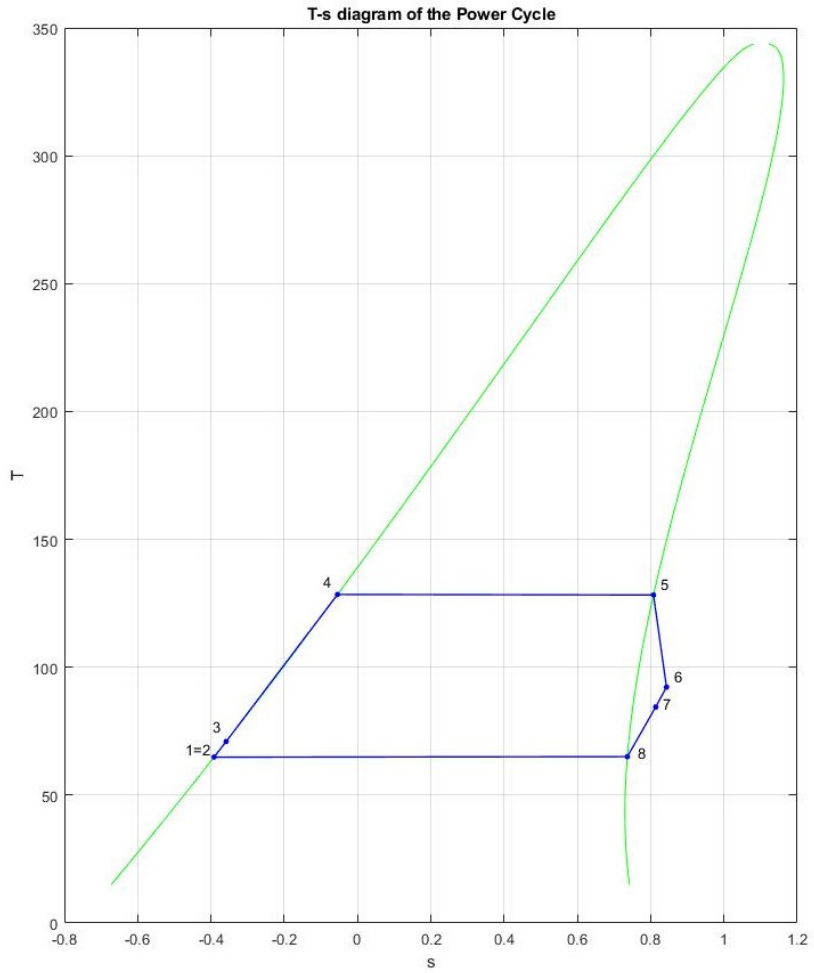


Figure 3.14: Ts diagram of the organic Rankine cycle

Once the charge cycle calculation has been completed, the discharge cycle is analyzed. Considering the configuration in which the low temperature heat source is available during the whole year, there are essentially four unknowns. They are:

- $T_1$ : temperature at the end of the condensation
- $T_4$ : temperature at the begin of the evaporation
- $T_7$ : temperature at the outlet of the recuperator (hot side)
- $T^*$ : intermediate temperature of the district heating water

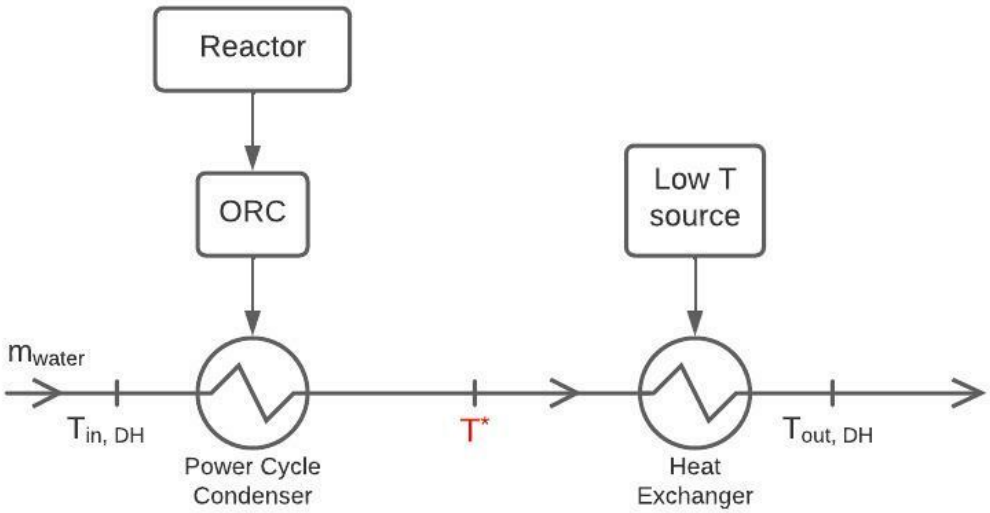


Figure 3.15: Conceptual scheme of the district water heating

Figure 3.15 shows the heat exchanges that the district heating water undergoes. In case the low temperature heat source is available throughout the year, the condensation heat released by the power cycle raises the water temperature from its initial temperature up to $T^*$. Then, the low temperature source finishes the heating of the water up to the target outlet temperature.

The MATLAB function which was developed for the calculation of the discharge cycle assumes four initial guesses for these temperatures, uses them to calculate the thermodynamic points of the cycle and finally calculates the parameters of interest. In particular, as for the charging cycle, the areas of the exchangers are calculated. These must coincide with the areas previously calculated during the charge cycle analysis, since the components are the same.

If the values of the areas of the eschangers do not coincide with those calculated in the charge cycle, the function updates the first attempt values and recalculates the areas of the exchangers. When these coincide with to those of the charge cycle, the function is interrupted and the four temperatures initially assumed are obtained.

This process is shown in Figure 3.19

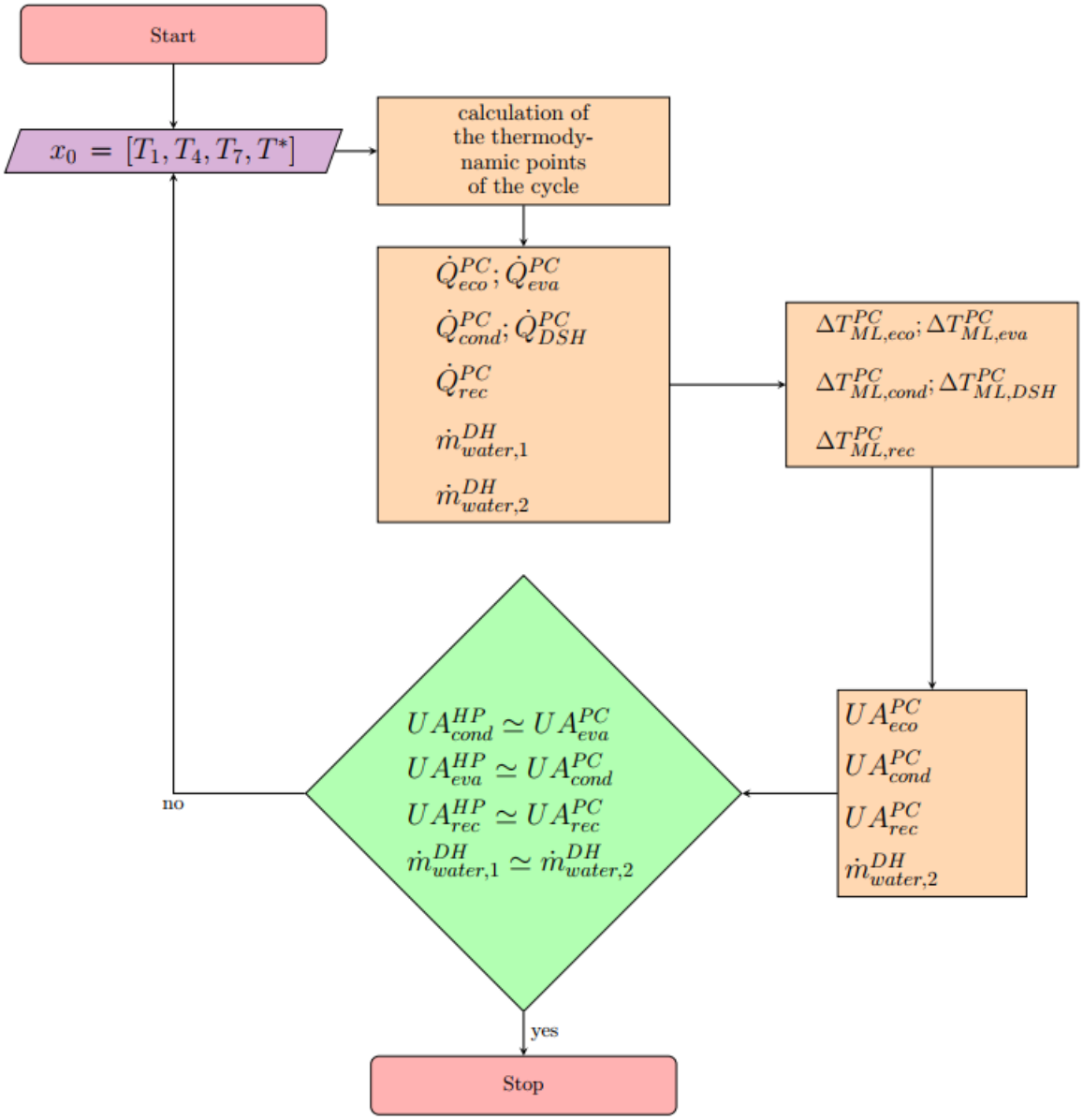


Figure 3.16: Conceptual scheme of the Power Cycle calculation

The first step is to calculate the thermodynamic properties of the points at the end of condensation and at the beginning of evaporation, using the guesses end condensation and start evaporation temperature:

$$\begin{aligned} [P_1, h_1, s_1, d_1] &= refprop(T_1, Q = 0) \\ [P_4, h_4, s_4, d_4] &= refprop(T_4, Q = 0) \end{aligned} \tag{3.41}$$

The temperature at the end of evaporation is obtained through the losses that occur inside

this component.

$$T_5 = T_4 - \Delta T_{eva,PC} \tag{3.42}$$

This temperature is then used to calculate the other thermodynamic properties at that point.

$$[P_5, h_5, s_5, d_5] = refprop(T_5, Q = 1) \tag{3.43}$$

Subsequently, the pressure at the inlet of the economizer (through the losses inside the recuperator, $\Delta P_{HE,gas}$) and the pressure at the inlet of the recuperator itself (through the pressure drop inside the recuperator, liquid side, $\Delta P_{rec,liq}$) are identified.

$$\begin{aligned} P_3 &= P_4 + \Delta P_{HE,gas} \\ P_2 &= P_3 + \Delta P_{rec,liq} \end{aligned} \tag{3.44}$$

Now, using the definition of isentropic efficiency of the pump, it is possible to calculate the temperature of the working fluid at the pump outlet (point 2). The steps are as follows:

$$\begin{cases} h_{2,is} = refprop(P_2, s_1) \\ h_2 = h_1 + \frac{(h_{2,is} - h_1)}{\eta_{is,pump}} \\ [T_2, s_2, d_2] = refprop(P_2, h_2) \end{cases} \tag{3.45}$$

As regards the conditions at the beginning of condensation, they can be calculated as follows:

$$\begin{aligned} T_8 &= T_1 + \Delta T_{cond,PC} \\ [P_8, h_8, s_8, d_8] &= refprop(T_8, Q = 1) \end{aligned} \tag{3.46}$$

Furthermore, the conditions at the inlet of the recuperator (hot side, $point7$) can be calculated using the first guess temperature and knowing that the pressure in that point is equal to the pressure at the start of condensation ($P_7 = P_8$).

$$[h_7, s_7, d_7] = refprop(T_7, P_7) \tag{3.47}$$

From $P_7$, it is possible to calculate the pressure at the end of compression, assuming a $\Delta P_{rec,gas}$:

$$P_6 = \frac{P_7}{1 - \Delta P_{rec,gas}} \tag{3.48}$$

At this point, using the definition of isentropic efficiency of the turbine,the temperature at the outlet of this component is calculated, adopting a procedure similar to that described for the pump:

$$\begin{cases} h_{7,is} = refprop(P_6, s_5) \\ h_6 = h_5 + \frac{(h_5 - h_{7,is})}{\eta_{is,turb}} \\ [T_6, s_6, d_6] = refprop(P_6, h_6) \end{cases} \tag{3.49}$$

As done in the previous section during the charge cycle analysis, through an energy balance at the recuperator, it is now possible to calculate the enthalpy of the fluid at the entrance of the recuperator:

$$h_3 - h_2 = h_6 - h_7 \tag{3.50}$$

Knowing the enthalpy and the pressure of *point*3, the other thermodynamic properties are calculated:

$$[T_3, s_3, d_3] = refprop(P_3, h_3) \tag{3.51}$$

## 3.6. Power Cycle parameters

The heat released by the inverse, exothermic reaction depends on the efficiency of the thermochemical storage, which is linked to the storage time:

$$\dot{Q}_{reaction,charge} = \eta_{storage} \dot{Q}_{reaction,discharge} \tag{3.52}$$

As discussed in Chapter 1, this efficiency can be considered uniform without making major mistakes. In the previous equation, $Q_{reaction,discharge}$ correspond to $\dot{m}_{PC}(h_5 - h_3)$, since the heat supplied by the discharge reaction is used to evaporate the working fluid of the power cycle:

$$\dot{Q}_{reaction,charge} = \dot{m}_{PC}(h_5 - h_3) \tag{3.53}$$

From this one, the mass flow rate of the working fluid of the discharge cycle is obtained.

As described above, the water is heated firstly by the heat released by the condensation of the working fluid up to $T^*$, and then it finishes the heating up to $T_{out,DH}$ through the heat deriving from the source at low temperature.

Through two energy balances in these two exchangers, the code calculates two values of

the district heating water.

As regards the energy balance at the condenser, it can be expressed as follows:

$$\dot{m}_{water,DH} C_{P,water} (T^* - T_{in,DH}) = \dot{m}_{PC} (h_7 - h_1) \tag{3.54}$$

From this, the first value of $\dot{m}^{DH}_{water,1}$ is obtained.

From this balance, the first value of the mass flow rate of district heating water is obtained. This value will then be compared with the water flow obtained from the second balance.

The code continues with the calculation of the electrical power generated by the turbine, that absorbed by the compressor and that released to the district heating water.

$$P_{el,turb} = \dot{m}_{PC} (h_5 - h_6) \tag{3.55}$$

$$P_{el,pump} = \dot{m}_{PC} (h_2 - h_1) \tag{3.56}$$

$$\dot{Q}_{out} = \dot{Q}_{cond} + \dot{Q}_{DSH} = \dot{m}_{PC} (h_7 - h_1) \tag{3.57}$$

The code verifies that the global heat balance is verified. It can be expressed as follows:

$$P_{el,pump} + \dot{Q}_{reaction} = \dot{Q}_{out} + P_{el,turb} \tag{3.58}$$

### 3.6.1. High pressure heat exchanger

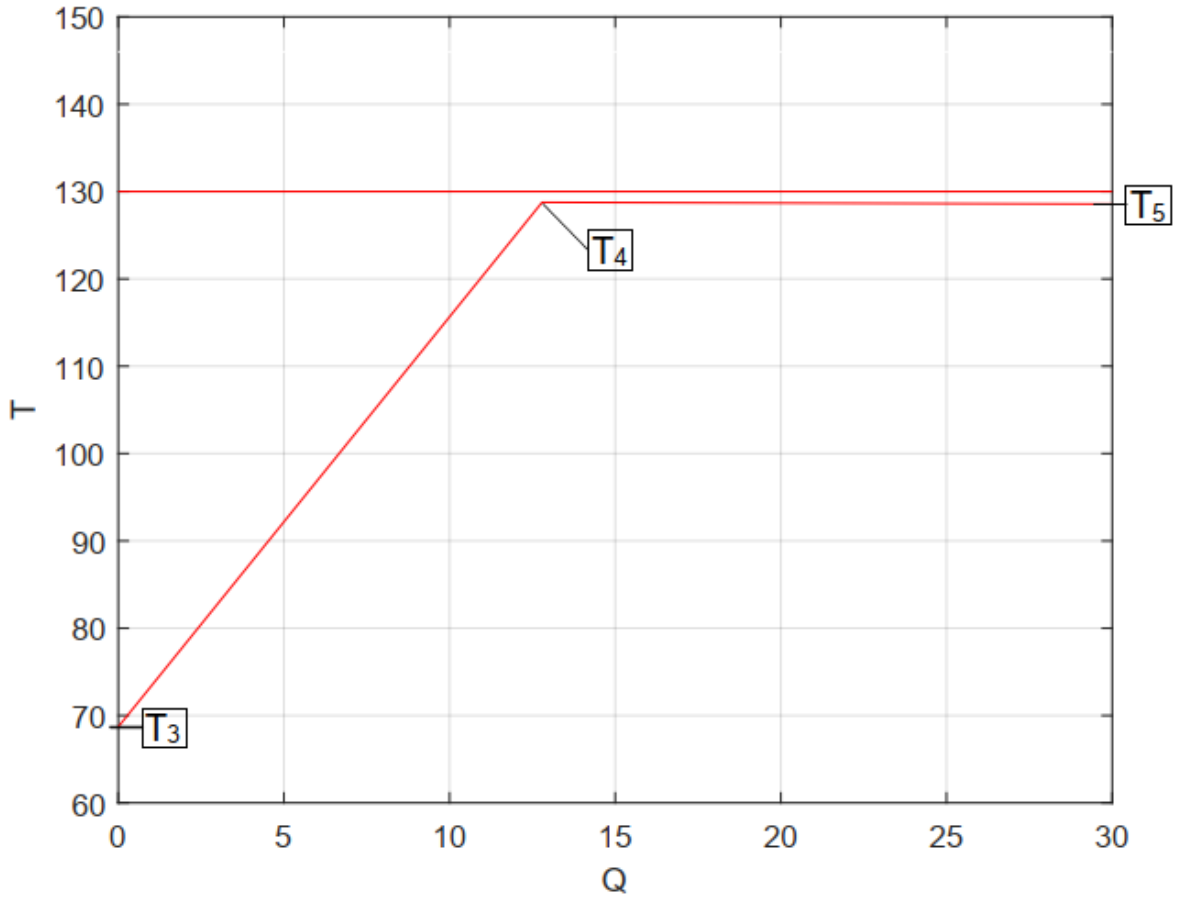


Figure 3.17: TQ diagram of the high pressure heat eschanger

The working fluid condenses in the high pressure exchanger during heat pump operation. In power cycle operation, the preheating and evaporation of the fluid takes place in this component.

The code, as previously done for the charge cycle, calculates the thermal power in each section, the $\Delta T_{ML}$ and finally obtains the parameter UA.

$$\dot{Q}_{eco}^{PC} = \dot{m}_{PC}(h_4 - h_3) \tag{3.59}$$

$$\dot{Q}_{eva}^{PC} = \dot{m}_{PC}(h_5 - h_4) \tag{3.60}$$

$$\Delta T_{ML,eva} = \frac{(T_{discharge} - T_5) - (T_{discharge} - T_4)}{\ln \frac{(T_{discharge} - T_5)}{(T_{discharge} - T_4)}} \tag{3.61}$$

$$\Delta T_{ML,eco} = \frac{(T_{discharge} - T_4) - (T_{discharge} - T_3)}{\ln \frac{(T_{discharge} - T_4)}{(T_{discharge} - T_3)}} \tag{3.62}$$

$$UA_{eva,TOT} = \frac{\dot{Q}^{PC}_{eva}}{\Delta T_{ML,eva}} + \frac{\dot{Q}^{PC}_{eco}}{\Delta T_{ML,eco}} \tag{3.63}$$

## Overall heat transfer calculation

At this point, unlike what was done for the charge cycle, the internal and external heat transfer coefficients are calculated by scaling them with respect the assumed values in the charging phase.

The internal heat transfer coefficient during a change of phase (condensation or evaporation) in a shell-and-tube heat exchanger is calculated using Formula 3.64 [47]:

$$h_i = 0.729 \left[ \frac{\rho_l(\rho_l - \rho_v) g i^*_{lv} k_l^3}{\mu_l (T_{sat} - T_{wall}) d_0} \right]^{0.25} \tag{3.64}$$

In that relation, the subscript $l$ and $v$ indicates the conditions of saturated liquid and saturated vapour respectively. These thermodynamic properties of the fluid are calculated using $REFPROF$, at the film temperature, defined as follows:

$$T_{film} = \frac{T_{in} - T_{out}}{2} \tag{3.65}$$

The term $i^*_{lv}$ is a function of the latent heat ($i_{lv}$) and of the specific heat of the saturated liquid as follows:

$$i^*_{lv} = i_{lv} + 0.68 c_{p_l} (T_{sat} - T_{wall}) \tag{3.66}$$

The term $(T_{sat} - T_{wall})$ is assumed to remain constant. So, given that $g$ is a constant and the geometric parameter $d_0$ remains constant, making the ratio between the heat exchange coefficient in the discharging cycle and the one in the charging cycle, the following relationship is obtained:

$$\frac{h_{i,EVA,discharge}}{h_{i,EVA,charge}} = \frac{\left[\frac{\rho_l(\rho_l-\rho_v)i^*_{lv}k_l^3}{\mu_l}\right]^{0.25}_{discharge}}{\left[\frac{\rho_l(\rho_l-\rho_v)i^*_{lv}k_l^3}{\mu_l}\right]^{0.25}_{charge}} \tag{3.67}$$

from which, the internal heat transfer coefficient referred to the evaporator of the power cycle is calculated:

$$h_{i,EVA,discharge} = h_{i,EVA,charge}\frac{\left[\frac{\rho_l(\rho_l-\rho_v)i^*_{lv}k_l^3}{\mu_l}\right]^{0.25}_{discharge}}{\left[\frac{\rho_l(\rho_l-\rho_v)i^*_{lv}k_l^3}{\mu_l}\right]^{0.25}_{charge}} \tag{3.68}$$

At this point it is possible to calculate the global heat exchange coefficient for this exchanger, through which the evaporator area is calculated.

$$U = \left(\frac{1}{h_{i,EVA,discharge}A_{ratio,1}} + \frac{1}{h_{i,EVA,discharge}A_{ratio,2}} + \frac{R_{f,int,EVA}}{A_{ratio,1}} + \frac{R_{f,ext,EVA}}{A_{ratio,2}}\right)^{-1} \tag{3.69}$$

The same procedure is done for the economizer. The only difference is the heat transfer correlation used: in this case, for a liquid that is being heated up, the well-known Dittus-Boelter correlation is preferred. It links the Nusselt number with the Reynolds number and the Prandtl number:

$$Nu = \frac{hD}{k} = 0.023Re^{0.8}Pr^{0.4} \tag{3.70}$$

In which the two non-dimensional numbers are calculated through the following two equations:

$$Re = \frac{\rho Du}{\mu} = \frac{\dot{m}Du}{\mu A_c} = \frac{4\dot{m}}{\pi D^2\mu} \tag{3.71}$$

where $A_c = \frac{\pi D^2}{4}$ since the tubes of the heat exchangers are cylinders.

$$Pr = \frac{\mu c_p}{k} \tag{3.72}$$

From 3.70 the heat transfer coefficient is obtained:

$$h = \frac{0.023 k Re^{0.8} Pr^{0.4}}{D} \tag{3.73}$$

So, making some calculations, the ratio between the heat transfer coefficient in the discharging cycle and that in the charging cycle is:

$$\frac{h_{i,ECO,d}}{h_{i,ECO,c}} = \frac{k_d}{k_c} \frac{(\frac{\dot{m}_d}{\mu_d})^{0.8}}{(\frac{\dot{m}c}{\mu_c})^{0.8}} \frac{(\frac{\mu_d c_p}{k_d})^{0.4}}{(\frac{\mu_c c_p}{k_c})^{0.4}} \tag{3.74}$$

The subscripts $d$ and $c$ are referred to the discharging cycle properties and the charging cycle one. From 3.74 the heat transfer coefficient in the economizer section of the high pressure heat exchanger is calculated. Finally, the U parameter and the area of the economizer can be computed.

Eventually, the total area of the high pressure heat exchanger is obtained by the sum of the two sections:

$$A_{HP} = A_{EVA} + A_{ECO} \tag{3.75}$$

### 3.6.2. Low pressure heat exchanger

During operation in power cycle mode, the low pressure exchanger is responsible for desuperheating and condensation of the working fluid.

$$\dot{Q}^{PC}_{cond} = \dot{m}_{PC}(h_8 - h_1) \tag{3.76}$$

$$\dot{Q}^{PC}_{dsh} = \dot{m}_{PC}(h_7 - h_8) \tag{3.77}$$

In order to calculate the UA parameter referred to the only condensation section, it is necessary to calculate the district heating water temperature at the end of the condensation section only.

This temperature can be seen in the $TQ$ shown in Figure 3.18.

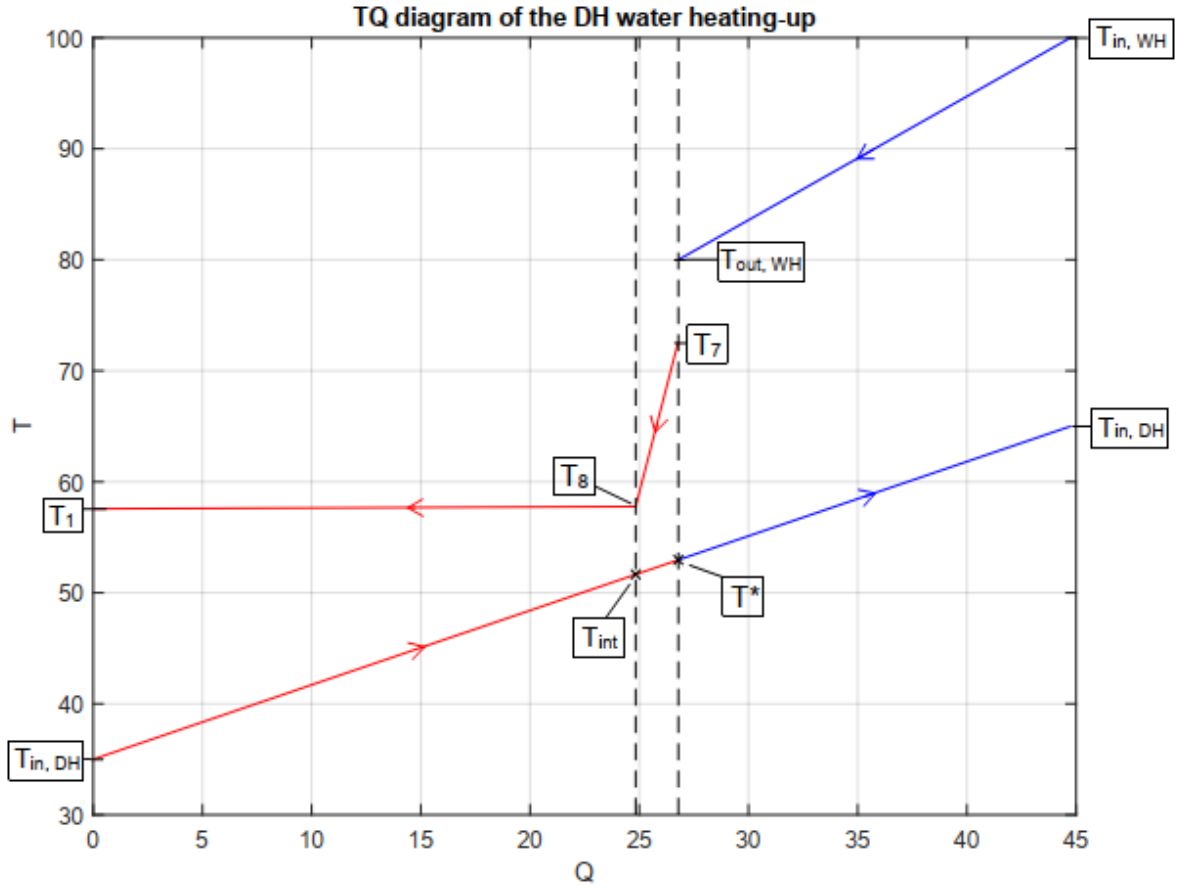


Figure 3.18: TQ diagram of the low pressure heat exchanger

The energy balance of the condensation section is:

$$\dot{Q}_{cond}^{PC} = \dot{m}_{water,1}^{DH} C_{p,water}(T_{int} - T_{in,DH}) \tag{3.78}$$

From this, $T_{int}$ is calculated, and then used to obtain $\Delta T_{ML,cond}$, $\Delta T_{ML,dsh}$ and then the respective UA parameters.

$$\Delta T_{ML,cond} = \frac{(T_1 - T_{in,DH}) - (T_8 - T^*)}{\ln \frac{(T_1 - T_{in,DH})}{(T_8 - T^*)}} \tag{3.79}$$

$$\Delta T_{ML,dsh} = \frac{(T_7 - T^*) - (T_8 - T_{int})}{\ln \frac{(T_7 - T^*)}{(T_8 - T_*)}} \tag{3.80}$$

$$UA_{cond} = \frac{\dot{Q}^{PC}_{cond}}{\Delta T_{ML,cond}} \tag{3.81}$$

$$UA_{dsh} = \frac{\dot{Q}^{PC}_{dsh}}{\Delta T_{ML,ssh}} \tag{3.82}$$

Now the two global heat exchange coefficients and finally the areas of the two sections are calculated. As regards the condensation section, the procedure is the same as indicated for the condensation part of the charge cycle. Through the correlation 3.64 the internal heat transfer coefficient is computed (liquid water from the district heating flows in the shell part of the exchanger and the heat transfer coefficient in assumed in Table 3.3). For the desuperheating section, the Dittus-Boelter is used and the conceptual scheme is the same as described above.

## Recuperator

The heat exchanged in this component is calculated as:

$$\dot{Q}^{PC}_{rec} = \dot{m}_{PC}(h_3 - h_2) \tag{3.83}$$

In the recuperator, the hot working fluid at the outlet of the turbine cools down from $T_6$ to $T_5$, heating the cold working fluid exiting the pump from $T_2$ to $T_3$. So, the $\Delta T_{ML,rec}$ and the $UA_{rec}$ are the following:

$$\Delta T_{ML,rec} = \frac{(T_6 - T_3) - (T_7 - T_2)}{\ln \frac{(T_6 - T_3)}{(T_7 - T_2)}} \tag{3.84}$$

$$UA_{rec} = \frac{Q^{PC}_{rec}}{\Delta T_{ML,rec}} \tag{3.85}$$

In order to calculate the internal heat transfer coefficient relative to the recuperator, Dittus-Boelter correlation is used. As for the external heat transfer coefficient, the Zukauskas correlation is better representative of the heat exchange in this component **??**.

$$Nu = \frac{hD}{k} = cRe^m Pr^n \left(\frac{Pr}{Pr_s}\right)^{0.25} \tag{3.86}$$

where $c$ is a constant and $Pr_s$ is the Prandtl number evaluated at the superficial temeprature of the tubes (while, as in all other cases, the thermodynamic properties of the fluid are evaluated at the film temperature).

The procedure is the same: the heat transfer coefficients are scaled with respect to those assumed for the charging phase. With these calculated values of $h_{i,REC}$ and $h_{e,rec}$, the global heat transfer coefficient U is computed, and finally the area of this component is obtained.

### 3.6.3. Second District Heating water heat exchanger

At this point the energy balance is applied to the second district heating water exchanger (shown in Figure 3.15).

$$\dot{Q}_{WH} = \dot{m}^{DH}_{water,2} C_{p,water}(T_{out,DH} - T^*) \tag{3.87}$$

From this balance, the second value of the mass flow rate of the district heating water is calculated.

$$\dot{m}^{DH}_{water,2} = \frac{\dot{Q}_{WH}}{C_{p,water}(T_{out,DH} - T^*)} \tag{3.88}$$

So far, the MATLAB function has calculated the $UA$ parameters of the power cycle and, through the energy balances of the two exchangers that heat up the district heating water, it has calculated two values of the mass flow rate of this water.

Now, as shown in the block diagram of Figure 3.8, the last step is to compare the $UA$ values just calculated with the actual ones (those calculated in the heat pump cycle) and compare the two values of the mass flow rate involving in the district heating system.

The MATLAB solver $fsolve$ repeats the procedure of Figure 3.8 until these four differences are close to 0 (the admitted error is of the order of $10^{-6}$).

### 3.6.4. No thermal integration

In the situations in which there is no thermal integration, that is when the low temperature heat source is available only in summer and not during the whole year, the code does the same procedure except for the calculation of the fourth variable, $T^*$. Indeed, in this case the heating of the district heating water is due only to the condensation heat available from the power cycle. The code only calculates the areas of the exchangers and uses them to calculate the three unknown temperatures.

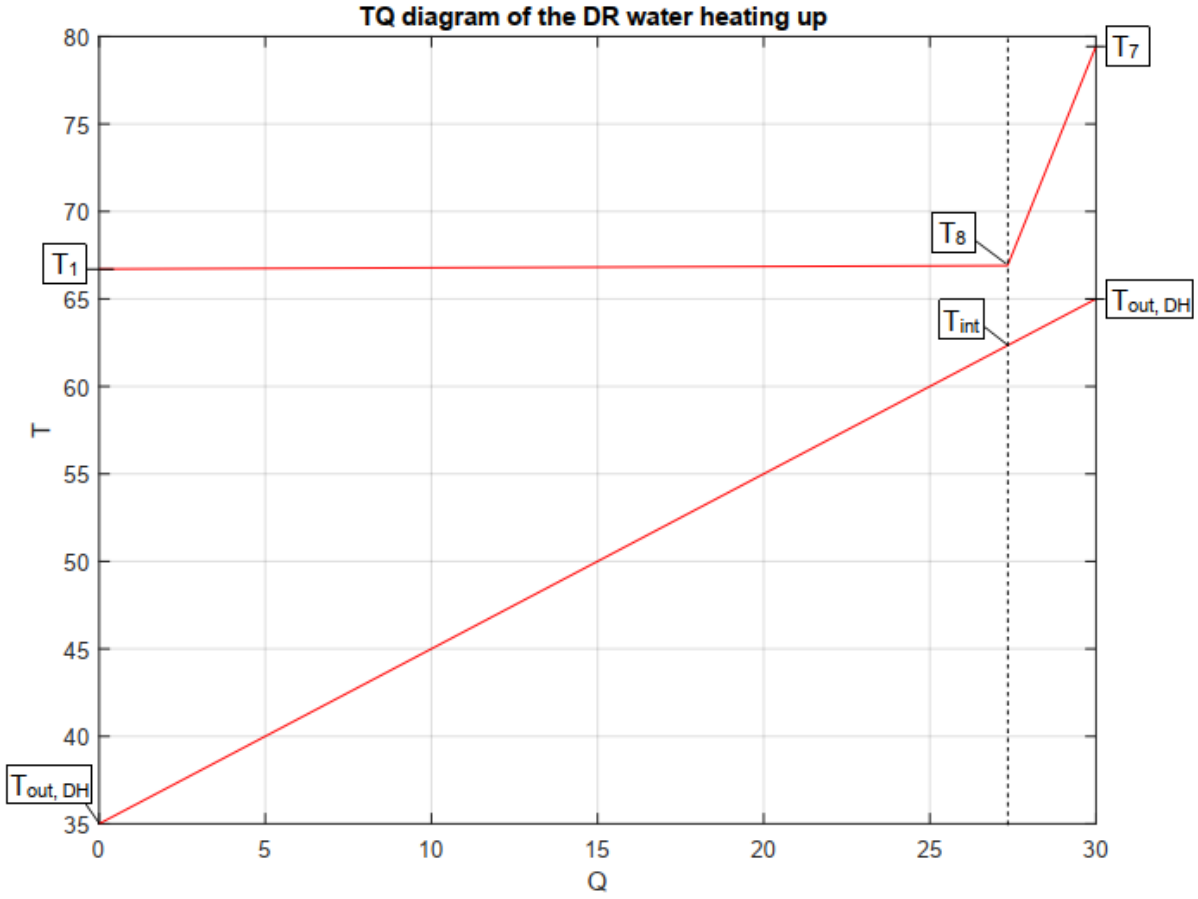


Figure 3.19: District water heating diagram

Figure 3.19 shows the heating up of the district heating water if there is no thermal integration, considering a fourth generation district heating network. The water is heated from $T_{in,DH}$ $(35^oC)$ to $T_{out,DH}$ $(65^oC)$ exploiting only the heat deriving from the condensation and the desuperheating of the working fluid of the charging cycle.

In this chapter the code developed for the study of this thermochemical energy storage

system was described.

Definitely, the code calculated the thermodynamic points of the two charge and discharge cycles as a function of the temperature at which the reaction takes place, the conditions of the low-temperature heat source and the district heating system (hence the desired inlet and output).

In the following chapter a reference case will be defined and the results obtained will be analyzed. Subsequently, some sensitivity analyzes are made to see if under certain conditions the optimal fluids are other than the one of the reference case.

# 4 | Results and fluids classification

After having described the methodology and the MATLAB code used to carry out the simulations of the storage system analyzed in the present thesis, the results referring to a reference case are presented. Finally, some sensitivity analyses will be done to see if there are any variations in terms of better fluids.

## 4.1. Reference case definition

The temperature at which the chemical reaction takes place in the reactor is considered equal to 150°C for each simulation performed. The same for the reverse reaction, which takes place at a temperature of 130°C .

As regards the low temperature heat source, for all the simulations it was considered water at a temperature of 100°C which cools down to 80 °C, evaporating the working fluid of the heat pump cycle.

Table 4.1 summarizes the temperatures used.

| | °C |
|---|---|
| $T_{reaction,charge}$ | 150 |
| $T_{reaction,discharge}$ | 130 |
| $T_{in,WH}$ | 100 |
| $T_{out,WH}$ | 80 |

Table 4.1: Characteristic temperature of the reference case

As described in the section concerning the different district heating networks analyzed in this thesis, the inlet and outlet temperatures of the water sent to the district heating can vary greatly depending on the generation being considered. Therefore, the performance of the system are strictly dependent on the generation of district heating used.

In the reference case, a base fourth generation district heating network is treated. Thus,

the water is heated from a temperature of 35°C (which is the return temperature) to a temperature of 65°C (which is the supply temperature).

| | °C |
|---|---|
| $T_{in,DH}$ | 35 |
| $T_{out,DH}$ | 65 |

Table 4.2: District Heating temperatures of the reference case

As explained earlier in this thesis, if the low temperature heat source is available throughout the year, the system can be thermally integrated. The heat source could be a renewable one, for example solar, available only at certain times of the year, or a waste heat coming from an industrial process and therefore available all year round.

In the reference case, the performances of the system are analyzed by considering two diametrically opposite situations:

- *No thermal integration.* The heat source is available only in the summer. The district heating water is heated only by the heat released by the power cycle.
- 100 % *thermal integration.* The heat source is available all year round. The heating of the district heating water is carried out in two exchangers in series.

## 4.2. Reference case results

The most important parameter that characterizes the performance of the analyzed system is the round trip efficiency (RTE). It is defines as the ratio between the useful electric power delivered by the power cycle and the electric power absorbed by the compressor of the charge cycle. Analytically, this corresponds to:

$$RTE = \frac{P_{PC}}{P_{compr,HP}} = \frac{P_{turbine,PC} - P_{pump,PC}}{P_{compr,HP}} \tag{4.1}$$

Given that the performance parameters of the two charge and discharge cycles are:

- $COP = \dfrac{Q_{reaction}}{P_{compr,HP}}$
- $\eta_{PC} = \dfrac{P_{PC}}{Q_{reaction}}$

the round trip efficiency can be rewritten as:

$$RTE = COP * \eta_{PC} \tag{4.2}$$

In Chapter 3 it was discussed the MATLAB function that calculates the minimum and maximum temperatures of the compressor inlet and outlet. As anticipated, the code calculates the RTE for each fluid in this computed temperature range.

Figure 4.1 shows the most significant trends of the round-trip-efficiency. It can be immediately noticed that the most promising fluids in this case are Benzene and Dmc, which have the highest RTE when the compressor outlet temperature is the maximum allowable. Also Toluene and Mxylene have a good RTE (Oxylene and Pxylene have about the same performances, but slightly lower, therefore in the next graphs only Mxylene is reported).

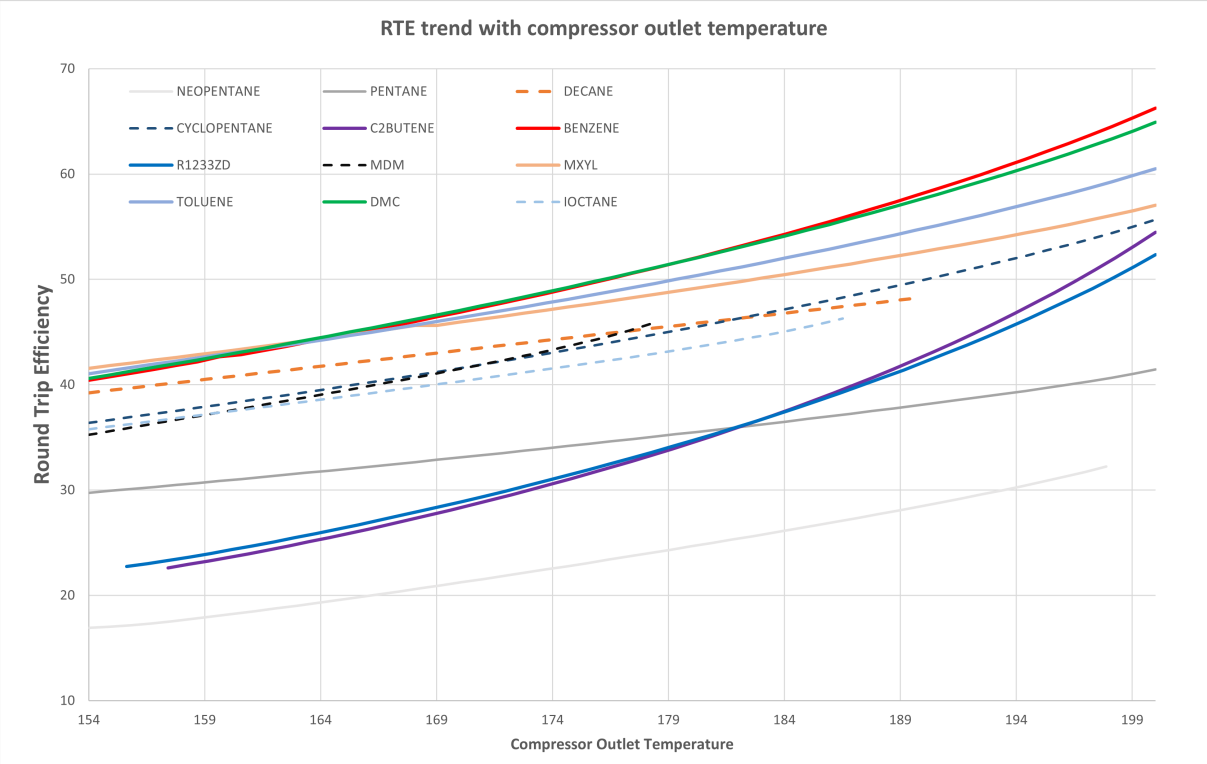


Figure 4.1: RTE trend as the compressor outlet temperature increases, for the reference case with no thermal integration

Particular trends are those of R1233ZD and C2butene, which show a large relative increase in RTE with the increasing of the compressor outlet temperature. Indeed, when this temperature is the lowest, they have a very low RTE, but at the maximum temperature,

their RTE is almost that of Cyclopentane or Mxylene, which have a much higher RTE when the compressor outlet temperature is the lowest.

Fluids as MDM (MM and MD2M are not showed in the graph since they have the same trend but slightly lower) have a good increasing trend, but their maximum outlet temperature allowable is small (lower than 180°C). This is due to their shape of the saturation bell: Figure 4.2 shows the two thermodynamic cycles of MDM when the compressor inlet and outlet temperature is the maximum possible.

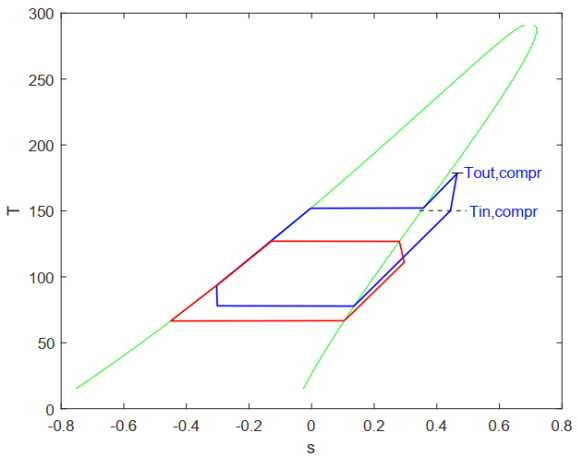


Figure 4.2: Ts diagram of MDM

For the sake of completeness, trends of Neopentane (the worst fluid in terms of RTE), Pentane, Ioctane and Decane are reported. All the other fluids not showed in the graph of Figure 4.1

So, looking and the trends of the RTE, a first conclusion is derived: increasing the outlet compressor temperature, the round-trip-efficiency of the system increases monotonously for all fluids. This means that, where permitted by the turbomachine, exploiting the maximum temperature allowed by thermodynamics is beneficial in terms of performance of the whole system.

This first conclusion was also obtained in the circumstance in which there is a 100 % thermal integration. This case is reported in Figure 4.3.

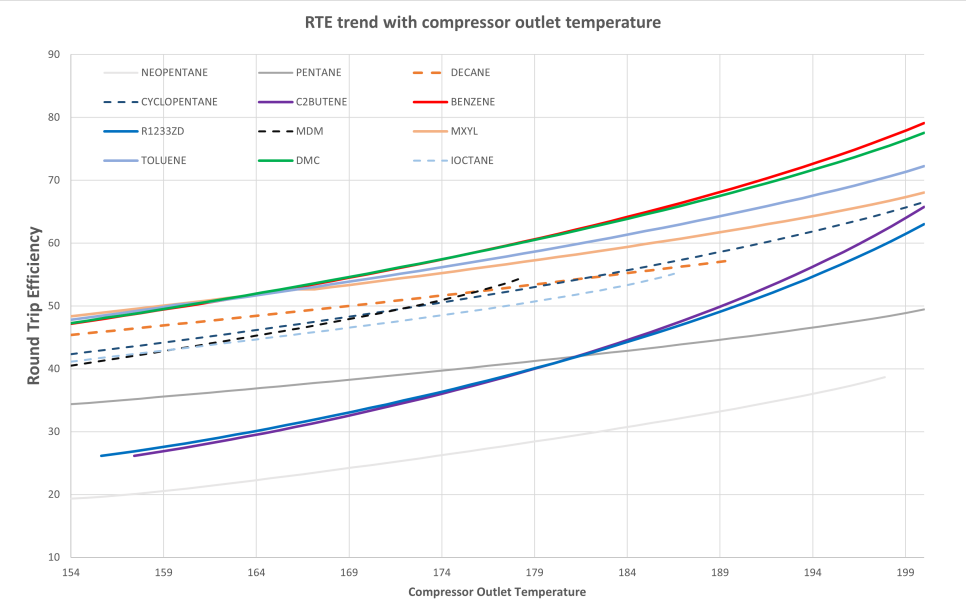


Figure 4.3: RTE trend as the compressor outlet temperature increases, for the reference case with 100% thermal integration

Even in this situation, an increase in the temperature at the compressor outlet results in an increase in performance.

As expected, in case there is thermal integration throughout the year, the round trip efficiency is greater for a given outlet compressor temperature. This is due the fact that the heat released to the district heating water is produced in series in two exchangers (Figure 3.15), the condensation temperature of the discharge cycle is lowered, hence its efficiency increases, leading to a RTE increase (Equation 4.2). Graphically, this is observable from the fact that the fluid curves are 'translated' upwards, towards major RTEs.

A first classification of the fluids is made (table **??**) according to the efficiency obtained. As shown in the graphs of figures 4.1 and 4.3, when there is 100% thermal integration throughout the year, the RTE of each fluid increases. It is noted that the ordering of the best performing fluids does not vary substantially.

The greater the RTE of a fluid in the stand alone case, the greater the benefit that fluid obtains when there is thermal integration. For example, benzene obtains the greatest increase in RTE ($+12,817\%$), followed by $DMC$ ($+12,663\%$) and *toluene* ($+11,792\%$), while *neopentane* present the lowest increase ($+6,415\%$).

Henceforth, only the fluids with the best performance will be considered.

| Stand Alone | RTE |
|---|---|
| BENZENE | 66.259 |
| DMC | 64.915 |
| TOLUENE | 60.515 |
| MXYLENE | 57.053 |
| OXYLENE | 57.020 |
| PXYLENE | 56.954 |
| R123 | 56.588 |
| CYCLOPENTANE | 55.660 |
| C2BUTENE | 54.476 |
| R1233ZD | 52.341 |
| CYCLOHEXANE | 49.047 |
| DECANE | 48.205 |
| C11 | 48.802 |
| C3CC6 | 48.376 |
| T2BUTENE | 48.261 |
| NONANE | 47.869 |
| MD2M | 47.643 |
| D5 | 47.480 |
| OCTANE | 47.374 |
| C1CC6 | 47.228 |
| HEPTANE | 46.451 |
| IOCTANE | 46.292 |
| MM | 45.189 |
| MDM | 45.834 |
| HEXANE | 44.807 |
| R245CA | 44.056 |
| IHEXANE | 43.836 |
| PENTANE | 41.445 |
| RE245FA2 | 39.630 |
| R365MFC | 39.325 |
| IPENTANE | 39.260 |
| NOVEC649 | 36.115 |
| RE347MCC | 34.616 |
| NEOPENTANE | 32.250 |

| 100% Thermal Integration | RTE |
|---|---|
| BENZENE | 79.116 |
| DMC | 77.545 |
| TOLUENE | 72.248 |
| MXYLENE | 68.055 |
| OXYLENE | 67.992 |
| PXYLENE | 67.955 |
| R123 | 67.938 |
| CYCLOPENTANE | 66.544 |
| C2BUTENE | 65.780 |
| R1233ZD | 63.024 |
| T2BUTENE | 58.439 |
| CYCLOHEXANE | 58.349 |
| C11 | 58.202 |
| DECANE | 57.247 |
| C3CC6 | 57.524 |
| NONANE | 56.885 |
| MD2M | 56.792 |
| D5 | 56.726 |
| OCTANE | 56.341 |
| C1CC6 | 56.207 |
| HEPTANE | 55.277 |
| IOCTANE | 55.104 |
| MDM | 54.453 |
| MM | 53.733 |
| HEXANE | 53.347 |
| R245CA | 52.705 |
| IHEXANE | 52.261 |
| PENTANE | 49.465 |
| RE245FA2 | 47.388 |
| R365MFC | 46.925 |
| IPENTANE | 46.870 |
| NOVEC649 | 42.243 |
| RE347MCC | 41.351 |
| NEOPENTANE | 38.663 |

Table 4.3: Classification of fluids based on their RTE, in the stand alone case (left) and 100% thermal integration case (right)

Just looking at the RTE parameter, it is immediately noticed which are the most performing fluids. But the choice of the optimal fluid is not based only on thermodynamic performance. However, it is also necessary to analyze how the heat exchange surfaces vary as the compressor outlet temperature increases. To do this, the values of the exchangers areas are analyzed.

The overall is given by the sum of the individual areasof the three exchangers present in the system.

$$A_{TOT} = A_{HP} + A_{LP} + A_{REC} \tag{4.3}$$

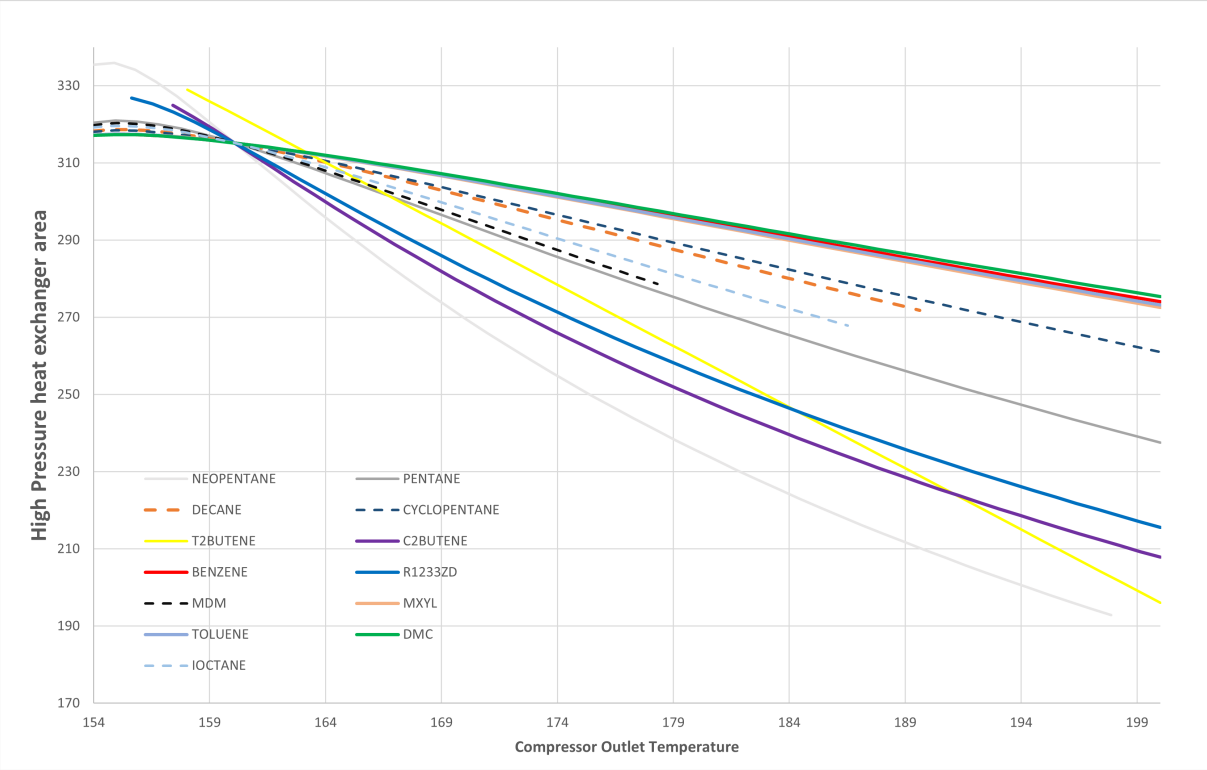


Figure 4.4: Trend of the high pressure HX area as the compressor outlet temperature increases

Figure 4.4 shows the behaviour of the high pressure heat exchanger area for some relevant fluids. It decreases as the compressor outlet temperature increases. The decrease can be very different for the various fluids: for example, looking at the Benzene and Pentane curves, it is noticed that they have approximately the same area when the compressor outlet temperature is the minimum admissible, but the area Pentane decreases more drastically than that of the Benzene.

From the graph it can be seen that the fluids that allows to have the lower area for the high pressure heat exchanger are T2butene and Neopentane (which is the fluid with the poorest performance).

Among the three fluids that have the highest RTE (Benzene, DMC and R1233ZD), the first two have similar curves. Their area is the largest when the compressor outlet temperature is the maximum. On the contrary, R123ZD shows a great area reduction.

The same analysis is made for the low pressure exchanger. Figure 4.5 shows the $UA_{LP}$ trend for the same fluids analyzed previously.

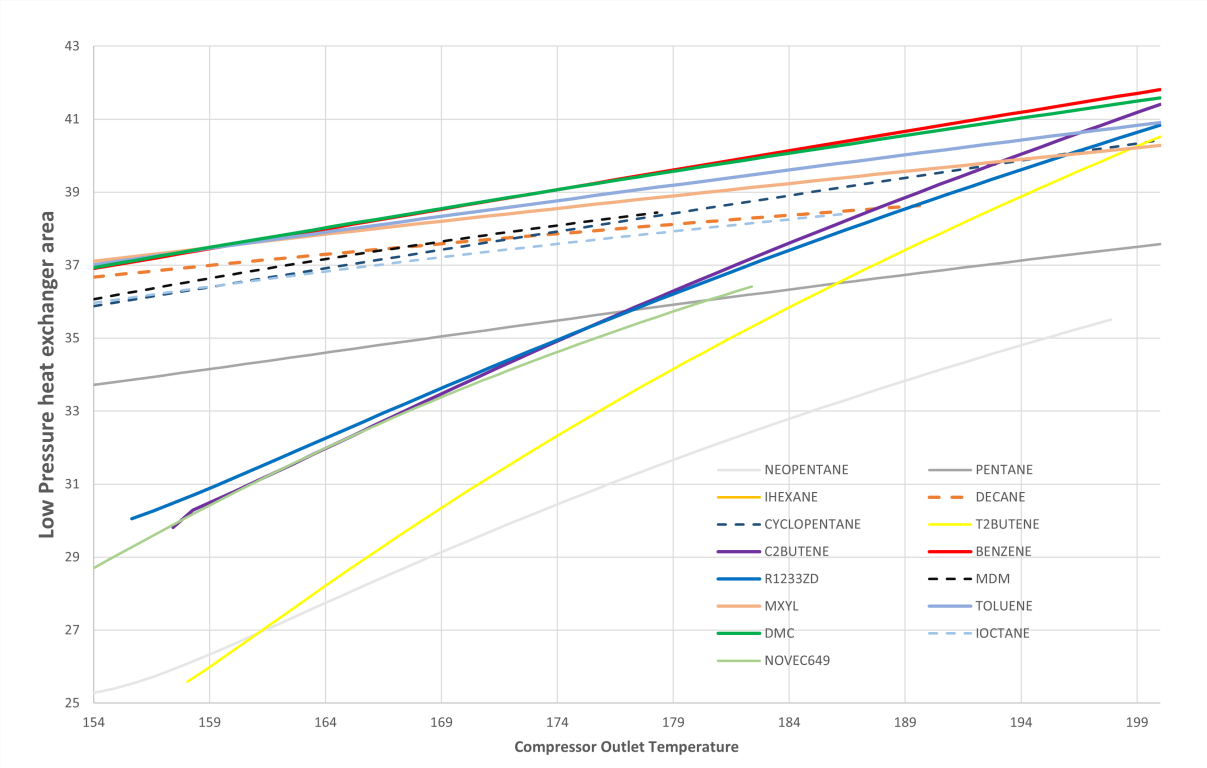


Figure 4.5: Trend of the low pressure HX area as the compressor outlet temperature increases

In this case, as the compressor outlet temperature increases, the area of the exchanger increases. Also in this case, depending on the working fluid, the increase can be more or less significant.

As for the high pressure exchanger, Benzene and DMC have approximately the same trend. Even in this case they need the largest areas when the temperature at the compressor outlet is the maximum.

T2butene had the greatest area increase and it reaches a value close to those of the three fluids that have a higher RTE.

As for as it concerns the recuperator, it represents the component most subject to variations in the heat exchange surfaces. As the compressor outlet temperature increases, the areas increase exponentially, as shown in Figure 4.6.

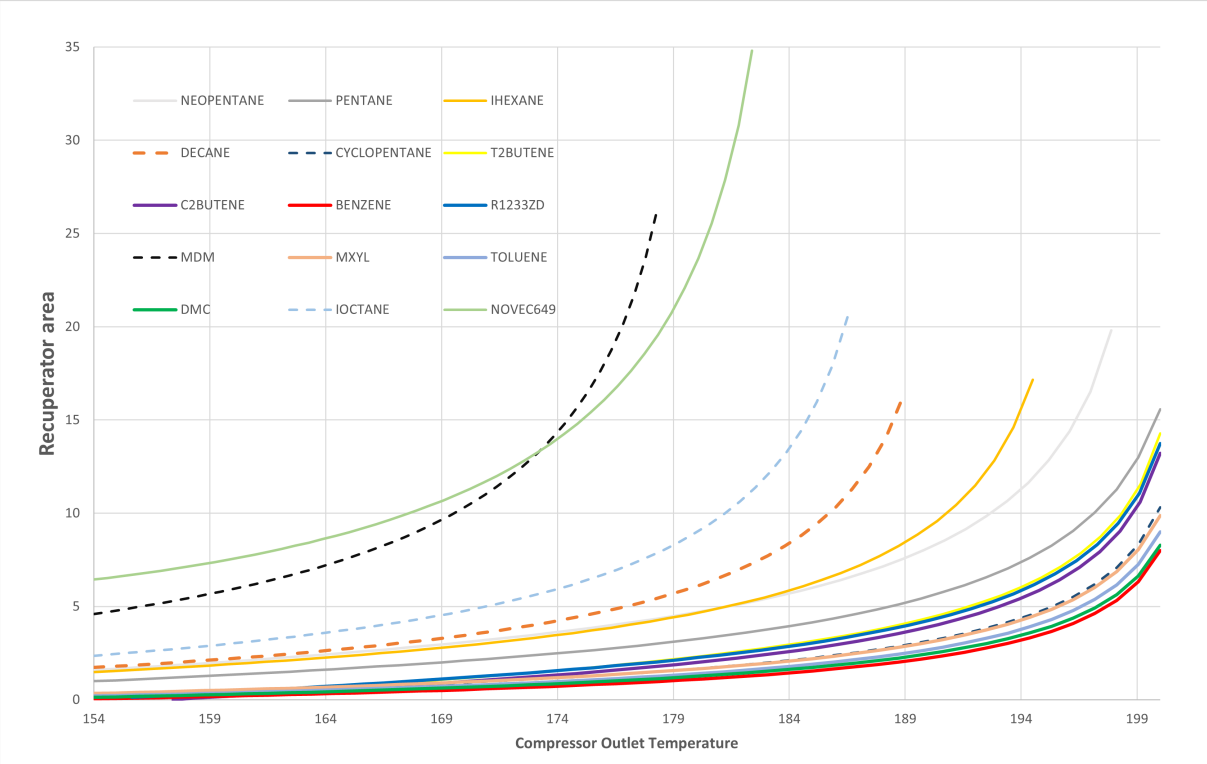


Figure 4.6: Trend of the recuperator area as the compressor outlet temperature increases

This is due to the fact that by increasing the compressor outlet temperature, the inlet temperature also increases accordingly. Therefore, the logarithmic mean temperatures difference inside this exchanger tend to decrease and this leads to an exponential increase of the areas. This aspect leads to excessive costs for this component.

Even in this case, Benzene and DMC. Their trend is good if compared with other fluids, as Ihexane, Decane, Ioctane or Pentane, which present an higher area at a lower temperature.

At the maximum compressor outlet temperature, R1233ZZD leads to an higher area than the previous two fluids. It is noted that the fluids that lead to an excessive increase in the areas of the recuperator are Novec649 and MDM.

However, the area of the recuperator, even at maximum temperatures, is not the most

relevant parameter among those involved. Indeed, the values of the other two exchangers (especially the high pressure one) are much larger.

The trends of the total area of the three heat exchangers are plotted in the graph of Figure 4.7.

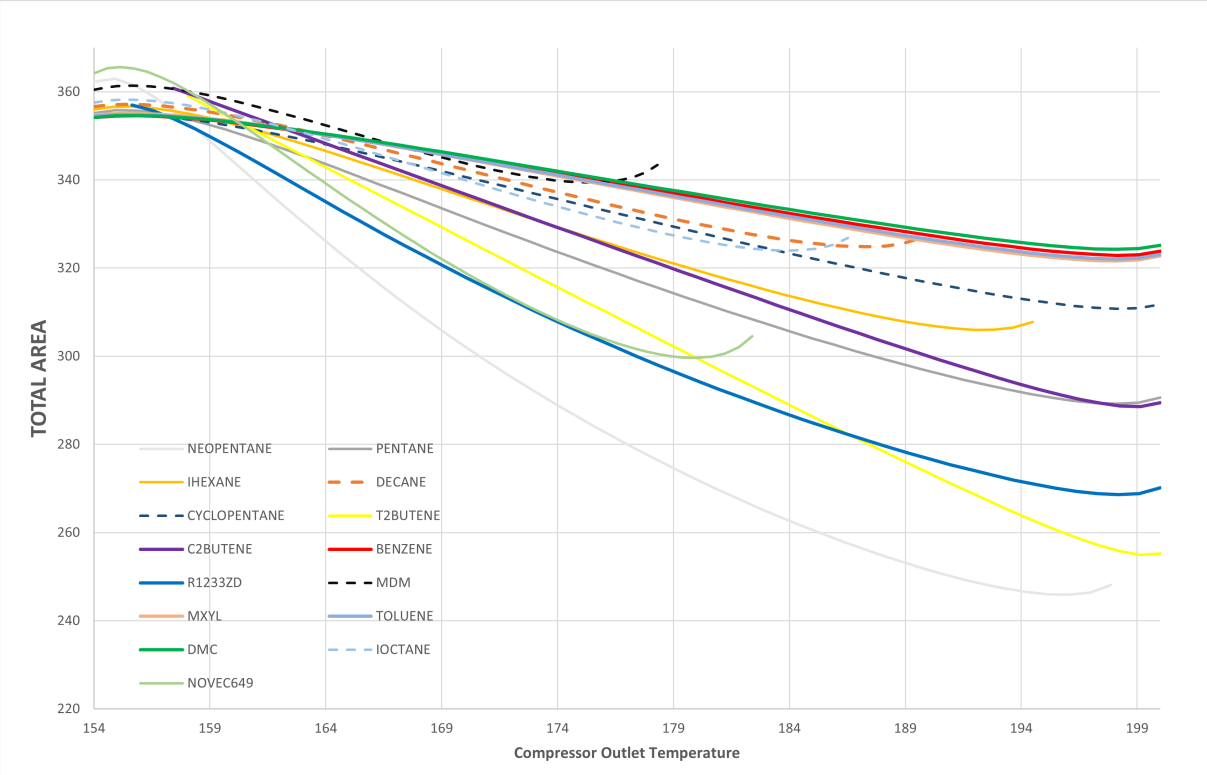


Figure 4.7: Trend of the total eschangers area as the compressor outlet temperature increases

As just said, the greatest weight is given by the high pressure heat exchanger. Therefore, T2butene is favored, as it is the fluid that has the greatest decrease in the area of that exchanger.

For some fluids (in particular Novec649 and MDM) the influence of the increase in the recuperator area at their maximum temperature can be noted.

DMC and Pentane have the same trend, and at the maximum temperature they have the maximum values of the total area (like Toluene and Mxylene, which however have lower RTE values). R1233ZD seems to be promising: indeed, compared to the other two fluids with the maximum RTE it has a quite lower value of the total area of the exchangers.

At this point, having analyzed the behavior of the RTE and the areas of the exchangers,

a combined analysis of these parameters is necessary to define which are the best fluids to use in the presented system.

## 4.3. RTE/AREA parameter

Pushing towards high temperatures at the compressor outlet has negative consequences for the recuperator and the low pressure heat exchanger, but is beneficial for the round-trip-efficiency of the cycle and for the high pressure heat exchanger.

For this reason, it is necessary to carry out an analysis that simultaneously takes into account all these aspects. Therefore, to understand which are the best fluids, the ratio between the RTE and the total area of the three involved exchangers has been computed.

This obtained values are plotted as a function of the compressor outlet temperature in Figure 4.8.

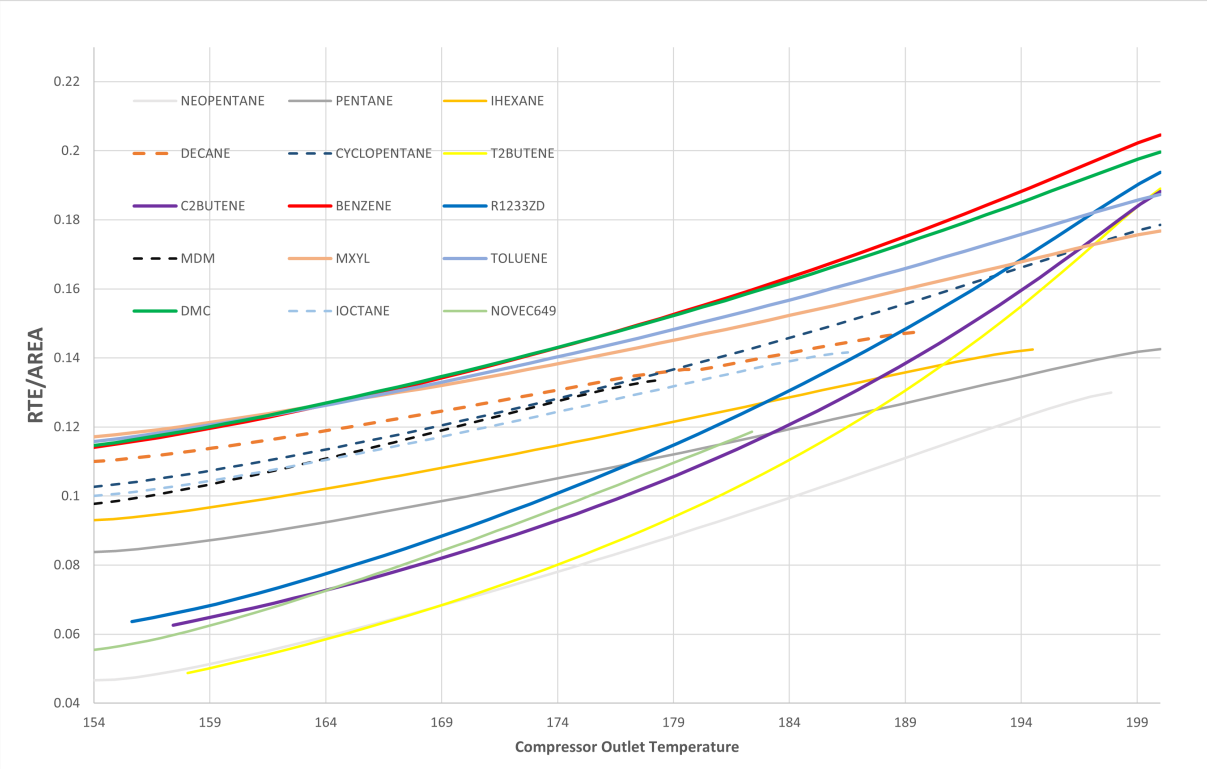


Figure 4.8: Trend of the RTE/A parameter (0% thermal integration)

Figure 4.8 shows that, considering the whole stretch from the minimum to the maximum compressor outlet temperature, the fluids with the higher RTE (Benzene, DMC and R1233ZD) remain the best to use. Indeed, they guarantee the higher $\frac{RTE}{A}$ parameter

when the outlet compressor temperature is the minimum, and maintain a fairly high value when the outlet temperature is the maximum.

The three xylenes (only Mxylene is shown in the graph for reasons of clarity) have the same behaviour as the previously commented fluids, with slightly lower values.

On the contrary, T2butene and C2butene have low values when the outlet temperature is the minimum, then their curves increase rapidly. Their final value is good, and they become considerable fluids. Even if they do not have the best RTE, the reduction in exchange surfaces that they entail is considerable.

The graph also shows the trend of the Neopentane, which have a great reduction of the high pressure heat exchanger area when the compressor outlet temperature increase and it have low values of the area of the low pressure heat exchanger, but its RTE is too low and this heavily affects the trade-off.

Therefore, from the technical-economic point of view, the results show that could be convenient to use fluids that have the best RTE. Obviously, a further analysis on the costs of the exchangers would be necessary to complete this aspect in the best possible way. Indeed, based on the cost of the exchangers, it might be preferable to use fluids that have a lower efficiency, but guarantee lower areas (and therefore costs).

## 4.4. Thermal Integration case

As mentioned above, in the situation in which the heat source is available throughout the year, the round trip efficiency of the system improves. On the other hand, the areas of the three heat exchangers remains the same. Indeed, the power cycle is simulated by equaling the areas calculated in the charge cycle. These areas are not affected by whether or not there is thermal integration (as detailed in Figure 3.4, Chapter 3).

Therefore, as can be seen in the figure below, the values of $\frac{RTE}{A}$ increase.

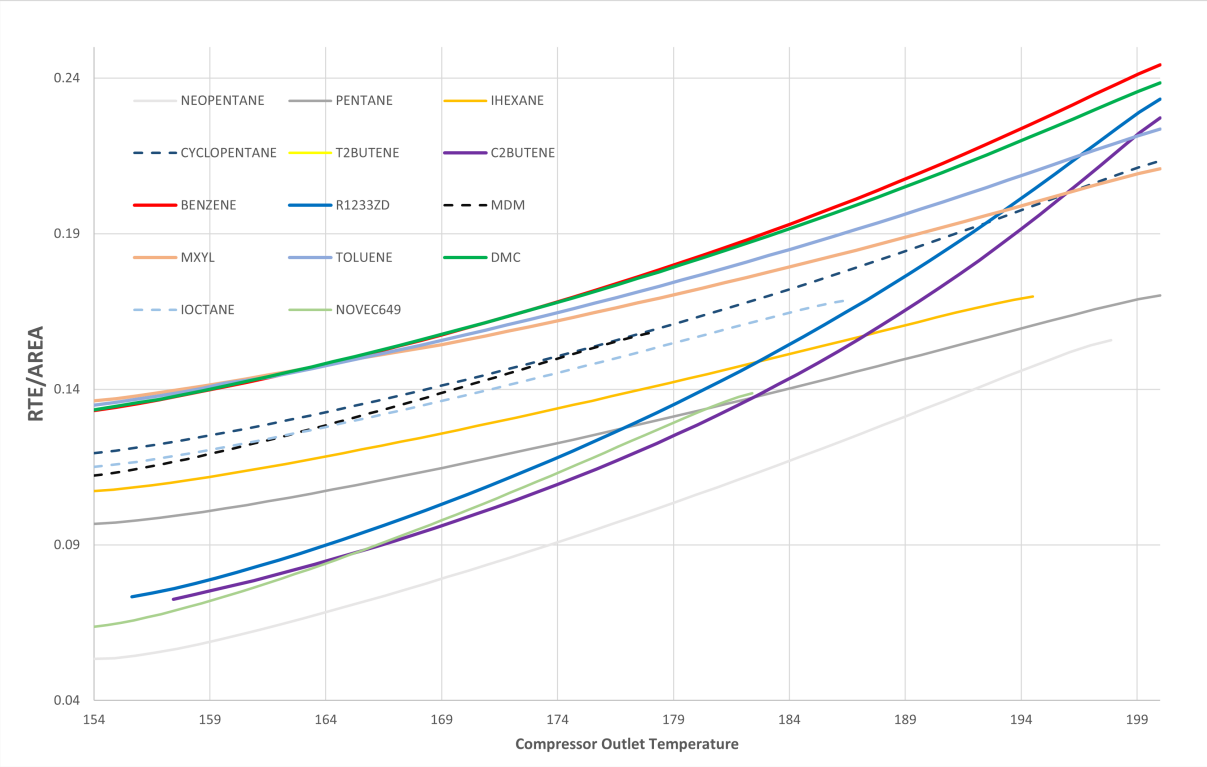


Figure 4.9: Trend of the RTE/A parameter (100% thermal integration)

The comments regarding the trends of the various fluids remain the same as for the stand alone case and the classification of the best fluids is the same.

If the compressor outlet temperature is the maximum allowable, the best fluids are Benzene, DMC and R1233ZD, which benefit from a high round-trip-efficiency. These are the best fluids for the whole compressor outlet temperature range.

## 4.5. Sensitivity Analysis

The results concerning the choice of the optimal working fluid in the reference case were analyzed. Here, a sensitivity analysis is carried out when some characteristic inputs vary.

In particular, the performance of the system are analyzed according to the variation of the generation of the district heating network used (therefore to the variation of its temperatures) and to the variation of the low temperature heat source.

The trends of the RTEs are analyzed for the three different generations of district heating considered in this thesis. These three generations are:

1. 3G DHC. Supply and return temperatures of 90 $^oC$ and 65 $^oC$.
2. 4G DHC - base. Supply and return temperatures of 65 $^oC$ and 35 $^oC$.
3. 4G DHC - advanced. Supply and return temperatures of 35 $^oC$ and 20 $^oC$.

Analyzing the best fluid (Benzene), it is immediately notice (Figure 4.12) that if a more advanced generation of district heating is used, the RTE substantially increase. On the contrary, an older generation (therefore with higher supply and return temperatures), lowers the performance of the system.

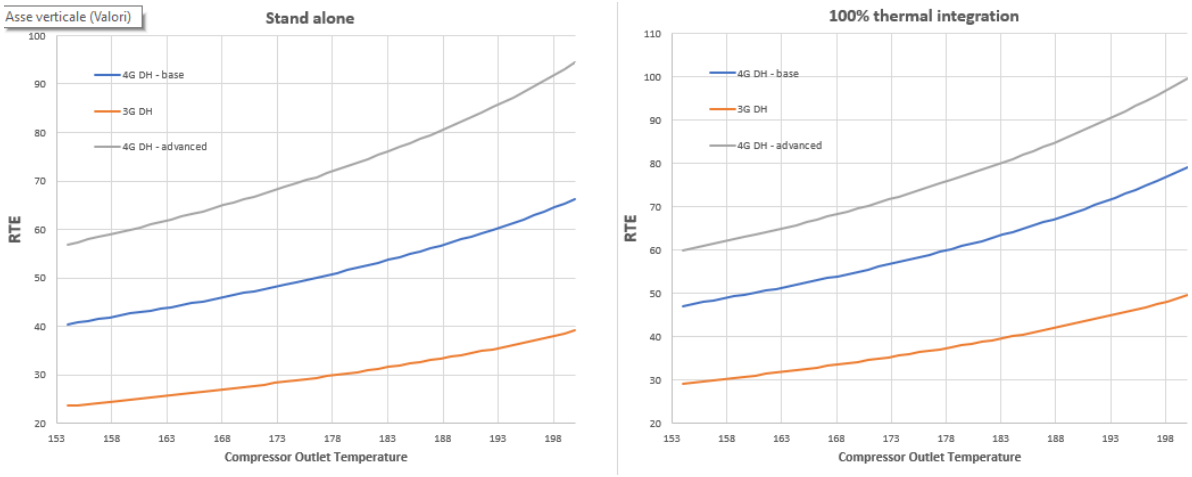


Figure 4.10: Benzene RTE trend for the three DH generations

It is immediately evident that adopting a more modern generation of district heating is beneficial for the whole system. Therefore, the lower is the supply and return temperatures, the higher will be the system RTE.

Indeed, the 3G DH has the lowest efficiencies. The increase obtained by passing from the minimum to the maximum compressor outlet temperature is also smaller.

In table 4.4 the values of the RTEs for the three district heating generation are showed. As shown graphically, an RTE of 99.62 can be obtained if the system is totally thermally integrated and there is an advanced fourth generation of district heating.

| | Stand alone | 100% thermal int. |
|---|---|---|
| BENZENE | RTE | |
| 4G DH (adv) | 94.37 | 99.62 |
| 4G DH (base) | 66.26 | 79.12 |
| 3G DH | 39.11 | 49.60 |

Table 4.4: Sensitivity analysis on the DH system (Benzene)

The relative increase obtained by passing from the third generation to the most modern generation of district heating is shown graphically in Figure 4.11. The first block (the darker one) indicates the RTE in the case of the third generation, while the two blocks above indicate the RTE increment.

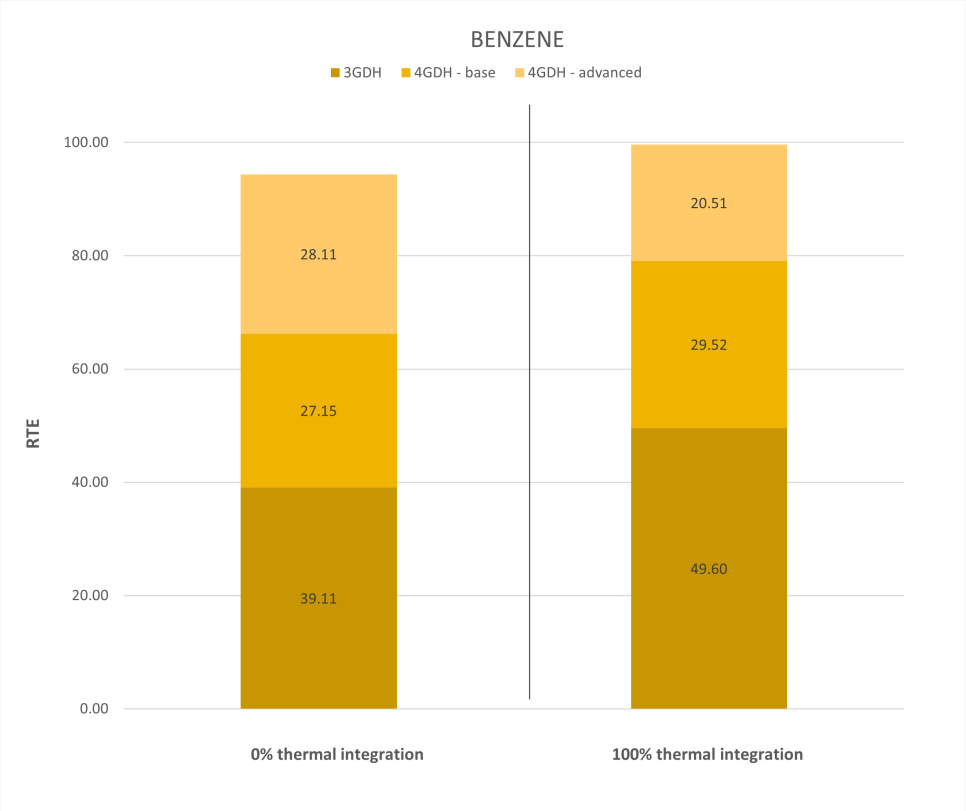


Figure 4.11: RTE relative increase in the three generations

The T-s diagram of the two thermodynamic cycles in the case of 100% integration and 4G-DH is shown in the following figure:

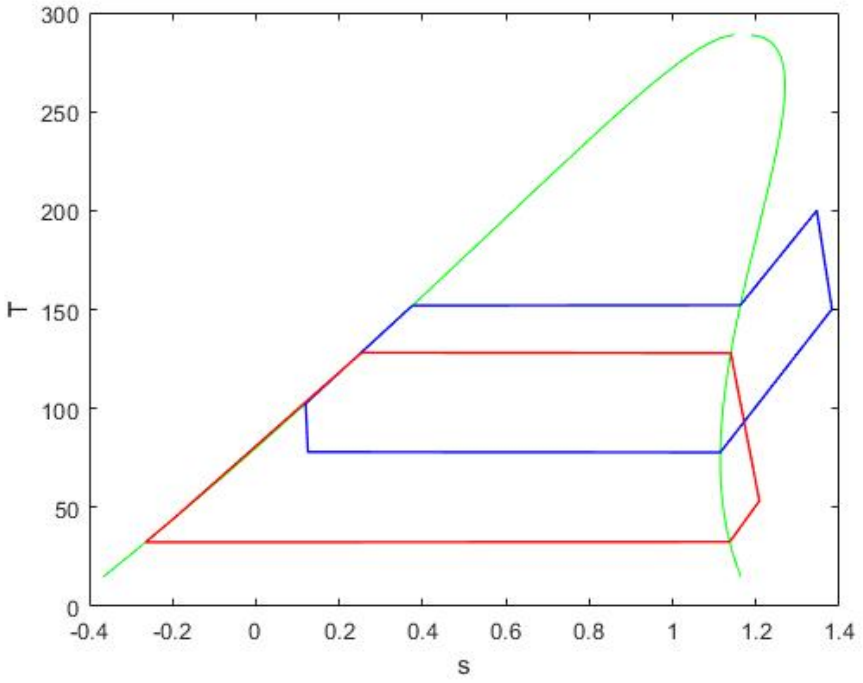


Figure 4.12: Ts diagram of Benzene, 100% thermal integration, 4G-DH (advanced)

Table 4.5 reports the results for the DMC. As it could be seen graphically, the RTE of this fluid is slightly lower than that of benzene in each of the investigated situations.

| | Stand alone | 100% thermal int. |
|---|---|---|
| DMC | RTE | |
| 4G DH (adv) | 92.73 | 97.98 |
| 4G DH (base) | 64.92 | 77.54 |
| 3G DH | 38.25 | 48.50 |

Table 4.5: Sensitivity analysis on the DH system (DMC)

The Ts diagrams of the DMC is reported in Figure 4.13. Figure 4.14 shows the diagram of the other promising fluid, the R1233ZD.

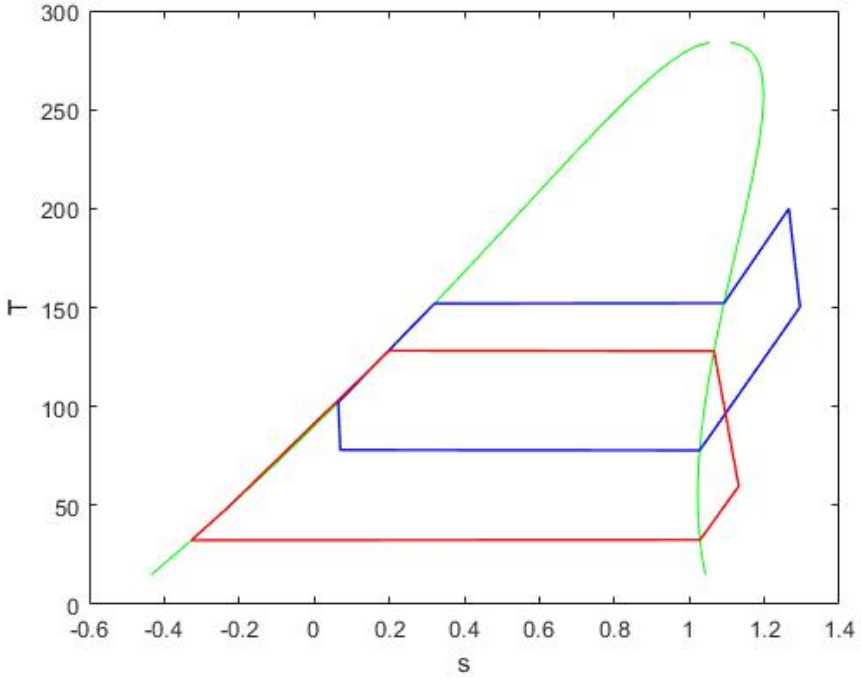


Figure 4.13: Ts diagram of DMC, 100% thermal integration, 4G-DH (advanced)

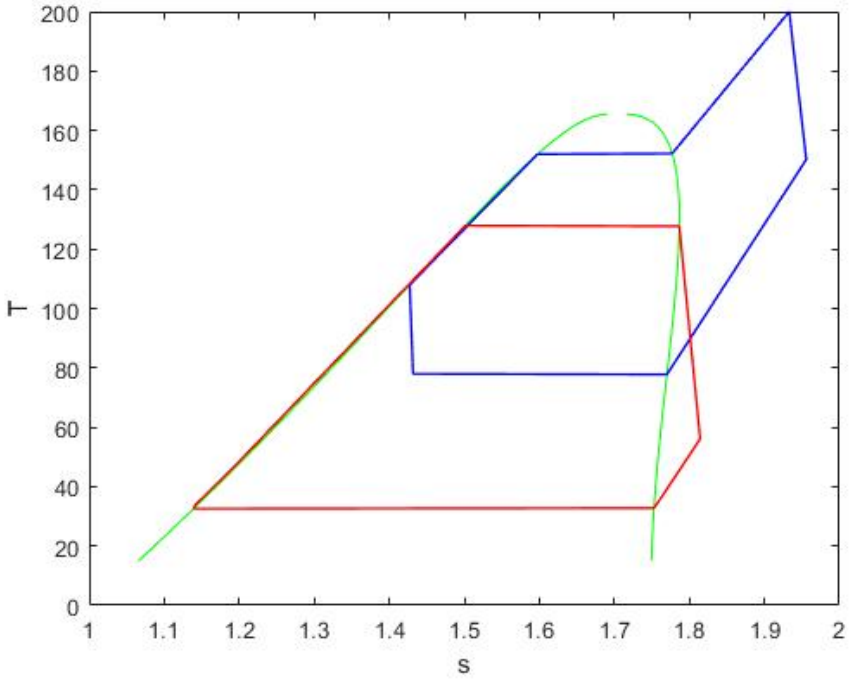


Figure 4.14: Ts diagram of R1233ZD, 100% thermal integration, 4G-DH (advanced)

At this point, for the best possible solution in terms of district heating (4G-DH, advanced), it is analyzed what happens by varying the temperature of the heat source. As initially mentioned, in this system it has been considered that the heat is available in the form of water at a certain temperature (100°C in the reference case), which is cooled down to another temperature (80°C), giving up heat to the thermodynamic charging cycle. The following combinations of water temperatures were considered:

- $T_{in,WH} = 110C$, $T_{in,WH} = 90C$
- $T_{in,WH} = 110C$, $T_{in,WH} = 80C$
- $T_{in,WH} = 90C$, $T_{in,WH} = 70C$
- $T_{in,WH} = 90C$, $T_{in,WH} = 60C$

| | RTE |
|---|---|
| $T_{in} = 120C, T_{out} = 100C$ | 96.64 |
| $T_{in} = 100C, T_{out} = 80C$ | 99.63 |
| $T_{in} = 110C, T_{out} = 90C$ | 98.29 |
| $T_{in} = 110C, T_{out} = 80C$ | 97.36 |
| $T_{in} = 90C, T_{out} = 70C$ | 100.69 |
| $T_{in} = 90C, T_{out} = 60C$ | 99.24 |
| $T_{in} = 80C, T_{out} = 60C$ | 101.52 |

Table 4.6: Sensitivity analysis on the heat source temperatures

As the results show, slightly higher RTE values could be obtained if the heat source were available at a lower temperature (90°C or 80 °C) and if it was cooled down to 70°C or 60°C. In this case, the RTE can reach the value of 101.52, which is the largest obtained value in the overall study of this thesis

Having a higher temperature source does not bring great benefits in terms of performance. Indeed, the worst result among those analyzed is obtained when the source is available at 120°C and is cooled down to 100°C. This last analysis is also valid for the other fluids analyzed, in particular for DMC and R1233ZD.

This aspect leads to the conclusion that the temperature at which the heat source is made available does not heavily affect the performance of the system.

This means that the system can be adapted to a wide range of applications. Any industrial plant (large or small) could benefit from this system.

# 5 | Conclusions and future developments

The electricity generation from renewable sources keeps growing and there is an urgent need to make up for the fact that these sources are aleatory.

An excellent solution (for some considered the only one) is to develop and implement innovative energy storage systems. These systems have been studied for many years and can be very varied, according to their operating principle. The thermochemical storage of energy is certainly a brilliant method to exploit renewables (or waste sources) and use them when needed. Indeed, the characteristic of being theoretically storable for very long periods of time (seasonal storage) makes it attractive to studious and investors.

The innovative system investigated in this thesis is a termochemical heat storage based on a Heat Pump cycle and a Organic Rankine Cycle (ORC). This technology is suitable for long storage times.

The results obtained are highly dependent on the input data: the generation of district heating (and so, its supply and return temperatures) and the temperature of the available heat source influence the round trip efficiency. If on one side the temperature of the heat source does not involve a large change in the RTE when it is varied, district heating temperatures do that.

This means that this thermochemical storage system produces excellent results when coupled with a modern district heating network. The most modern district heating networks (fourth generation) are being gradually installed all over the world, therefore the feasibility of these systems, with high performances, can be guaranteed in the years to come.

As far as the heat source is concerned, rather than the temperature at which it is available, as just mentioned, the time of year in which it is available is important. In fact, as illustrated in the chapter concerning the results, if the source is available throughout the year, with a thermal integration the performances of the system increase profusely.

Two extreme cases have been analyzed in this thesis. One in complete absence of thermal integration (stand alone case) and one with the heat source available at 100% of the power throughout the year. This last case means that the heat to be transferred to the district heating water is lower, therefore the condensation temperature of the ORC rises, increasing its efficiency and therefore the RTE of the whole system. Obviously there can be many intermediate solutions, depending on the type and the availability of the medium temperature heat source.

Thus, when this system is installed near an industrial plant, it can be thermally integrated throughout the year and the performance will be greater. While, if powered by renewables (in particular solar) the thermal integration will be lower, and then also the performance. In any case, it would help to harness low-temperature heat in a clever engineering way.

With regard to the best the working fluid, among the 34 fluids initially selected, Benzene is the one that guarantees the best performance in terms of RTE in any case. Indeed, by changing the generation of district heating or the temperatures at which the heat source is available, it guarantees the best round-trip-efficiency, both in the case of thermal integration and in the stand-alone case.

Benzene, as trans-2-butene (T2butene) and cis-2-butene (C2butene) belongs to aliene and alkynes family. These fluids are not environmentally dangerous. Indees, benzene has an ODP equal to 0 and a GWP equal to 3.4 [58]. Among the other fluids, the ones most similar to Benzene are DMC and R1233ZD. R1233ZD belongs to a class of refrigerants that are not environmentally dangerous (GWP=1, ODP=0.00034).

## 5.1. Future developments

In this thesis, a innovative thermochemical energy storage system has been studied and investigated into the details, many aspects can be studied in a deeper way.

A first analysis which could enlarge the results presented in this work involves the turbomachinery used. In this thesis a power of 300 kW was assumed (coming from the chemical reaction in the reactor). Obviously the same results would be obtained (in terms of better fluids) even using lower or higher power. Therefore, in the analyzed system, given the size of the plant, the turbomachinery (turbine and compressor) are two different components. But in case the size is few kW, it can be used the same reversible machine (a volumetric one). This involves a considerable saving of costs. In this case, a volume ratio analysis should be performed, in order to have the possibility to use the same machine.

In this work, regarding the turbine and the compressor, thir isentropic efficiency has been assumed consulting the literature and relying on similar systems. For sure, all the values adopted for the simulations are well representative of real components, but a more detailed study, involving the modelling of the components, would allow to evaluate the performance of the investigated system.

The second analysis which could definitely enlarge the obtained results, is an economic one. Here the areas of the three heat exchangers involved are calculated. The total area is used, together with the RTE, to classify the analyzed fluids but it is not calculated how much each heat exchanger actually costs. For example, the materials to build the recuperator could be much more expensive than those used to build the high pressure heat exchanger. Therefore, even if the area of the higher (or lower) pressure heat exchanger is greater, the weight of the recuperator in terms of costs could be greater.

As regards the heat exchange, in this thesis the values of the internal and external heat transfer coefficient was initially assumed. An improvement in this aspect could be to calculate these coefficients, designing the geometry of each heat exchanger (e.g. number of pipes, dimensions, position). The geometric analysis is in fact the last step in the study of heat exchangers, and allows to better model the thermal exchange phenomena that occur within them.

Finally, by calculating the cost of each component, the cost of the electrical and thermal energy needed to run the heat pump and the revenues coming from the sale of the energy produced during the discharge of the system, it could be possible to compute the Levelized Cost Of Storage (LCOS). Unfortunately, it is not easy to determine the lifespan of this kind of systems, neither is easy to predict the cost of the purchased and sold energy. However, it could be possible to have an idea of how much it costs to store energy in this way, and compare it to other existing ways of storing energy.

# Bibliography

[1] European Commission and Directorate-General for Energy. *EU energy in figures : statistical pocketbook 2018*. Publications Office, 2018.

[2] Haisheng Chen, Thang Ngoc Cong, Wei Yang, Chunqing Tan, Yongliang Li, and Yulong Ding. Progress in electrical energy storage system: A critical review. *Progress in Natural Science*, 19(3):291–312, 2009.

[3] IEA. Technology roadmap energy storage.

[4] Mukrimin Sevket Guney and Yalcin Tepe. Classification and assessment of energy storage systems. *Renewable and Sustainable Energy Reviews*, 75:1187–1197, 2017.

[5] Mathew Aneke and Meihong Wang. Energy storage technologies and real life applications – a state of the art review. *Applied Energy*, 179:350–377, 2016.

[6] Xing Luo, Jihong Wang, Mark Dooner, and Jonathan Clarke. Overview of current development in electrical energy storage technologies and the application potential in power system operation. *Applied Energy*, 137:511–536, 2015.

[7] A.G. Olabi, C. Onumaegbu, Tabbi Wilberforce, Mohamad Ramadan, Mohammad Ali Abdelkareem, and Abdul Hai Al – Alami. Critical review of energy storage systems. *Energy*, 214:118987, 2021.

[8] Edward Barbour, I.A. Grant Wilson, Jonathan Radcliffe, Yulong Ding, and Yongliang Li. A review of pumped hydro energy storage development in significant international electricity markets. *Renewable and Sustainable Energy Reviews*, 61:421–432, 2016.

[9] Bahtiyar Dursun and Bora Alboyaci. The contribution of wind-hydro pumped storage systems in meeting turkey's electric energy demand. *Renewable and Sustainable Energy Reviews*, 14(7):1979–1988, 2010.

[10] Chi Zhang and King Jet Tseng. Design and control of a novel flywheel energy storage system assisted by hybrid mechanical-magnetic bearings. *Mechatronics*, 23(3):297–309, 2013.

[11] Samuel Wicki and Erik G. Hansen. Clean energy storage technology in the making: An innovation systems perspective on flywheel energy storage. *Journal of Cleaner Production*, 162:1118–1134, 2017.

[12] S. Koohi-Fayegh and M.A. Rosen. A review of energy storage types, applications and recent developments. *Journal of Energy Storage*, 27:101047, 2020.

[13] Ioannis Hadjipaschalis, Andreas Poullikkas, and Venizelos Efthimiou. Overview of current and future energy storage technologies for electric power applications. *Renewable and Sustainable Energy Reviews*, 13(6):1513–1522, 2009.

[14] Jianjun Zhang, Shengni Zhou, Shuaiqi Li, Wenji Song, and Ziping Feng. Performance analysis of diabatic compressed air energy storage (d-caes) system. *Energy Procedia*, 158:4369–4374, 2019. Innovative Solutions for Energy Transitions.

[15] A. Foley and I. Díaz Lobera. Impacts of compressed air energy storage plant on an electricity market with a large renewable energy portfolio. *Energy*, 57:85–94, 2013.

[16] Peter J. Hall and Euan J. Bain. Energy-storage technologies and electricity generation. *Energy Policy*, 36(12):4352–4355, 2008. Foresight Sustainable Energy Management and the Built Environment Project.

[17] John Baker. New technology and possible advances in energy storage. *Energy Policy*, 36(12):4368–4373, 2008. Foresight Sustainable Energy Management and the Built Environment Project.

[18] Lidia Navarro, Alvaro de Gracia, Shane Colclough, Maria Browne, Sarah J. McCormack, Philip Griffiths, and Luisa F. Cabeza. Thermal energy storage in building integrated thermal systems: A review. part 1. active storage systems. *Renewable Energy*, 88:526–547, 2016.

[19] Philipp Geyer, Martin Buchholz, Reiner Buchholz, and Mathieu Provost. Hybrid thermo-chemical district networks – principles and technology. *Applied Energy*, 186:480–491, 2017. Sustainable Thermal Energy Management (SusTEM2015).

[20] US Energy. Employment report. *US Department of Energy, January*, 2017.

[21] T. Schmidt, D. Mangold, and H. Müller-Steinhagen. Central solar heating plants with seasonal storage in germany. *Solar Energy*, 76(1):165–174, 2004. Solar World Congress 2001.

[22] AMIT KUMAR and V.V.N. KISHORE. Construction and operational experience of a 6000 m2 solar pond at kutch, india. *Solar Energy*, 65(4):237–249, 1999.

[23] Ming Liu, Wasim Saman, and Frank Bruno. Review on storage materials and thermal performance enhancement techniques for high temperature phase change thermal storage systems. *Renewable and Sustainable Energy Reviews*, 16(4):2118–2132, 2012.

[24] Parfait Tatsidjodoung, Nolwenn Le Pierrès, and Lingai Luo. A review of potential materials for thermal energy storage in building applications. *Renewable and Sustainable Energy Reviews*, 18:327–349, 2013.

[25] Bruno Cárdenas and Noel León. High temperature latent heat thermal energy storage: Phase change materials, design considerations and performance enhancement techniques. *Renewable and Sustainable Energy Reviews*, 27:724–737, 2013.

[26] Atul Sharma, V.V. Tyagi, C.R. Chen, and D. Buddhi. Review on thermal energy storage with phase change materials and applications. *Renewable and Sustainable Energy Reviews*, 13(2):318–345, 2009.

[27] A. Abhat. Low temperature latent heat thermal energy storage: Heat storage materials. *Solar Energy*, 30(4):313–332, 1983.

[28] Jana Stengler and Marc Linder. Thermal energy storage combined with a temperature boost: An underestimated feature of thermochemical systems. *Applied Energy*, 262:114530, 2020.

[29] Sike Wu, Cheng Zhou, Elham Doroodchi, and Behdad Moghtaderi. Techno-economic analysis of an integrated liquid air and thermochemical energy storage system. *Energy Conversion and Management*, 205:112341, 2020.

[30] K. Edem N'Tsoukpoe, Hui Liu, Nolwenn Le Pierrès, and Lingai Luo. A review on long-term sorption solar energy storage. *Renewable and Sustainable Energy Reviews*, 13(9):2385–2396, 2009.

[31] T. Desrues, J. Ruer, P. Marty, and J.F. Fourmigué. A thermal energy storage process for large scale electric applications. *Applied Thermal Engineering*, 30(5):425–432, 2010.

[32] Alexander White, Geoff Parks, and Christos N. Markides. Thermodynamic analysis of pumped thermal electricity storage. *Applied Thermal Engineering*, 53(2):291–298, 2013. Includes Special Issue: PRO-TEM Special Issue.

[33] Liang Wang, Xipeng Lin, Han Zhang, Long Peng, and Haisheng Chen. Brayton-cycle-based pumped heat electricity storage with innovative operation mode of thermal energy storage array. *Applied Energy*, 291:116821, 2021.

[34] Bernd Eppinger, Lars Zigan, Jürgen Karl, and Stefan Will. Pumped thermal energy storage with heat pump-orc-systems: Comparison of latent and sensible thermal storages for various fluids. *Applied Energy*, 280:115940, 2020.

[35] Henning Jockenhöfer, Wolf-Dieter Steinmann, and Dan Bauer. Detailed numerical investigation of a pumped thermal energy storage with low temperature heat integration. *Energy*, 145:665–676, 2018.

[36] Sebastian Staub, Peter Bazan, Konstantinos Braimakis, Dominik Müller, Christoph Regensburger, Daniel Scharrer, Bernd Schmitt, Daniel Steger, Reinhard German, Sotirios Karellas, Marco Pruckner, Eberhard Schlücker, Stefan Will, and Jürgen Karl. Reversible heat pump–organic rankine cycle systems for the storage of renewable electricity. *Energies*, 11(6), 2018.

[37] Daniel Steger, Christoph Regensburger, Bernd Eppinger, Stefan Will, Jürgen Karl, and Eberhard Schlücker. Design aspects of a reversible heat pump - organic rankine cycle pilot plant for energy storage. *Energy*, 208:118216, 2020.

[38] Guido Francesco Frate, Marco Antonelli, and Umberto Desideri. A novel pumped thermal electricity storage (ptes) system with thermal integration. *Applied Thermal Engineering*, 121:1051–1058, 2017.

[39] Miles Abarr, Jean Hertzberg, and Lupita D. Montoya. Pumped thermal energy storage and bottoming system part b: Sensitivity analysis and baseline performance. *Energy*, 119:601–611, 2017.

[40] Miles Abarr, Brendan Geels, Jean Hertzberg, and Lupita D. Montoya. Pumped thermal energy storage and bottoming system part a: Concept and model. *Energy*, 120:320–331, 2017.

[41] Giovanni Manente, Yulong Ding, and Adriano Sciacovelli. Organic rankine cycles combined with thermochemical sorption heat transformers to enhance the power output from waste heat. *Applied Energy*, 304:117980, 2021.

[42] O. Dumont and V. Lemort. Mapping of performance of pumped thermal energy storage (carnot battery) using waste heat recovery. *Energy*, 211:118963, 2020.

[43] Samuel Henchoz, Florian Buchter, Daniel Favrat, Matteo Morandin, and Mehmet Mercangöz. Thermoeconomic analysis of a solar enhanced energy storage concept based on thermodynamic cycles. *Energy*, 45(1):358–365, 2012. The 24th International

Conference on Efficiency, Cost, Optimization, Simulation and Environmental Impact of Energy, ECOS 2011.

[44] Wolf-Dieter Steinmann, Dan Bauer, Henning Jockenhöfer, and Maike Johnson. Pumped thermal energy storage (ptes) as smart sector-coupling technology for heat and electricity. *Energy*, 183:185–190, 2019.

[45] Marco Astolfi. An innovative approach for the techno-economic optimization of organic rankine cycles, 2014.

[46] Ki Won Nam, Ji Hwan Jeong, Kui Soon Kim, and Man Yeong Ha. The effects of heat transfer evaluation methods on nusselt number for mini-channel tube bundles. pages 361–370, 2010.

[47] Francesco Calise, Adriano Macaluso, Pasquale Pelella, and Laura Vanoli. A comparison of heat transfer correlations applied to an organic rankine cycle. *Engineering Science and Technology, an International Journal*, 21(6):1164–1180, 2018.

[48] M.R. Salimpour. Heat transfer coefficients of shell and coiled tube heat exchangers. *Experimental Thermal and Fluid Science*, 33(2):203–207, 2009.

[49] Todd M. Bandhauer, Akhil Agarwal, and Srinivas Garimella. Measurement and Modeling of Condensation Heat Transfer Coefficients in Circular Microchannels. *Journal of Heat Transfer*, 128(10):1050–1059, 03 2006.

[50] D. Connolly, H. Lund, B.V. Mathiesen, S. Werner, B. Möller, U. Persson, T. Boermans, D. Trier, P.A. Østergaard, and S. Nielsen. Heat roadmap europe: Combining district heating with heat savings to decarbonise the eu energy system. *Energy Policy*, 65:475–489, 2014.

[51] European Commission. 2020–2030–2050, common vision for the renewable heating and cooling sector in europe: European technology platform on renewable heating and cooling. *Luxembourg: EUR-OP*, 2011.

[52] Simone Buffa, Marco Cozzini, Matteo D'Antoni, Marco Baratieri, and Roberto Fedrizzi. 5th generation district heating and cooling systems: A review of existing cases in europe. *Renewable and Sustainable Energy Reviews*, 104:504–522, 2019.

[53] Mennel S. Sulzer M. Hangartner D., Kodel J. Grundlagen und erlauterungen zu thermischen netzen. *Swiss Federal Office of Energy SFOE.*, 2018.

[54] National Institute of Standards and Technology.

[55] Selahattin Göktun. Selection of working fluids for high-temperature heat pumps. *Energy*, 20(7):623–625, 1995.

[56] Marco Astolfi Ennio Macchi. *Organic Rankine Cycle (ORC) Power Systems - Technologies and Applications*, volume 107, chapter 8, pages 22–24. Woodhead Publishing series in energy, 2017.

[57] United States Environmental Protection Agency.

[58] Zhong Ge, Jian Li, Yuanyuan Duan, Zhen Yang, and Zhiyong Xie. Thermodynamic performance analyses and optimization of dual-loop organic rankine cycles for internal combustion engine waste heat recovery. *Applied Sciences*, 9:680, 02 2019.

# List of Figures

# List of Tables

# Acronyms and nomenclature

| Acronyms | Description |
|---|---|
| PHES | Pumped Heat Energy Storage |
| CAES | Compressed Air Energy Storage |
| ORC | Organic Rankine Cycle |
| HP | Heat Pump |
| TES | Themal Energy Storage |
| LHS | Latent Heat Storage |
| SHS | Sensible Heat Storage |
| TCS | Thermochemical Energy Storage |
| PCM | Phase Change Material |
| CHP | Combined Heat and Power |
| PES | Primary Energy Saving |
| RTE | Round-Trip Efficiency |
| HX | Heat Exchanger |